
Towards a microscopic Description of classical Solutions in Field Theory

Lukas Gründig



München 2016

Towards a microscopic Description of classical Solutions in Field Theory

Lukas Gründing

Dissertation
an der Fakultät für Physik
der Ludwig–Maximilians–Universität
München

vorgelegt von
Lukas Gründing
aus Köln

München, den 16. Dezember 2016

Erstgutachter: Prof. Georgi Dvali

Zweitgutachter: Prof. Stefan Hofmann

Tag der mündlichen Prüfung: 17. Februar 2017

Contents

Zusammenfassung	xiii
Abstract	xv
1 Introduction	1
1.1 Classical and Semi-Classical General Relativity	4
1.1.1 Anti-de Sitter Space-Time	8
1.1.2 Semi-classical Black Holes	9
1.2 Black Hole Information	11
1.3 Black Hole Portrait	13
1.4 Solitons	19
1.4.1 Soliton in 1 + 1 dimensions	19
1.4.2 Supersymmetric Soliton	22
1.4.3 Monopole in 3 + 1 dimensions	24
1.5 Instantons	26
1.5.1 Instanton in 0 + 1 dimensions	27
1.5.2 Yang-Mills Instanton	27
1.6 AdS/CFT Correspondence	28
2 Resolution of the Black Hole Bound State in Scattering Experiments	33
2.1 Microscopic Structure of the Black Hole	35
2.2 Time Ordering	39
2.3 Operator Product Expansion of the Absorption Tensor \mathcal{A}	40
2.4 Analytic properties of the Forward Scattering Amplitude \mathcal{C}	42
2.5 Conclusions and Summary	43
3 Coherent State Picture for Solitons	45
3.1 Corpuscular Soliton	46
3.1.1 Coherent State Picture of the Non-Topological Soliton	48
3.1.2 Coherent State Picture of the Topological Soliton	52
3.1.3 Corpuscular Algebra vs. Asymptotic Algebra	53
3.1.4 Topology-Energy decomposition of Solitons	55
3.1.5 Quantum meaning of the Soliton-Anti-Soliton interaction	60

3.2	Corpuscular SUSY Breaking	63
3.2.1	Coherent state picture for the supersymmetric kink	64
3.2.2	Corpuscular Corrections: Commutator Method	66
3.2.3	Corpuscular Corrections: Bogoliubov Method	72
3.3	Conclusions	74
4	Coherent State Picture for Instantons	77
4.1	Instantons in $0 + 1$ dimensions as Solitons in $1 + 1$ dimensions	80
4.1.1	Non-topological Instanton	80
4.1.2	Topological Instanton	83
4.1.3	Explicit Embedding of an Instanton I	86
4.1.4	Explicit Embedding of an Instanton II	89
4.2	Gauge Instanton as Tunneling Monopole	93
4.3	Instantons in $3 + 1$ dimensions	97
4.3.1	$3 + 1$ dimensional Instanton in a Scalar Field Theory	97
4.3.2	BPST-Instanton	99
4.4	Conclusions	102
5	Coherent State Picture for Classical Gravitational Backgrounds	105
5.1	Corpuscular Resolution of arbitrary gravitational Backgrounds	107
5.2	Corpuscular Picture for Linearized Anti-de Sitter	108
5.3	Non-Linear Corpuscular AdS	111
5.4	Randall-Sundrum Geometry	114
5.5	Corpuscular Corrections to scalar Propagators in AdS	116
5.5.1	Scalar Propagator	116
5.5.2	Unruh Effect in AdS	121
5.6	Conclusion	125
6	Summary and Outlook	127
A	Supersymmetry Breaking	131
B	Corpuscular corrections to the scalar propagator in AdS	133
	Acknowledgements	143

List of Figures

1.1	Quantum depletion by a $2 \rightarrow 2$ scattering process of constituent gravitons (curly lines).	17
1.2	The kink profile versus the spatial direction x . For $x \rightarrow \pm\infty$ the scalar field acquires the vacuum expectation values $\pm\frac{m}{g}$	20
1.3	The non-topological soliton profile versus the the spatial direction x	21
2.1	The left figure shows the tree-level diagram for the scattering experiment we consider in this chapter. A scalar field scatters on a black hole bound state with constituent degrees of freedom. As usual, the wiggly line denotes the propagator of the virtual graviton which is exchanged between the scalar field and the black hole. In the right figure, the black hole is resolved into N constituents to properly visualize the scattering on individual constituents.	37
2.2	The integration contour in the complex u -plane is depicted. While the left figure shows the integration contour given by the radius of convergence, the right figure displays the physical parameter u -region ($P^2 > Q^2$). Sending the radius of the circle to infinity, we can relate the physical and the unphysical region by performing a contour deformation.	43
3.1	The function \mathcal{G}_{kink}/m^2 is depicted versus the normalized spatial coordinate xm . Note that in this figure the logarithm is normalized to $\log(\Lambda_{UV}/\mu_{IR}) = 1$. \mathcal{G}_{kink}/m^2 directly measures the violation of the BPS condition and, furthermore, it exactly corresponds to the profile of the second Goldstino.	69
4.1	Non-topological Soliton evolving an euclidean distance L through a barrier. The dashed box represents the barrier, while the profile corresponds to the soliton. The soliton is created on the left side of the barrier and discharges again on the right side. Correspondingly, this virtual process describes the tunneling through the barrier in terms of the Euclidean motion of a soliton.	81
4.2	The dashed line represents the background kink-anti-kink layer created by the background field χ . The straight line corresponds to the solitonic excitation of $\tilde{\phi}$ on the background. For a large layer thickness L , this configuration is well approximated by a standard kink.	88

- 4.3 The dashed profile corresponds to the background χ . In the transition region of χ the ψ profile representing the $\tilde{\phi}$ soliton is different from 0. In particular, the maxima of ψ are given by $\pm \frac{m}{g}$. As a consequence, Alice observes the transition $-\frac{m}{g} \rightarrow \frac{m}{g}$ when the profile passes her. 90
- 4.4 In both figures the ψ profile is depicted, but at different times. The profile moves across the transition region of the χ background kink and passes Alice. Alice measures a vacuum expectation value $\phi = -m/g$ when the minimum of the soliton profile passes her, while she observes $\phi = m/g$ when the maximum is passing by. This means that Alice measures a sign flipping of the vacuum expectation values. Since Alice cannot resolve the spatial extension, she interprets this effect as an instanton. 92
- 4.5 Wall-anti-wall profile with $L = 10/m$. $\Phi^a = 0$ outside the layer, while inside the barrier it acquires the expectation value $\Phi^a = \delta_3^a v$ 95
- 4.6 The white region depicts the Higgs phase, while the grey regions correspond to the surrounding confining phases. Inside the Higgs phase, magnetic point charges can exist. The magnetic field of these charges is screened at large distances. Since there exist magnetic mirror charges on both sides of the layer, this is even the case in the direction longitudinal to the Higgs phase layer. 96
- 5.1 The figure depicts a scalar particle of momentum k propagating through a corpuscular resolved AdS. In particular, the scalar scatters on the individual AdS constituents by exchanging off-shell gravitons. 109
- 5.2 This diagram shows the quantum correction to the full propagator given by $\mathcal{O}_q G_c$ as a function of the coordinate x_1 . The other parameters are chosen as $x_2 = y_1 = y_2 = 0$, $z_1 = 7$, $z_2 = 1$, $t_1 = 1$, $t_2 = 0$. We consider three different choices for the scalar mass: $m^2 = -1$ (largely dashed), $m^2 = 0$ (straight) and $m^2 = 1$ (dashed). The unit length scale in this figure is given by R_{AdS} 118
- 5.3 This diagram shows the quantum correction to the full propagator given by $\mathcal{O}_q G_c$ as a function of the coordinate x_1 . The other parameters are chosen as $x_2 = y_1 = y_2 = 0$, $z_1 = 7$, $z_2 = 1$, $t_1 = 1$, $t_2 = 0$, $m^2 = 1$. We consider two different choices for the curvature radius R_{AdS} : $R_{AdS} = 0.8$ (straight) and $R_{AdS} = 1$ (dashed). The unit mass scale in this figure is given by m 119
- 5.4 This diagram shows the quantum correction to the full propagator given by $\mathcal{O}_q G_c$ as a function of the coordinate z_1 . The other parameters are chosen as $x_1 = x_2 = y_1 = y_2 = 0$, $z_2 = 1$, $t_1 = 1$, $t_2 = 0$. We consider three different choices for the scalar mass: $m^2 = -1$ (largely dashed), $m^2 = 0$ (straight) and $m^2 = 1$ (dashed). The unit length scale in this figure is given by R_{AdS} 120

-
- 5.5 This diagram shows the quantum correction to the full propagator given by $\mathcal{O}_q G_c$ as a function of the coordinate z_2 . The other parameters are chosen as $x_1 = x_2 = y_1 = y_2 = 0$, $z_1 = 5$, $t_1 = 1$, $t_2 = 0$, $m^2 = 1$. We consider two different choices for the curvature radius R_{AdS} : $R_{AdS} = 1$ (straight) and $R_{AdS} = 1.5$ (largely dashed). The unit mass scale in this figure is given by m . 121
- 5.6 This figure shows the quantum derivation from the KMS condition $\Delta \equiv W_{q_1}(\tau, 0) - W_{q_1}(0, \tau + i\beta)$ as a functions of τ . For the additional parameter we choose $z_0 = 1$. We choose three different accelerations for the Rindler observer (all satisfying $a > 1/R_{AdS}$): $a = 2$ (straight), $a = 3$ (largely dashed) and $a = 4$ (dashed). The unit length scale in this figure is given by R_{AdS} . . 124

List of Tables

1.1	The table shows the different physical limits, where M_B is the black hole mass and M_P is the Planck mass.	14
-----	-------------------------------------------------------------------------------------------------------------------------	----

Zusammenfassung

In der Kosmologie und Quantenfeldtheorien (QFT) gibt es viele Experimente, die darauf hinweisen, dass die Natur Quantengesetzen gehorcht. In dieser Dissertation wollen wir, von dieser Prämisse ausgehend, die Konsequenzen untersuchen. Insbesondere folgt daraus, dass wir jedes klassische Objekt als einen Quantenbindungszustand aus mikroskopischen Freiheitsgraden verstehen sollten. Alle klassischen Eigenschaften müssen aus Konsistenzgründen aus der zugrunde liegenden Physik folgen. Dieser Denkweise folgend entwickeln wir Methoden, um verschiedene klassische Felder durch ihre Konstituenten auszudrücken.

Unter dieser Annahme müssen QFT und dementsprechend Unitarität auch innerhalb eines schwarzen Loches weiterbestehen. Daraus folgt unmittelbar, dass ein schwarzes Loch ein Quantenbindungszustand sein muss. Demnach können wir das innere des schwarzen Loches durch Hochenergiestreuexperimente untersuchen, wie dies zum Beispiel in der Quantenchromodynamik (QCD) der Fall ist. Insbesondere wenn wir Streuenergien von der Größe des inversen Schwarzschildradius in Betracht ziehen, folgt automatisch, dass wir die Verteilungsfunktion der individuellen Konstituenten des schwarzen Loches bestimmen können. Es stellt sich heraus, dass diese direkt proportional zum entsprechenden Wirkungsquerschnitt ist.

Außerdem entwickeln wir in dieser Arbeit eine Methode um allgemeine klassische Felder mit Hilfe von kohärenten Zuständen als Bindungszustände darzustellen. Dies erlaubt uns eine mikroskopische Beschreibung von Solitonen zu entwickeln. Vor allem stellen wir fest, dass die Stabilität des topologischen Solitons gegenüber dem Zerfall in Verbindung mit einer divergierenden Besetzungszahl von langwelligen Quanten steht. Als ein weiterer Aspekt der quantenmechanischen Beschreibung bricht das supersymmetrische Soliton alle Supersymmetrien durch die Quantenkorrekturen, die aus einer Rückkopplung mit den individuellen Solitonkonstituenten resultieren.

Es ist nicht möglich die gleichen Techniken direkt auf das Instanton anzuwenden. Daher bilden wir das Instanton auf ein höher dimensionales Soliton ab, welches in euklidischer Zeit propagiert. Dementsprechend erbt das Instanton alle quantenmechanischen Eigenschaften des Solitons. Durch diese Beschreibung lässt sich feststellen, dass die Skaleninvarianz des Belavin-Polyakov-Schwarz-Tyupkin (BPST) Instantons gebrochen ist, da die Besetzungszahl direkt proportional zur Ausdehnung des Instantons ist.

Zudem untersuchen wir klassische Hintergrundmetriken in der allgemeinen Relativitätstheorie von dem mikroskopischen Standort aus. Zum Beispiel beschreiben wir die Anti-de Sitter (AdS) Raumzeit mit Hilfe der oben genannten kohärenten Zustände. Folglich

lässt sich feststellen, dass die Besetzungszahl in der Hauptmasse von AdS mit der Entropie der konformen Feldtheorie auf der Umgrenzung der Raumzeit übereinstimmt. Dies verdeutlicht den quantenmechanischen Ursprung des holographischen Prinzips. Außerdem führt die Auflösung von AdS zu ähnlichen Quantenkorrekturen, wie jenen die wir oben im Zusammenhang mit supersymmetrischen Solitonen eingeführt haben. Diese Korrekturen beeinflussen die Propagation von Skalarfeldern durch die AdS-Raumzeit und die korrespondierende Unruhstrahlung.

Abstract

Many experiments, for instance in cosmology and quantum field theory (QFT), imply that nature is fundamentally quantum. In this thesis we want to take this perspective as a starting point and investigate its consequences. From this point of view, every classical object should be understood as a quantum bound state of proper microscopic degrees of freedom. As a consequence, consistency requires that all the classical features should emerge from these underlying physics. Following this logic, we develop methods to represent classical fields in various examples in terms of constituents.

If we take this premise seriously, it follows that QFT and subsequently unitarity even preexist inside a black hole. In other words, we should understand the black hole as a quantum bound state. Therefore, we can probe the black hole interior by high energy scattering experiments as it is usually done in quantum chromodynamics (QCD) for hadrons. We would expect by default that when we consider scattering energies of the order of the inverse Schwarzschild radius, we can measure the momentum distribution of the individual black hole constituents. Thus, we perform a consistency check that, indeed, the corresponding cross-section is proportional to the occupation number.

As a next step, we develop the coherent state technique which can be used to represent generic classical fields as bound states. Using this method, we show how we can treat solitons in a microscopic description. In particular, we observe that the stability of the topological soliton can be associated with a diverging occupation number of large wavelength quanta. In ongoing work, we consider supersymmetric solitons from this perspective. It turns out that supersymmetry is completely broken by the quantum effects resulting from the back-reaction on the individual constituents.

To apply these techniques to the instanton is more subtle. Therefore, instead of defining a coherent instanton state, we map the instanton on a higher dimensional soliton evolving in Euclidean time. More explicitly, we manufacture a situation where a soliton tunnels through an energetically forbidden barrier. A low energy observer which is confined to this region interprets this effect as an instanton from his lower dimensional point of view. Correspondingly, the instanton inherits all its features from the soliton. In this description, we observe that the scale invariance of the Belavin-Polyakov-Schwarz-Tyupkin (BPST) is broken, since the occupation number of the instanton is proportional to the size of the instanton.

Furthermore, we investigate gravitational background metrics from the microscopic point of view. However, this is still work in progress. For instance, we discuss how we can

use the very same coherent state techniques to describe Anti de-Sitter (AdS). Most notably, in this description the occupation number of the AdS bound state in the bulk seems to coincide with the entropy of the conformal field theory (CFT) on the boundary. This makes the holographic principle manifest from the quantum point of view. In addition, the compositeness of AdS leads to quantum corrections similar to the ones we uncovered for supersymmetric solitons. These corrections affect the propagation of a scalar in AdS and the Unruh radiation which is observed by a Rindler observer.

Chapter 1

Introduction

There is great experimental evidence that nature is fundamentally quantum. This is implied by the experimental success of the tests of quantum field theories (QFT) as, for instance, the electroweak theory and the discovery of the Higgs particle [1], but additionally by observations of the cosmic microwave background [2]. Nevertheless, in many occasions in physics objects are introduced on purely classical grounds. For example, in general relativity (GR) background metrics are usually treated as fundamentally classical objects. In particular, this means that the background does not emerge from a microscopic quantum theory. As a consequence, back-reactions on the background are neglected by default. Furthermore, we know of many field configurations which usually arise as solutions to the classical equations of motions in quantum field theories. In the standard framework, these solutions are treated as purely classical backgrounds, while we consider only quantum fluctuations around the solution on a perturbative level. However, if nature is quantum these classical solutions which are known as solitons should have a microscopic description. In other words, they should emerge from underlying quantum degrees of freedom.

Let us briefly clarify what is meant by 'quantum' in this context. We should not confuse this with the usual perturbative computation of quantum loop contributions to classical observables. These effects always arise when we consider small quantum fluctuations on a classical background and a non-vanishing Planck constant \hbar , while the back-reaction is neglected. We will refer to this limit as semi-classical limit. On the contrary, in this work we are interested in a resolution of classical solutions into N constituents. In other words, we want to identify the real microscopic degrees of freedom from which the classical solution emerges. For instance, let us consider the hydrogen atom. It can be treated as a classical field by a low energy observer. However, when one considers scattering experiments with exchanged energies of the order of the inverse atomic radius, one observes that the atom has a microscopic substructure. Namely, the constituents of the atom are given as the electron and the proton. Considering even higher energy scales, it was found in quantum chromodynamics (QCD) that the proton as well is only a bound state of quantum degrees of freedoms. Thus, according to these examples the true quantum case is achieved when we take the compositeness of classical fields into account (N is finite in this case) and additionally set $\hbar \neq 0$. We can always obtain the semi-classical limit from the pure

quantum case for $N \rightarrow \infty$. In this thesis we are interested in generalizing this bound state logic to several objects in quantum field theories which are usually introduced on purely classical grounds.

The most famous of these objects which are usually treated semi-classically is the black hole. This case is of particular interest, since due to the proof of gravitational waves created by black hole mergers by the LIGO experiment [3], a new era of probing gravitational features seems to arise. Therefore, it is necessary to develop a complete understanding of gravity and, in particular, black holes to predict future measurements. However, in the common semi-classical description of black holes many open questions and mysteries exist which need still to be resolved. In order to achieve this goal, Dvali and Gomez [4, 5, 6] took first steps towards a quantum mechanical description of black holes, where the number of black hole constituents N is finite. In contrast to the semi-classical approach, this framework known as black hole portrait takes back-reactions on the background into account. In the work of Hofmann and Rug [7], further steps were taken to quantum mechanically describe black holes in terms of auxiliary currents. From the quantum theory point of view any bound state resolved into a finite number of constituents should sense deviations from the classical value due to interactions between the constituents. These effects are, of course, highly suppressed as $1/N$. As already mentioned, we can exactly recover the semi-classical limit from the quantum picture for the $N \rightarrow \infty$ limit. Accordingly, we can safely ignore any constituent effects in this limit. Note that this is exactly the main assumption of the semi-classical work of Hawking [8, 9]. The Hawking radiation computation was done in the black hole mass $M_B \rightarrow \infty$ limit. Correspondingly, the constituent number N diverges as well. Therefore, any back-reactions are neglected in this approach. Let us assume, for the moment, we would have established a quantum notion for black holes. How can this help in resolving, for example, the information paradox? The answer is connected to the back-reaction which is not neglected in the full quantum description. One can restate the information paradox simply as: How does a pure state evolve into a mixed one? In a full quantum description, of course, such a non-unitary time evolution does not occur. When we allow quantum effects due to compositeness, the information is encoded in the constituents of the black hole and the Hawking radiation.

As mentioned before this quantum bound state logic is more general and should be applied to all classical gravitational backgrounds. In particular, in this thesis we will apply it to the Anti-de Sitter (AdS) background which was originally proposed in [4, 6]. Of course, this is currently of particular interest due to the AdS/Conformal Field Theory (CFT) correspondence [10, 11, 12]. For instance, we can give an interpretation for the holographic principle [13] in this picture, since the total number of AdS constituents in the bulk is proportional to the number of degrees of freedoms on the boundary.

So far we we only discussed the difference between the quantum and the semi-classical approach in the gravity context as there are many open questions which need to be answered. Nevertheless, as pointed out before the reasoning presented here is much more general. There are many other examples of classical fields in physics which can be resolved into constituents. Take, for example, the well known Laser beam which can be seen as a coherent state of the corresponding monochromatic photons. The coherent state [14] is, in

some sense, the most classical quantum state, since it is the eigenvector of the annihilation operator meaning that only higher order operators can lead to deviations from classical results. In particular, this is the reason why we can represent the classical electric field of a Laser as a coherent state. However, this state is still intrinsically quantum. For instance, it contains the notion of N constituent photons of the Laser. Thus, in principle it allows to calculate $1/N$ corrections for the electric field. Of course, the Laser behaves nearly classical due to the enormous occupation number.

Since the universe is fundamentally quantum, every classical solution should have a microscopic notion in terms of quantum degrees of freedom. Correspondingly, in this thesis we want to extend the quantum bound state description to solitons and instantons because these are usually treated as classical backgrounds. Note that, in contrast to the black hole case, we are not forced to think about a new description of these objects due to obvious inconsistencies of the semi-classical treatment. Rather, as mentioned above there is broad evidence that implies that we live in a fundamentally quantum world. Therefore, the only logical perspective is that every classical solution of field theory like, for example, the soliton should be resolved into its quantum constituents. Since solitons can be seen as some kind of standing wave, it is straightforward to apply the coherent state reasoning of the Laser to the case at hand.

At this point, let us summarize the general philosophy of this thesis. Nature seems to be intrinsically quantum. Therefore, let us take the perspective that every classical object can be described in terms of constituent degrees of freedom. In the following we try to give a consistent description for many of these objects.

The outline of this thesis is as follows. In the rest of this chapter, we give an overview of the usual classical and semi-classical treatment. First we consider classical general relativity and quantum field theory on curved space-time. In particular, we point out which problems arise in this treatment for black holes. Furthermore, we present the black hole portrait by Dvali and Gomez [4, 5, 6] which is a first proposal to represent the black hole as a bound state of gravitons. Then we briefly discuss semi-classical solitons and instantons in sections 1.4 and 1.5, respectively. Finally, we present the essence of the AdS/CFT correspondence.

Due to the new evidence for black hole mergers, it is a very interesting question how the microscopic structure of black holes would affect the outcome of scattering processes on black holes. Naturally, we would expect that in the quantum treatment the corresponding cross-section is proportional to the occupation number of constituent gravitons. In chapter 2 we perform a consistency check to show that this is, indeed, the case. To achieve this, we use similar techniques as in deep inelastic scattering (DIS) on hadrons in QCD [15].

In the third chapter we discuss our bound state proposal for solitons put forward in [16]. In this case we use coherent states to represent solitons in terms of its quantum degrees of freedom. We recover all the known classical results for the non-topological and topological soliton in the first section of this chapter which is, of course, a necessary condition for every quantum framework. Moreover, we give a physical interpretation of the different types of quanta. We can relate the stability of the topological soliton against vacuum decay to an infinite occupation number of long wavelength modes. In addition, we investigate solitons in supersymmetric theories in 3.2. The results indicate that the constituent picture of

solitons leads to $1/N$ type quantum effects (similar to the black hole portrait) which break all the supersymmetries. Note, however, that this is still work in progress and some open questions remain.

The quantum resolution of instantons is discussed in the fourth chapter. For that purpose, we present an understanding of instantons in terms of the tunneling of solitons. In fact, we will consider explicit situations where solitons evolving in Euclidean time are interpreted as instantons by a low energy observer. Note that this means that we can map instantons on solitons in one more dimension. Due to this duality the instanton inherits the microscopic structure of the soliton if it is represented as a bound state. We will consider many different examples like the Belavin-Polyakov-Schwarz-Tyupkin (BPST) instanton [17] and the kink [67].

The coherent state method can also be used to describe gravitational backgrounds as it was proposed in [4, 6]. This is done in chapter 5 for the explicit example of Randall-Sundrum space-time [18, 19] and AdS. As mentioned before, the metric is described as an emergent phenomenon of many quanta in a coherent state similar to the soliton. In particular, we want to understand if this sheds a new light on the AdS/CFT correspondence [10]. Additionally, we try to compute $1/N$ type corrections to the propagator of a scalar in AdS. These could potentially affect the correspondence as well. However, there are still many questions to be answered in this context. As an application, we can show that these effects would lead to deviations from the thermality of the Unruh radiation in AdS [20].

Finally, in chapter 6 we give a summary and an outlook for future projects.

Conventions

In this thesis, we will use the unit convention $\hbar = c = 1$, where \hbar is the Planck constant and c is the vacuum speed of light, respectively. In some situations, we will restore the appropriate powers of \hbar if it is necessary. When it is convenient, we put 'hats' on the operators to make the difference to classical functions manifest. Additionally, we will use the 'mostly $-$ ' convention for the Minkowski space-time in the QFT part of this thesis, while we use the 'mostly $+$ ' convention for GR. The Planck mass is defined as $M_P = 1/\sqrt{8\pi G}$, where G is Newton's constant. In many occasions in this thesis we discuss quantum effects which are suppressed as $1/N$. Note that strictly speaking these effects always behave as \hbar/N .

1.1 Classical and Semi-Classical General Relativity

In this section we briefly review the important features of GR [21, 22] and quantum field theory on curved space-time (reviewed for instance in [23]). For a more detailed review of GR the reader is referred to [24, 25].

Classical GR is a geometric theory meaning that all objects move along geodesics. These geodesics depend on the curvature in the given amount of space. The curvature is generated by the sources of GR, i. e. the energy-momentum tensor $T_{\mu\nu}$. In particular,

any mass or energy bends the space-time. Correspondingly, it affects the surrounding geodesics. The dynamical object in GR which has to be determined in order to construct the geodesics for each particle is given by the metric $g_{\mu\nu}$.

Einstein formulated fundamental postulates in order to define GR. First of all, he introduced the principle of equivalence stating that any mass or energy couples with the same strength to gravity. Secondly, he claimed that physics is independent of the coordinate choice. This simply means that we can switch to physically equivalent metrics by a diffeomorphism

$$\tilde{g}_{\mu\nu} = \frac{\partial x^\alpha}{\partial \tilde{x}^\mu} \frac{\partial x^\beta}{\partial \tilde{x}^\nu} g_{\alpha\beta} . \quad (1.1)$$

Given a curve which is parametrized by τ , we now define the corresponding tangent vector given by $u^\alpha = dx^\alpha/d\tau$. This curve is a geodesic if the tangent vector is parallel transported along itself meaning simply that the covariant derivative vanishes,

$$\frac{Du^\alpha}{D\tau} = \frac{\partial u^\alpha}{\partial \tau} + \Gamma_{\beta\gamma}^\alpha u^\beta u^\gamma = 0 . \quad (1.2)$$

Here we introduced the Christoffel symbols

$$\Gamma_{\beta\gamma}^\alpha = \frac{1}{2} g^{\alpha\mu} (\partial_\gamma g_{\mu\beta} + \partial_\beta g_{\mu\gamma} - \partial_\mu g_{\gamma\beta}) . \quad (1.3)$$

Note that the Christoffel symbols are not a tensor, since they do not transform according to (1.1) under diffeomorphisms. Now we simply have to find the metric produced by the energy-momentum tensor at hand. For that purpose, we consider the fundamental action of GR given as the famous Einstein-Hilbert action

$$S_{EH} = \int d^4x \left(\sqrt{-g} \frac{M_P^2}{2} (R - 2\Lambda) + g_{\mu\nu} T^{\mu\nu} \right) , \quad (1.4)$$

where M_P is the Planck mass, Λ the cosmological constant, R is the trace of the Ricci tensor $R_{\mu\nu}$ and g the determinant of the metric $g_{\mu\nu}$. We will clarify the meaning of Λ later in this section. In addition, $T^{\mu\nu}$ is the energy-momentum tensor acting as the source in general relativity. The kinetic term for the metric is encoded in the Ricci tensor, since it is defined as

$$R_{\mu\nu} = R_{\alpha\mu\nu}^\alpha = \partial_\mu \Gamma_{\alpha\nu}^\alpha - \partial_\nu \Gamma_{\alpha\mu}^\alpha + \Gamma_{\beta\mu}^\alpha \Gamma_{\alpha\nu}^\beta - \Gamma_{\beta\nu}^\alpha \Gamma_{\alpha\mu}^\beta . \quad (1.5)$$

$R_{\mu\nu}$ is a measure for the curvature of the corresponding space-time and is invariant under coordinate transformations. By varying (1.4) with respect to $g_{\mu\nu}$, we obtain the equation of motion known as the Einstein equation

$$M_P^2 \left(R_{\mu\nu} - \frac{1}{2} R g_{\mu\nu} + \Lambda g_{\mu\nu} \right) = T_{\mu\nu} . \quad (1.6)$$

Now it becomes manifest how $T_{\mu\nu}$ influences the space-time metric. To determine the geodesics of an object, we just solve equation (1.6) for the metric. The principle of equivalence which was postulated by Einstein is exactly reflected in (1.6). Mass and Energy represented by $T_{\mu\nu}$ couple with the same strength to gravity. The corresponding coupling constant is the Planck mass M_P .

Note, however, that this feature is not unique to gravity, but can also be achieved in certain scalar field theories [26]. Similarly, the principle of coordinate invariance is not unique. To understand this, one has to keep in mind that it simply means that we should use redundancies to implement the correct number of degrees of freedom in the corresponding field. Obviously, this is similar to usual gauge theories where we use gauge redundancies instead of coordinate invariance. This will become more clear below.

As nature is quantum, let us take a further step and try to understand gravity from the QFT point of view. When trying to quantize the full Einstein-Hilbert action (1.4) one runs into several problems. First of all, since the Hamiltonian of gravity is zero, we cannot easily apply the canonical quantization method as for other classical field theories like Maxwellian theory¹ [27]. Secondly, treating the metric as a quantum field $\hat{g}_{\mu\nu}$ the highly non-linear operators in (1.4) like the determinant term $\sqrt{-\hat{g}}$ lead to an infinite series of higher order operators when expanded. The appearance of the non-renormalizable terms in the Lagrangian was a puzzle for some time, since the Standard Model contains usually only renormalizable or super-renormalizable terms. We further elaborate on this topic in a moment, but first let us discuss the usual strategy to combine quantum theory and gravity which is called QFT on curved space-time. As was pointed out above, this is a purely semi-classical treatment, since it does not allow for the resolution of the classical background, but only takes finite \hbar effects into account. This means that one considers small quantum fluctuations around the classical metric $g_{\mu\nu}$, but neglects any back-reactions on $g_{\mu\nu}$. Starting from pure Einstein gravity, we therefore obtain an interacting quantum theory of these massless fluctuations. As it turns out, these are spin 2 particles referred to as gravitons. From this point of view, it makes more sense to uniquely define GR as the interacting theory of massless spin 2 particles. The equivalence principle and coordinate invariance directly follow from this statement.

Accordingly, the strategy to quantize the theory is as follows. We do not quantize the whole metric $\hat{g}_{\mu\nu}$, but simply consider small quantum fluctuations known as gravitons on top of the classical background $g_{\mu\nu}$. For that purpose, we split the metric as follows

$$\hat{g}_{\mu\nu} \rightarrow g_{\mu\nu} + \frac{1}{M_P} \hat{h}_{\mu\nu} . \quad (1.7)$$

We have to include the factor of M_P to canonically normalize the graviton $\hat{h}_{\mu\nu}$. Let us stress, again, that only $\hat{h}_{\mu\nu}$ is a quantum field, while the background metric stays classical. Consequently, the graviton corresponds to the gauge boson responsible for gravitational

¹ The Hamiltonian of GR is simply a constraint which has to vanish. This is, of course, problematic since in usual quantum theories the Hamiltonian generates time translations. However, in classical GR all coordinates are treated on equal footing.

interaction. Note that we will from now on denote the graviton quantum field by $h_{\mu\nu}$ instead of $\hat{h}_{\mu\nu}$. In the context of general relativity, the gauge symmetries are called diffeomorphisms and exactly correspond to the coordinate invariance of the classical metric in equation (1.1). As in gauge theories, the diffeomorphism invariance is used to enforce constraints on the symmetric tensor field $h_{\mu\nu}$ such that only two propagating degrees of freedom remain [27]. In contrast to the photon, the graviton has two symmetric space-time indices. Correspondingly, it is a spin 2 boson.

As mentioned above, the Einstein-Hilbert Lagrangian contains non-renormalizable interaction terms for the graviton even in the semi-classical description. However, from a modern effective field theory point of view this is not a problem [28, 29, 30]. These irrelevant operators are simply suppressed for energies far below the Planck mass. When the energy scale approaches the Planck scale, we have to include higher order operators to still obtain the correct results. One could argue that such a theory would not be predictive, but this is not true. Before doing any computations, we have to determine up to which energy scale we want to be predictive. Then we have to do a finite amount of measurements to determine the coefficients of the contributing operators.

Of course, this strategy only works as long as we consider energy scales $\Lambda_{UV} < M_P$. For energy scales above the Planck scale, all the dimensionless couplings are at least of order one. Accordingly, we cannot trust perturbation theory anymore at this point. This simply means that a new, unknown type of physics comes into play at those scales which unitarizes the theory. The most famous approach to UV complete general relativity is possibly String Theory [31, 32] which tries to solve the problem by introducing a hard UV cut-off by replacing point particles by strings. In this thesis we will always operate far below the Planck scale such that we do not have to consider any kind of UV completion.

There are many classical objects in our universe like planets with masses $M \gg M_P$. Thus, one could argue that already at the level of Newtonian mechanics the unitarity bound is violated. Of course, this is not the case, since we do not need to include anti-particles for extremely massive non-relativistic objects. Consequently, planets can only occur as external legs in an effective field theory description. For sure they cannot run in loops causing unitarity violations.

Note that already in equation (1.7) we see the M_P suppression for higher order graviton operators. With this in mind we can expand the Einstein Hilbert action to linearized order in the graviton as is for instance shown in [33],

$$S_h = \int d^4x \left(-\frac{1}{2} \partial_\lambda h_{\mu\nu} \partial^\lambda h^{\mu\nu} + \partial_\mu h_{\nu\lambda} \partial^\nu h^{\mu\lambda} - \partial_\mu h^{\mu\nu} \partial_\nu h + \frac{1}{2} \partial_\lambda h \partial^\lambda h \right). \quad (1.8)$$

Here we considered a Minkowski background $g_{\mu\nu} = \eta_{\mu\nu}$ and defined $h = h_\mu^\mu$. To go to a non-trivial background, we have to perform the simple replacement $\partial_\alpha \rightarrow \nabla_\alpha$, since the covariant derivative contains all the background information. Now we can simply apply the Hamilton method as is, for example, described in [33] to quantize the system by imposing non-vanishing equal time commutators for the graviton and its conjugated momentum Π

$$[h(x), \Pi(y)]_{x_0=y_0} = i\hbar \delta^{(3)}(\vec{x} - \vec{y}). \quad (1.9)$$

We can express the graviton in terms of creation and annihilation operators \hat{a}_k and \hat{a}_k^\dagger to fulfill this requirement via the usual free wave expansion

$$h_{\mu\nu}(x) = \int \frac{d^3k}{\sqrt{(2\pi)^3 2\omega(k)}} \sum_{\lambda} \left(\epsilon_{\mu\nu}(\lambda) \hat{a}_k e^{ikx} + \epsilon_{\mu\nu}^*(\lambda) \hat{a}_k^\dagger e^{-ikx} \right). \quad (1.10)$$

Here we introduced the polarization tensor $\epsilon_{\mu\nu}$. As for usual quantum field theories, we can compute correlators by using Wick's theorem. For instance, we find the following graviton propagator

$$\langle 0 | T h_{\mu\nu}(x) h_{\alpha\beta}(y) | 0 \rangle = \Delta_{\mu\nu\alpha\beta}^{grav}(x-y) = \int d^4k \frac{-i}{k^2 + i\epsilon} e^{ik(x-y)} S_{\mu\nu\alpha\beta}, \quad (1.11)$$

where we introduced the tensor structure

$$S_{\mu\nu\alpha\beta} = \eta_{\mu\alpha}\eta_{\nu\beta} + \eta_{\nu\alpha}\eta_{\mu\beta} - \eta_{\mu\nu}\eta_{\alpha\beta}. \quad (1.12)$$

Now we have everything in place to, for instance, write down the Feynman rules of the theory or compute the partition function of the theory. As mentioned above, introducing a background metric would simply lead to a coupling to a classical background field. Furthermore, we could include the graviton self-interaction by including the next-to leading order term of the form $(\partial h)^2 h / M_P$. Of course, this is the first non-renormalizable operator and is suppressed as Λ_{UV} / M_P . This approach now allows to compute quantum corrections to classical observables via contributions from higher loop diagrams.

1.1.1 Anti-de Sitter Space-Time

Anti-de Sitter space-time is one of the simplest special space-times. It is characterized by a negative cosmological constant Λ which leads to many interesting features. In general, we can represent $d+1$ dimensional AdS as a hyperboloid embedded in $d+2$ dimensions [11],

$$-x_0^2 - x_{d+1}^2 + \sum_{i=1}^d x_i^2 = -R_{AdS}^2. \quad (1.13)$$

Here R_{AdS} is the AdS curvature radius. This leads to the line element of the global patch of Anti-de Sitter given as

$$ds^2 = R_{AdS}^2 \left(-\cosh^2 \rho d\tau^2 + d\rho^2 + \sinh^2 \rho d\Omega_{d-1}^2 \right), \quad (1.14)$$

where $d\Omega_{d-1}^2$ represents the solid angle. It possesses the maximal symmetry group $SO(d,2)$, but in contrast to Minkowski it is a hyperbolic space.

The coordinate system we will mostly use here is the Poincaré patch which covers half of the AdS. The corresponding metric is given as

$$ds^2 = \frac{R_{AdS}^2}{z^2} \left(dz^2 + dx^\mu dx_\mu \right), \quad (1.15)$$

where the index μ corresponds to the usual Minkowski coordinates. The z coordinate denotes the conformal direction. In some sense, AdS can be seen as a Minkowski space at each z , but conformally rescaled. Due to the large symmetry of pure AdS we can easily compute its Ricci scalar

$$R = \frac{-(d+1)d}{R_{AdS}^2}. \quad (1.16)$$

Additionally, for a $d+1$ dimensional AdS, we can express Λ in terms of its curvature radius R_{AdS}

$$\Lambda = \frac{-d(d-1)}{R_{AdS}^2}. \quad (1.17)$$

Brown and Henneaux [34, 35] showed that we can associate an asymptotic symmetry group to the boundary of AdS. However, in contrast to Minkowski which is invariant under the BMS symmetry group [36, 37, 38, 39] the boundary of AdS preserves conformal symmetry. This is reflected by the fact that no massive particle can reach the boundary of AdS. Thus, in some sense AdS acts as a box imprisoning the massive particles. We will get to this point again when we discuss the AdS/CFT correspondence in section 1.6.

1.1.2 Semi-classical Black Holes

In classical general relativity, there exists a special solution which is called the black hole or Schwarzschild solution [24, 40]. The gravitational pull of such an object is large enough to trap light on its horizon. Any object of mass M whose physical radius r_p is smaller than the Schwarzschild radius $r_g = 2GM$ fulfills this requirement. The line element for this Schwarzschild solution is given as

$$ds^2 = -\left(1 - \frac{r_g}{r}\right) dt^2 + \frac{1}{\left(1 - \frac{r_g}{r}\right)} dr^2 + r^2 d\Omega^2. \quad (1.18)$$

As usual, the line element can be computed from the metric via $ds^2 = g_{\mu\nu} dx^\mu dx^\nu$. In general, this is the metric for any object of mass M for $r \gg r_p$. The black hole simply corresponds to the special case $r_p < r_g$. Note that although this metric is ill defined at $r_g = r$, nothing special happens at this point for an infalling observer. This is simply an artefact of a wrongly chosen coordinate system. In principle, we can get rid of this problem by introducing Kruskal coordinates [24]

$$ds^2 = \frac{4r^3}{r} e^{-r/r_g} (-dT^2 + dX^2) + r^2 d\Omega^2, \quad (1.19)$$

where we performed the coordinate transformation

$$T = \sqrt{\frac{r}{r_g} - 1} e^{r/2r_g} \sinh\left(\frac{t}{2r_g}\right), \quad (1.20)$$

$$X = \sqrt{\frac{r}{r_g} - 1} e^{r/2r_g} \cosh\left(\frac{t}{2r_g}\right) \quad (1.21)$$

for the exterior of the black hole and

$$T = \sqrt{1 - \frac{r}{r_g}} e^{r/2r_g} \cosh\left(\frac{t}{2r_g}\right), \quad (1.22)$$

$$X = \sqrt{1 - \frac{r}{r_g}} e^{r/2r_g} \sinh\left(\frac{t}{2r_g}\right) \quad (1.23)$$

for the interior where $r < r_g$. As one can see, the time and the radial coordinate exchange their roles at the Schwarzschild radius. Therefore, we cannot define a global timelike Killing vector for the interior and the exterior. This usually happens for time dependent backgrounds. Notice that this property ultimately leads to the Hawking radiation phenomenon which we will consider below.

The $r = r_g$ surface is called the event horizon, since we cannot exchange information with any object which passes the Schwarzschild surface. Thus, by no means we can test the Kruskal coordinates in the interior on classical grounds without entering the black hole. However, obviously an observer inside the black hole cannot communicate with the exterior. The only true classical singularity of this background occurs at $r = 0$ where the curvature of the black hole diverges.

To compute the famous Hawking radiation of a black hole, let us allow quantum fluctuation on top of this classical background. Naively, we can interpret this effect as follows. A pair of particles created near the event horizon could be separated by the gravitational pull. Consequently, an anti-particle would enter the black hole, while the other one escapes as Hawking radiation.

Let us be more explicit at this point and repeat the computation of Hawking [8, 9]. We want to work in the semi-classical limit during this computation:

$$\hbar \neq 0; \quad M_B \quad \text{and} \quad M_P \rightarrow \infty \quad \text{keeping} \quad r_g \quad \text{fixed.} \quad (1.24)$$

Consider now a quantum scalar field ϕ propagating on this background. It satisfies the free wave equation

$$\nabla^2 \phi = 0. \quad (1.25)$$

At this point, the derivative operator ∇^2 already contains the background as the covariant derivative contains all the metric dependent Christoffel symbols. Since ϕ fulfills the usual equal time commutation relation, we can expand it in terms of creation and annihilation operators \hat{a} and \hat{a}^\dagger

$$\phi = \sum_i \left(\alpha_i \hat{a}_i + \alpha_i^* \hat{a}_i^\dagger \right), \quad (1.26)$$

where the α_i are the corresponding mode functions which have to satisfy the equation of motion (1.25). The \hat{a}_i and \hat{a}_i^\dagger are defined as creating and annihilating quanta at past infinity

$$\hat{a}_i |0_-\rangle = 0. \quad (1.27)$$

Furthermore, they satisfy the usual algebra

$$[\hat{a}_i, \hat{a}_j] = 0 \quad ; \quad [\hat{a}_i, \hat{a}_j^\dagger] = \delta_{ij} . \quad (1.28)$$

At the same time, we can define the scalar field in terms of a different set of creation and annihilation operators $\hat{b}_j, \hat{b}_j^\dagger, \hat{c}_j, \hat{c}_j^\dagger$ which act on a different vacuum. The \hat{b}_j create scalar particles at future infinity, while the \hat{c}_j create particle going in the black hole. Thus, we obtain

$$\phi = \sum \left(\beta_i \hat{b} + \beta_i^* \hat{b}_i^\dagger + \gamma_i \hat{c} + \gamma_i^* \hat{c}_i^\dagger \right) . \quad (1.29)$$

Here the γ_i and β_i are again the mode functions which have to fulfill the equation of motion. In particular, they might behave differently than the α_i , since the corresponding operators are defined on the future vacuum

$$\hat{b}_i |0_+\rangle = 0 \quad (1.30)$$

$$\hat{c}_i |0_+\rangle = 0 . \quad (1.31)$$

The Hawking radiation is explicitly encoded in the difference of the vacua. To be more explicit, we can relate the different creation and annihilation operators via a Bogoliubov transformation. Correspondingly, there is a non-zero occupation number of \hat{b} -quanta from the point of view of the vacuum at past infinity $|0_-\rangle$,

$$\langle n_i \rangle = \langle 0_- | \hat{b}_i^\dagger \hat{b}_i | 0_- \rangle \propto \frac{1}{(e^{\omega/T_g} - 1)} . \quad (1.32)$$

Here ω is the frequency of the Hawking quanta. This is exactly the spectrum of the radiation of a black body with temperature $T_g = 1/r_g$.

It is the thermality of the spectrum which leads to the conclusion that there is an information paradox, since thermal radiation cannot contain any information. This would mean that measuring all the radiation of the black hole for an infinite time we could not gather any knowledge about the quanta which fell into the black hole. From a quantum mechanical perspective, this means that the black hole undergoes a non-unitary time evolution because starting from a pure state we arrived at a mixed state described by a density matrix.

1.2 Black Hole Information

To analyze the black hole from a quantum information point of view, let us consider the argument of Page [41, 42]². For that purpose, we view the Hawking radiation and the black hole as two quantum mechanical subsystems (with dimension n and m , respectively) of the same total Hilbert space of dimension nm . We assume that unitary time evolution is

²A useful review of the information paradox is, for example, given by [43].

preserved, since it is fundamental in quantum mechanics. If we consider a pure black hole state under this assumption, it can only evolve again into a pure state. In other words, the total density matrix for black hole and Hawking radiation still satisfies $\rho_t = \rho_t^2$.

Nevertheless, the subsystems can be in a mixed state. As usual, we can determine their density matrices by tracing over the other subsystem. Consequently,

$$\rho_{BH} = \text{tr}_{HR}\rho_t \quad (1.33)$$

$$\rho_{HR} = \text{tr}_{BH}\rho_t, \quad (1.34)$$

where ρ_{BH} and ρ_{HR} are the density matrices of the black hole and the Hawking radiation, respectively. We can define an entanglement entropy for both subsystems using the definition of von Neumann

$$S_{BH} = -\text{tr}_{BH}\rho_{BH}\log\rho_{BH} = -\text{tr}_{HR}\rho_{HR}\log\rho_{HR} = S_{HR}. \quad (1.35)$$

Page defines the notion of information of the black hole I_{BH} as the difference between the maximal entropy ($\log m$) for the black hole and the entanglement entropy in (1.35). The information of the radiation I_{HR} is defined accordingly,

$$I_{BH} = \log m - S_{BH} \quad (1.36)$$

$$I_{HR} = \log n - S_{HR}. \quad (1.37)$$

The smaller subsystem is nearly fully entangled and therefore contains hardly any information. It holds

$$I_{HR} \sim \frac{m}{2n} \quad (1.38)$$

for $1 < m < n$. This situation, however, is changed after a certain period of time which is called Page time t_P . After this amount of time, the Hilbert space of the Hawking radiation is larger than the one of the black hole. Correspondingly, the radiation cannot be totally entangled anymore with the black hole. In turn, the radiation starts to convey information according to equation (1.37).

The results of Page seem to be in total contrast to the ones of Hawking who found a completely thermal spectrum which cannot contain any information. To resolve this problem, one has to take a look at the time scales involved. The Page time is naturally given by the time scale which is needed to radiate away half of the black hole. If one trusts Hawking's computation, it is then given by

$$t_P \sim M_B. \quad (1.39)$$

Thus, since Hawking considers an infinitely heavy black hole, it takes an infinite amount of time until information starts to leave the black hole. According to Page, even if one could prove that no information comes out by perturbative processes, nothing could prevent non-perturbative processes to do so.

To summarize, if one considers a finite mass black hole, the Hawking radiation contains information as soon as half of the black hole is radiated away. In some sense, there exists no information paradox by default, since in a full quantum picture a unitary time-evolution is guaranteed. This is basically, the starting assumption of the black hole portrait of Dvali and Gomez we consider in the next section.

Standard Approaches

There are several different attempts to resolve the information paradox. As a remark, let us briefly comment on the two most common approaches. The first strategy tries to tackle the problem within the description of semi-classical black holes itself. Most famously, Susskind et al. proposed the concept of black complementarity [44, 45]. Their proposal states that it is unphysical to assume that there exists a pure physical state describing both the interior and the exterior of the black hole, since an outside observer could never gain any information about the interior. Without such a global superobserver, there seems to be no contradiction to assume that an infalling observer can retrieve the information after some time. Before evaporating, the information is stored on a stretched horizon which can contain all the microscopic degrees of freedom. However, one of the main assumptions of this proposal states that that an infalling observer should observe nothing special when he enters the black hole. This is questioned by the work of Polchinski et al. [46] who showed that this set-up necessarily leads to a firewall surrounding the black hole. Thus, this strongly hints that semi-classical solutions to the unitarity problem seem not to work so far.

The second type of solutions is based on string theory like the fuzzball proposal [47] or matrix models [48]. In these frameworks, however, the question arises why we have to introduce physics in the deep UV to resolve a problem which even occurs on extremely large scales. More explicitly, consider a large black hole of Schwarzschild radius $r_g \gg L_P$, where L_P is the Planck length. At these energy scales, we can totally trust common quantum gravity, since usually we expect new degrees of freedom to become important only at the Planck scale. Nevertheless, unitarity is violated by semi-classical black holes at these scales. Thus, it has to be clarified why a problem arising at macroscopic scales should be resolved by physics affecting a highly disconnected energy regime.

A third option is to resolve the black hole in its quantum degrees of freedom and is discussed in the next section.

1.3 Black Hole Portrait

At this point, let us discuss the black hole portrait by Dvali and Gomez [4, 5, 6]. In contrast to the semi-classical approach, the portrait gives a full quantum picture of the black hole. This means that the black hole is not treated as a classical background, but is resolved into its quantum degrees of freedom. As argued in the beginning of this chapter, this is a very reasonable perspective as many experiments indicate the fundamental quantumness of

nature. The different physical limits (classical, semi-classical, quantum) are shown in table 1.1. Obviously, if we work in a full quantum picture, unitary time evolution is guaranteed

classical	$\hbar \rightarrow 0$	$M_B, M_P \rightarrow \infty, M_B/M_P^2$ fixed
semi-classical	$\hbar \neq 0$	$M_B, M_P \rightarrow \infty, M_B/M_P^2$ fixed
quantum	$\hbar \neq 0$	M_B, M_P finite

Table 1.1: The table shows the different physical limits, where M_B is the black hole mass and M_P is the Planck mass.

by default. This leads, for instance, to the automatic resolution of the information paradox, since no pure state can evolve into a mixed state in such a description of black holes³.

The quantum description for the black hole is introduced by representing it as a bound state. In particular, the black hole is made out of N quantum constituents from this point of view. Since we consider black holes of finite mass, the corresponding occupation number N is finite as well. As we will see, this will lead to finite corrections to the Hawking spectrum of the order $1/N$. Although these corrections seem to be very small, they can still unitarize the Hawking radiation.

The constituents of the black hole are given as gravitons in the black hole portrait. This is a natural choice for several reasons. First of all, we know that black holes also exist in pure Einstein gravity, where the graviton is the only quantum particle we know of. Furthermore, as we will see below it is exactly the derivative structure of the graviton self-coupling which allows to construct black hole bound states of arbitrary size. These constituent gravitons are longitudinally polarized. In contrast to the usual transversal gravitons, the off-shell gravitons allow for the formation of bound states. Note, however, that the constituent gravitons behave completely differently than usual transversal gravitons. They simply cannot exist as asymptotic S -matrix states and have a non-trivial dispersion relation. Correspondingly, they can only exist in the bound state itself. In order to form black holes in this framework, one has to claim that the overlap between the asymptotic and the bound state quanta is non-zero.

For every bound state, the constituents have to be confined in a certain spatial volume. Additionally, there exists a momentum distribution of the bound state quanta. One of the crucial points of the black hole portrait is that the wavelength of the constituent gravitons is given by the Schwarzschild radius. Of course, this also means that we can only consider black holes with physical size $r_p = r_g$, since otherwise the gravitons cannot be confined inside the bound state. The mass of the black hole is simply given as the sum over the energy of the N constituents

$$M_B = N \frac{1}{r_g}, \quad (1.40)$$

³Note that it was shown in [49] that we do not need to consider a concrete quantum model for the black hole in order to resolve the paradox. As soon as we take back-reactions on the black hole into account (M_B, M_P finite), it directly follows that corrections to the thermality of Hawking radiation become important after Page time. These corrections are not exponentially suppressed.

where all gravitons contribute the same amount of energy. Note that this is only an approximation. The real momentum distribution of the constituent gravitons should be smeared out by a corresponding profile. Accordingly, it cannot be completely narrow in a more realistic approach. With this assumption, we can reexpress the classical parameters of the black hole in terms of the quantum parameters N and M_P

$$M_B = \sqrt{N}M_P, \quad (1.41)$$

$$r_g = \sqrt{N}L_P, \quad (1.42)$$

where L_P is the Planck length.

Naively, one could expect that the gravitational attraction between the constituents should be very strong. Therefore, totally unknown physics should dominate in this picture. To show that this is not true, let us compute the individual coupling of the gravitons of wavelength $\lambda_{grav} = r_g$

$$\alpha = \frac{L_P^2}{\lambda_{grav}^2} = \frac{1}{N}. \quad (1.43)$$

Here we focused on the lowest order graviton self-coupling term to compute α . Of course, this is much smaller than 1 in such way that we operate far below the Planck scale. For instance, for a solar mass black hole it holds

$$N \sim 10^{76}. \quad (1.44)$$

Correspondingly, we can neglect all the higher order interactions, since they are suppressed by even higher powers of α . This is also the reason why we can safely neglect loop contributions in this framework simply because we are far from the point of strong individual graviton interaction. Let us stress at this point that this description breaks down for small black holes because for $M_B \sim M_P$ it follows $N \sim 1$ such that the individual coupling becomes order 1 as well.

The bound state system we are describing here has the crucial feature that the coupling is the same for every constituent⁴. This is usually a property of Bose-Einstein condensates. Furthermore, all constituents of a condensate share the same quantum state. Dvali and Gomez claim that we can always represent the black hole as such a Bose-Einstein condensate of gravitons [50]. Naively, we could ask the question, why such a condensate does not decay if the individual coupling is extremely small. Note, however, that we can still have large collective effects due to the large occupation number N . Usually, we define the 't Hooft coupling

$$\lambda_{tH} = N\alpha. \quad (1.45)$$

in large N gauge theories to measure the collective coupling. The crucial difference to, for example, large N QCD [51, 52] is that we can have black holes of arbitrary N in

⁴Clearly, this feature is very special to gravity, since the coupling is universal.

gravity, while N is fixed in QCD⁵. Notice that the black hole condensate is in a very special situation, where

$$\lambda_{tH} = 1 . \quad (1.46)$$

This means that the condensate is at the quantum critical point. Therefore, the black hole is, in contrast to usual macroscopic objects, very far away from classicality. Let us stress again, that although the gravitons are weakly coupled individually, the black hole enters the quantum critical regime due to the large collective effects. Additionally, we can make the observation that λ_{tH} does, in fact, not depend on N , but is always 1 for the black hole condensate. This is totally unknown in usual Bose-Einstein condensates and is exactly related to the highly non-trivial derivative graviton self-coupling. In other words, it is a special property of quantum gravity.

Consequently, the black hole always corresponds to a situation where the gravitons are maximally packed. In particular, the binding potential and the kinetic energy of the graviton are of the same order

$$E_{kin} = \hbar\alpha N \frac{1}{\lambda_{grav}} , \quad (1.47)$$

$$V(r) = \hbar\alpha N \frac{1}{r} , \quad (1.48)$$

since the gravitational wavelength $\lambda_{grav} \sim r_g$. Again, this is related to the quantum criticality of the black hole. At this point, quantum depletion becomes highly probable reflecting that constituent gravitons can easily leave the black hole, since the confining potential is of the same order as the kinetic energy. Of course, this is related to the Hawking radiation.

Before evaluating the corresponding depletion rate, let us briefly discuss the black hole state. Since the black hole is described as a Bose condensate, the corresponding state can simply be viewed as a Fock state of N constituent gravitons in one mode

$$|B\rangle \sim (a_{1/r_g}^\dagger)^N |0\rangle . \quad (1.49)$$

Note, again, that these creation operators do not create asymptotic quanta. To guarantee consistency, the black hole state must have a non-zero overlap with a Fock state of N asymptotic gravitons. As a consequence, the black hole can be formed in scattering processes [53]. In this article, Dvali et al. consider the scattering of two ultra-planckian gravitons into N gravitons in the final state.

The criticality of the Bose condensate of gravitons is ultimately linked to the thermality of the black hole. In other words, gravitons can easily leave the condensate via usual quantum scattering processes. In contrast to other bound states, black holes can exist for any occupation number N . The black hole always stays at the quantum critical point even

⁵This is reminiscent of the fact that in the QCD context N is given by the gauge group $SU(N)$ which is fixed.

when the occupation number changes as λ_{tH} is independent of N . As a consequence, a black hole can decay completely via a series of black holes of smaller occupation number, but still at the critical point. Correspondingly, Hawking radiation occurs in a full quantum treatment as a byproduct of such a process. Obviously, this property is unique for black holes and GR.

In the black hole portrait, we can easily approximate the corresponding black hole decay rate from the bound state point of view. For that purpose, we simply consider the two-to-two scattering of constituent gravitons. Due to this scattering, a graviton can obtain enough kinetical energy to leave the black hole. This process is depicted in figure 1.1. To leading order in $1/N$, we obtain

$$\Gamma = N^2 \alpha^2 \frac{1}{r_g} = \frac{1}{r_g}. \quad (1.50)$$

Here N^2 occurs due to the multiplicity of gravitons, while $1/r_g$ is the energy scale of the outgoing quanta and α^2 is simply the coupling. For $\alpha = 1/N$ we exactly recover Hawking's result. Restoring the Planck constant \hbar , we subsequently obtain the Hawking temperature as in the semi-classical description

$$T = \frac{\hbar}{\sqrt{N} L_P} = \frac{1}{r_g}. \quad (1.51)$$

To compute this result we neglected quantum effects which are suppressed as $1/N$. Neglecting these contributions corresponds to the limit $N \rightarrow \infty$ which is exactly the semi-classical limit where Hawking's calculation is valid. Based on these ideas, the Hawking evaporation was further investigated in [54].

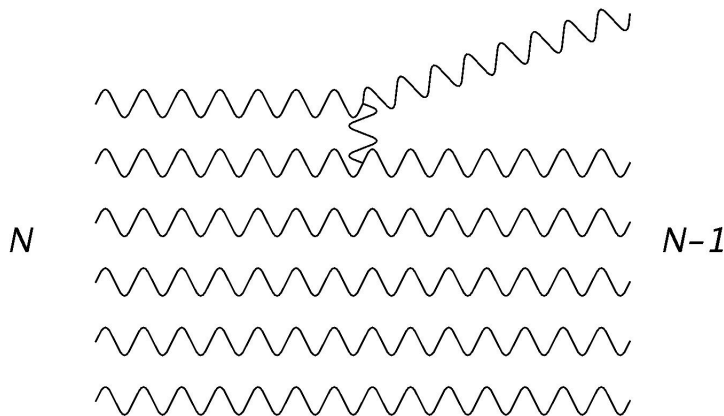


Figure 1.1: Quantum depletion by a $2 \rightarrow 2$ scattering process of constituent gravitons (curly lines).

Let us now consider the situation of finite N . Of course, the total occupation number changes in this case due to the radiation

$$\frac{dN}{dt} = -\frac{1}{\sqrt{N} L_P} + O(1/N^{3/2}). \quad (1.52)$$

This already explains the negative heat capacity of black holes. It is related to the fact that the occupation number is decreasing in time. Since the occupation number is not constant, we obviously get corrections to the decay rate. These are exactly the quantum corrections which are responsible for the purification of the Hawking radiation. In particular, they are not exponentially suppressed as usual perturbative corrections when we consider fluctuations around the saddle point. Rather, they are suppressed as $1/N$ and become order one after Page time t_P .

In other words, if we wait until half of the black hole is evaporated ($t_P \sim M_B/2$), information starts to leave the black hole. It is simply encoded in the $1/N$ corrections to Hawking radiation as Page suggested. Clearly, it is not surprising that the results are in accordance with Page, since both approaches claim that unitarity is a fundamental concept of nature. As a consequence, there is no black hole paradox in this formalism. The black hole constituents all evolve unitarily simply because they are quantum objects. Accordingly, the $1/N$ corrections unitarize the Hawking radiation.

Similarly, we can consider the no hair theorems [55, 56, 57, 58, 59, 60] from this point of view. They state that the only charges we can attribute to a black hole are its mass M_B , its angular momentum and its electrical charge Q . Let us investigate the theorem in the black hole portrait as in [5]. For that purpose, we assume that the black hole has some global charge B . Again, we can measure it by scattering processes, but the decay rate for quanta with global charge is suppressed as B/N . This follows from considering again $2 \rightarrow 2$ scattering with the difference that charged quanta only have a occupation number B . Hence, we obtain

$$\Gamma_B = NB\alpha^2 \frac{1}{r_g}, \quad (1.53)$$

$$\frac{dB}{dt} = -\frac{B}{N^{3/2}t_P}. \quad (1.54)$$

When considering the semi-classical limit $N \rightarrow \infty$, these effects vanish and the black hole seems to have no hair. On the contrary, the full quantum treatment reveals that black holes can, indeed, have quantum hair⁶.

Additionally, the black hole portrait sheds a new light on the Bekenstein entropy [62, 63] and how we can understand fast scrambling [64]. In the articles [65, 66] Dvali et al. consider a toy model of a complex scalar on a ring to mimic the behaviour of the black hole constituents in the interior of the black hole,

$$H = \int d^d x \left(\frac{\hbar^2}{2m} \nabla \phi^\dagger \nabla \phi - \frac{g}{2} (\phi^\dagger \phi)^2 \right). \quad (1.55)$$

This model still captures many of the black hole features like attractive interaction and condensation of scalars. One can explicitly determine the time scale after which fluctuations around the mean field background become important. This quantum break time can be

⁶Note that it was shown in [61] that skyrmion black holes have hair even on a classical level.

found to be

$$t_b \sim \log N . \quad (1.56)$$

This is the time scale directly related to the quantum depletion of the Bose Einstein condensate, since quantum effects become important when enough gravitons have left the condensate due to scatterings.

To summarize the work presented in this section, we can treat black holes as Bose condensates of N constituent gravitons. All typical results like geometry and Hawking radiation can emerge from this condensate. In particular, this treatment resolves the information paradox, since it avoids the unphysical $N \rightarrow \infty$ limit.

1.4 Solitons

1.4.1 Soliton in 1 + 1 dimensions

In general, solitons are solutions to non-linear equations which are non-dissipating. Moreover, they possess a certain energy and are localized on a corresponding length scale. For instance, in 1 + 1 dimensions the simplest of these objects is the kink which will be mostly considered in this section, but we will also briefly treat the magnetic monopole in higher dimensions. For a more detailed review of solitons the reader is, for instance, referred to [67].

Topological Soliton

The kink is obtained as a solution to the classical equation of motion corresponding to the action

$$S = \int dxdt \left[\partial_\mu \phi \partial^\mu \phi - g^2 \left(\phi^2 - \frac{m^2}{g^2} \right)^2 \right] , \quad (1.57)$$

where g is the coupling and m the mass of the scalar field ϕ . Note that the canonical dimension of ϕ in 1 + 1 dimensions is zero, while the dimension of g is one. The vacuum of this theory is degenerate due to the spontaneously broken \mathbb{Z}_2 symmetry ($\phi \rightarrow -\phi$). The two corresponding vacua are

$$\phi = \frac{m}{g} \text{ for } x \rightarrow \infty \text{ and} \quad (1.58)$$

$$\phi = -\frac{m}{g} \text{ for } x \rightarrow -\infty . \quad (1.59)$$

The solution to the equations of motion known as kink profile is

$$\phi_{top}(x) = \frac{m}{g} \tanh(mx) , \quad (1.60)$$

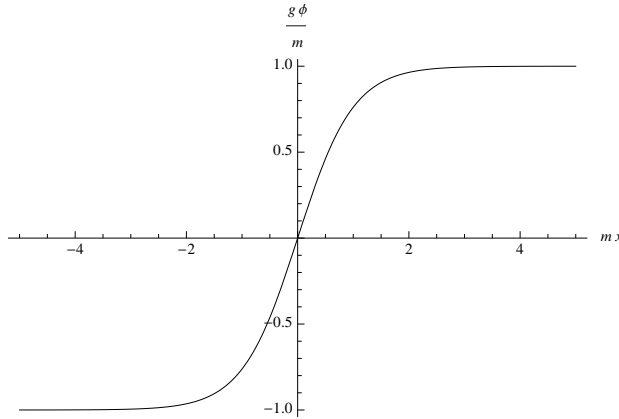


Figure 1.2: The kink profile versus the spatial direction x . For $x \rightarrow \pm\infty$ the scalar field acquires the vacuum expectation values $\pm \frac{m}{g}$.

which is shown in figure 1.2. The soliton has a modulus, since the theory is invariant under shifting the kink center in the spatial direction. A very interesting feature of this object is its topological charge. It guarantees that the kink or topological soliton is protected against decay into the non-topological sector. To make the topological charge Q manifest, we use the Bogomol'nyi split

$$\begin{aligned}
 S &= \int dx dt \left(\left[\partial_\mu \phi \pm g \left(\phi^2 - \frac{m^2}{g^2} \right) \right]^2 \mp 2(\partial_\mu \phi)g \left(\phi^2 - \frac{m^2}{g^2} \right) \right) \\
 &= \int dt \left(\int dx \left[\partial_\mu \phi \pm g \left(\phi^2 - \frac{m^2}{g^2} \right) \right]^2 \mp \underbrace{2 \int dx g \partial_x \left(\frac{\phi^3}{3} - \phi \frac{m^2}{g^2} \right)}_Q \right). \quad (1.61)
 \end{aligned}$$

Since the last term is a total derivative, we can identify it with topological charge of the model. The \pm sign refers to the kink or anti-kink solution, respectively. To classify the topological structure of the theory, one introduces the concept of homotopy. Two functions are homotopic if they can be continuously deformed into each other. In particular, this is not the case anymore if there exists a topological charge and a corresponding non-trivial vacuum structure. We cannot deform the kink to a topologically trivial mapping. This is simply rephrasing the statement that the kink is stable due to the conservation of the topological charge. The vacuum structure at hand corresponds to a non-trivial first homotopy group

$$\pi_0(\mathbb{Z}_2) = \mathbb{Z}. \quad (1.62)$$

This measures the winding around the one dimensional sphere. In particular, the winding number is given as the topological charge Q .

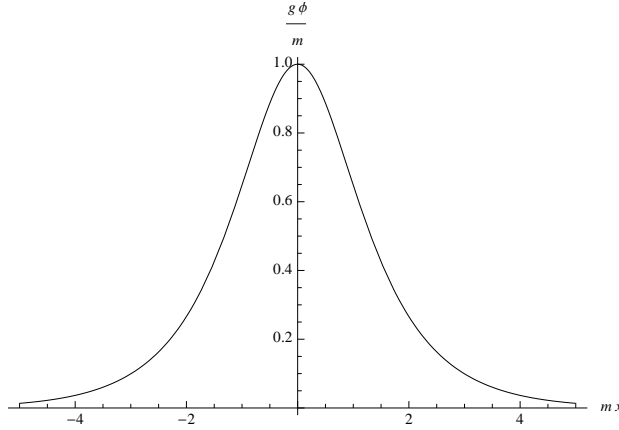


Figure 1.3: The non-topological soliton profile versus the the spatial direction x .

As mentioned in the beginning, every soliton has an associated finite energy

$$E_{top} = \int dx \left[\partial_\mu \phi \partial^\mu \phi + g^2 \left(\phi^2 - \frac{m^2}{g^2} \right)^2 \right] = \frac{8m^3}{3g^2} . \quad (1.63)$$

Note that the energy is always given by the typical energy scale m times the inverse dimensionless coupling

Non-Topological Soliton

Similar to the kink, there also exists a non-topological soliton when we interchange the signs of the mass and the interaction term

$$S = \int dx dt \left[\partial_\mu \phi \partial^\mu \phi - m^2 \phi^2 + g^2 \phi^4 \right] . \quad (1.64)$$

In contrast to the topological soliton, the vacuum is obviously non-degenerate in this case. Correspondingly, the theory is topologically trivial which also means that it has a trivial homotopy group according to our previous statements. As a consequence, the solitonic solution to this theory known as bounce is not protected against decay into the vacuum. It is given as

$$\phi_{non-top} = \frac{m}{\sqrt{2g}} \operatorname{sech}(mx) , \quad (1.65)$$

which is depicted in figure 1.3. This solution interpolates between the following field values

$$\begin{aligned} \phi &= 0 \text{ for } x \rightarrow -\infty \text{ (vacuum)} , \\ \phi &= \frac{m}{g} \text{ for } x = 0 \text{ (not stable)} , \\ \phi &= 0 \text{ for } x \rightarrow \infty \text{ (vacuum)} . \end{aligned}$$

Interpreting x as the time, the field starts at the vacuum $\phi = 0$ reaches $\phi = \frac{m}{\sqrt{2g}}$ and bounces back to the starting value. This solution is topologically not protected and can accordingly decay into the Minkowski vacuum. This effect is known as false vacuum decay investigated by Coleman in [68, 69].

Still this profile describes a legitimate soliton with the corresponding energy given by

$$E_{non-top} = \frac{2m^3}{3g^2} . \quad (1.66)$$

It is worth mentioning that the energy is of the same order as the one of the topological soliton.

1.4.2 Supersymmetric Soliton

In this section we review supersymmetry and in particular the supersymmetric soliton. Coleman and Mandula [70] showed that we cannot extend the Poincaré algebra without trivializing the theory (all scattering angles are fixed). However, there is a loophole to this proof when we consider the symmetry of transforming bosons into fermions and vice versa. This extension of the Poincaré algebra leads to the super-Poincaré algebra. Note that supersymmetry necessarily implies that every boson has a supersymmetric super-partner of the same mass. For a more detailed discussion of supersymmetry the reader is referred to [71, 72, 73, 74].

These additional symmetries are generated by the supercharges $Q_\alpha, \bar{Q}_{\dot{\alpha}}$, where we introduced Weyl indices [67]. In the following we are only interested in $\mathcal{N} = 1$ supersymmetry. This leads to the following algebra (additionally to the usual commutators)

$$\begin{aligned} \{Q_\alpha, \bar{Q}_{\dot{\alpha}}\} &= 2(\sigma^\mu)_{\alpha\dot{\alpha}}(P_\mu + Z_\mu) , \\ [Q_\alpha, P_\mu] &= 0 , \\ [M_{\mu\nu}, Q_\alpha] &= i(\sigma^{\mu\nu})_\alpha^\beta Q_\beta . \end{aligned}$$

Here the σ^μ are the Pauli matrices and Z_μ is the central charge which commutes with all the other generators. Furthermore, P_μ generates spatial translations, $M_{\mu\nu}$ generates the Lorentz transformations and $\sigma^{\mu\nu}$ is defined as

$$\sigma^{\mu\nu} \equiv \frac{1}{4} (\sigma^\mu \bar{\sigma}^\nu - \sigma^\nu \bar{\sigma}^\mu) . \quad (1.67)$$

In general, a state $|sol\rangle$ is supersymmetric when it is annihilated by all the super charges

$$Q_\alpha |sol\rangle = 0 . \quad (1.68)$$

Now let us turn to a concrete supersymmetric theory, where a soliton solution exists. For that purpose, consider the 1 + 1 dimensional Wess-Zumino model with semi-classical (kink not resolved microscopically) Lagrangian given as

$$\mathcal{L} = \frac{1}{2} \left[\partial_\mu \phi \partial^\mu \phi + \bar{\psi} i \gamma^\mu \partial_\mu \psi - \left(\frac{\partial \mathcal{W}}{\partial \phi} \right)^2 - \left(\frac{\partial^2 \mathcal{W}}{\partial^2 \phi} \right) \bar{\psi} \psi \right] , \quad (1.69)$$

where ψ is a two-component Majorana spinor which is simply the fermionic superpartner of the bosonic scalar field ϕ and the γ_μ matrices satisfy the standard Clifford algebra. The Dirac γ_μ matrices in $1 + 1$ dimensions can be represented in terms of the Pauli matrices σ^μ :

$$\begin{aligned}\gamma^0 &= \sigma^2, \\ \gamma^1 &= i\sigma^3.\end{aligned}$$

In order to define interaction terms respecting supersymmetry, we usually use the superpotential $W(\Phi)$ as a tool allowing for an easy construction of supersymmetric theories. In the particular model at hand, it is given by

$$W = \frac{m^2}{g}\phi - \frac{g}{3}\phi^3, \quad (1.70)$$

where the parameters are defined in accordance with the non-supersymmetric kink. Thus, g is simply the coupling constant, while m is the mass. From equation (1.69), we observe that m is the bosonic as well as the fermionic mass parameter which, of course, is a necessary condition for a supersymmetric theory. Furthermore, the bosonic part of (1.69) is obviously the same as the Lagrangian for the ordinary kink in equation (1.57). Correspondingly, this theory has a similar classical kink solution. In general, we would expect that a solitonic background should break the supersymmetries. However, there are some critical solutions which preserve some of the supersymmetries.

For that purpose, we perform the standard Bogomol'nyi completion trick, while keeping $\psi = 0$ for the moment. In particular, we can bring the Hamiltonian to the form

$$H = \int dx \frac{1}{2} \left[(\partial_x \phi) \pm \left(m^2/g - g\phi^2 \right) \right]^2 \mp \int dx \partial_x \phi \left(m^2/g - g\phi^2 \right). \quad (1.71)$$

Our intention is to find the critical solitonic solution minimizing the classical energy. Obviously, this is the case when the first term vanishes. Thus, the Bogomol'nyi-Prasad-Sommerfield (BPS) condition

$$\mathcal{O}_{BPS} \equiv \partial_x \phi \pm \left(m^2/g - g\phi^2 \right) = 0 \quad (1.72)$$

has to be satisfied. The critical classical profile can be found by solving this equation. Notice that the \pm sign corresponds to the anti-kink and kink solution, respectively. We will focus only on the kink solution which is given as

$$\phi_{top}(x) = \frac{m}{g} \tanh(xm). \quad (1.73)$$

The classical supersymmetric kink profile is the same as the usual kink given in equation (1.60). One could ask the question, how it is possible that this solution preserves some part of the supersymmetry. Clearly, there is not any fermionic kink in the theory. The

answer is related to the criticality of the kink. On the critical solution, the total energy of the kink is simply given by the second term of equation (1.71). We can rewrite this term as a total derivative

$$H = \int dx \partial_x \mathcal{W} = \mathcal{W}(x = \infty) - \mathcal{W}(x = -\infty) = Z, \quad (1.74)$$

where Z is the topological charge of the kink. The topological charge is equivalent to the central charge of the supersymmetry algebra of the theory. We can bring the algebra to the form

$$\{Q_1, Q_1\} = H - Z, \quad (1.75)$$

$$\{Q_2, Q_2\} = H + Z. \quad (1.76)$$

Accordingly, on the kink solution corresponding to $H = Z$ the charge Q_1 annihilates the soliton state, while Q_2 does not. In other words, evaluating the charges on the kink state we arrive at

$$Q_1 |sol\rangle = 0, \quad (1.77)$$

$$Q_2 |sol\rangle \neq 0. \quad (1.78)$$

Consequently, this simply means that half of the supersymmetries are preserved. Thus, we refer to this solution as 1/2 BPS.

Naturally, the question arises why the BPS condition is not spoiled by quantum effects. We can answer this question in the semi-classical treatment by introducing bosonic and fermionic quantum fluctuations around the classical background kink. These are simply represented by the fermion operator $\hat{\psi}$ which we neglected in the beginning of this section and a bosonic fluctuation $\hat{\phi}$ which is small compared to ϕ_{top} .

One of the features of supersymmetry is that it protects the BPS condition. In particular, renormalization effects due to quantum loops will not break supersymmetry on a quantum level [71]. This corresponds to the fact, that for each bosonic loop there always exists a canceling fermionic counterpart.

This concludes this brief review of supersymmetric kinks.

1.4.3 Monopole in 3 + 1 dimensions

In this section we will focus on magnetic monopoles which arise in more complicated situations. For that purpose, we consider the Georgi Glashow model [33, 67] with a matter sector containing a real scalar field ϕ^a in the adjoint representation. Additionally, there is a gauge field A_μ^a with the gauge group $SU(2)$ in the theory. Note that the index a refers to the scalar components in $SU(2)$ space. We use the three Pauli matrices σ_a as basis vectors. The corresponding Lagrangian is given as

$$\mathcal{L} = -\frac{1}{4g^2} G_{\mu\nu}^a G^{a\mu\nu} + \frac{1}{2} D_\mu \phi^a D^\mu \phi^a - \lambda ((\phi^a)^2 - v^2)^2. \quad (1.79)$$

Here we used the following definitions for the field strength tensor $G_{\mu\nu}^a$ and the covariant derivative $D_\mu\phi^a$

$$G_{\mu\nu}^a = \partial_\mu A_\nu^a - \partial_\nu A_\mu^a + \epsilon^{abc} A_\mu^b A_\nu^c \quad (1.80)$$

and

$$D_\mu\phi^a = \partial_\mu\phi^a + \epsilon^{abc} A_\mu^b \phi^c, \quad (1.81)$$

where g is the gauge coupling. The last term of the Lagrangian (1.79) enforces a non-trivial vacuum structure for the scalar field at $|x| \rightarrow \infty$

$$\phi^a = v\delta_3^a. \quad (1.82)$$

The vacuum still has a $U(1)$ symmetry, since the breaking pattern is $SU(2) \rightarrow U(1)$. Using color rotation, one can bring the direction of the vacuum vector always to this form. Of course, this amounts to simply choosing a certain gauge condition which in this case is called the unitary gauge.

What we presented so far is simply the usual Higgs mechanism [75]. Correspondingly, the gauge fields A_μ^1 and A_μ^2 form the massive W^\pm bosons, while A_μ^3 stays massless, since the vacuum is invariant under color rotations around the third axis. However, this model contains solitons which are topologically stable. In order to see this, note that $\phi^a\phi^a$ is constrained to the sphere of radius v^2 . Mapping the coordinate sphere corresponding to the monopole on this group space sphere, we find a non-trivial homotopy group

$$\pi_2(SU(2)/U(1)) = \mathbb{Z}. \quad (1.83)$$

The winding number of the mapping, again, reflects the topological charge of the soliton. We call these solitons magnetic monopoles because they create a long-ranged Coulomb type magnetic field. In particular, this is the reason why we need to consider a vacuum structure still allowing one massless gauge field A_μ^3 .

To see how the Coulomb type magnetic field arises, we consider the energy of a monopole

$$E_{mono} = \int d^3x \left[\frac{1}{2g^2} (B_i^a)^2 + \frac{1}{2} D_i\phi^a D^i\phi^a \right]. \quad (1.84)$$

Here we made the assumption that the magnetic and the scalar field should be time independent. The magnetic field B_i^a is simply extracted from the magnetic field strength

$$B_i^a = -\frac{1}{2}\epsilon_{ijk} G_{jk}^a. \quad (1.85)$$

Repeating the Bogolmon'nyi split for equation (1.84), we obtain

$$E_{mono} = \int d^3x \left[\frac{1}{2} \left(\frac{B_i^a}{g} - D_i\phi^a \right)^2 + \underbrace{D^i \frac{B_i^a}{g} \phi^a}_{vq} \right], \quad (1.86)$$

where we used the equation of motion for the magnetic field. The second term is simply a total derivative which we associated with the topological charge in the previous section. For the magnetic monopole, however, it can be interpreted as the magnetic charge q . To understand this more properly, let us apply the law of Gauss to the second term in equation (1.86). Far away from the monopole, the scalar field ϕ^a takes the vacuum expectation value as is described in equation (1.82) leading to

$$q = \int_S dA \frac{1}{g} B_i^3 . \quad (1.87)$$

This is nothing, but the magnetic analog of Gauss's law, where B_i^3 is the magnetic field of the monopole and S denotes the integration surface. Since the charge on the left-hand side is constant, we obtain the usual Coulomb type $1/r^2$ scaling behavior for large radii r . Consequently, the charge can be expressed as

$$q = \frac{4\pi}{g} . \quad (1.88)$$

Obviously, the energy of the monopole is minimized when the BPS condition

$$\frac{B_i^a}{g} - D_i \phi^a = 0 \quad (1.89)$$

is satisfied. This leads to the energy of the critical monopole

$$E_{mono} = qv . \quad (1.90)$$

Note that we can, in principle, use the BPS equation (1.89) to determine the profile for the scalar field and the gauge field as it can be done for the kink solution. However, so far this was only done approximately.

This concludes this small review on different types of solitons.

1.5 Instantons

So far we only considered topological objects with a codimension smaller than the dimension of space-time. Instantons, however, have the same codimension as there are space-time dimensions. They are saddle point solutions to the Euclidean path integral. In contrast to solitons, we usually refer to instantons as describing tunneling processes due to their dependence on Euclidean time.

Note that the occurrence of instantons requires, in general, a non-trivial vacuum structure. First, we will discuss the instanton for the double-well potential in $0+1$ dimensional quantum mechanics. In the second subsection we discuss Yang-Mills instantons in $3+1$ dimensions. For a more detailed review of instantons the reader is referred to [67].

1.5.1 Instanton in 0 + 1 dimensions

The Langrangian of the double-well instanton is quite similar to the one of the kink in 1 + 1 dimensions

$$\mathcal{L}_{0+1} = (\partial_t \phi)^2 - g^2(\phi^2 - m^2/g^2)^2. \quad (1.91)$$

This potential has two degenerate minima at $\phi = \pm m/g$ at $t = \pm\infty$. The instanton profile simply describes the tunneling between both vacua. Note that the profile is basically the same as for the solitonic kink as will become important in chapter 4. However, the instanton depends on the Euclidean time t instead of the spatial coordinate x . The corresponding profile is given as

$$\phi_{inst}(t) = \pm \frac{m}{g} \tanh(tm). \quad (1.92)$$

The instanton has a modulus corresponding to the translational invariance of the instanton center t_0 . For simplicity we will set $t_0 = 0$. The instanton action now plays the role of the soliton energy,

$$S_{inst} = 8m^3/3g^2. \quad (1.93)$$

In contrast to the solitonic kink, the action comes into play because instantons are defined to have a finite action instead of a finite energy. This is why they can give a non-zero contribution to the path integral.

Starting from the path integral, we can actually obtain multi-instanton contributions to partition functions. For instance, there exist instanton-anti-instanton situations which are considered in detail in [76]. In this context, the modulus becomes physical, since the instanton-anti-instanton interaction depends on the distance between both objects.

1.5.2 Yang-Mills Instanton

Similar to the case we just considered, Yang-Mills theory has a non-trivial vacuum structure as well. In particular, there exist instanton solutions in Yang-Mills which describe tunneling processes between the non-trivial prevacua of this theory [17]. To investigate this, consider the Euclidean action of pure Yang-Mills without any matter fields

$$S = \int d^4x \frac{1}{4} G_{\mu\nu}^a G_{\mu\nu}^a = \frac{1}{8} \int d^4x (G_{\mu\nu}^a - \tilde{G}_{\mu\nu}^a)^2 + \frac{8\pi^2}{g^2} G_{\mu\nu}^a \tilde{G}^{a\mu\nu}. \quad (1.94)$$

Here the non-abelian field strength tensor $G_{\mu\nu}^a$ is defined as $G_{\mu\nu}^a = \partial_\mu A_\nu^a - \partial_\nu A_\mu^a + g f^{abc} A_\mu^b A_\nu^c$, while $\tilde{G}_{\mu\nu}^a = 1/2 \epsilon_{\mu\nu\alpha\beta} G_{\alpha\beta}^a$ is its dual, f^{abc} is the structure constant and g is the Yang-Mills coupling. The second term can be expressed as the total derivative of the Chern-Simons current K_μ . This term, of course, can be identified with the topological charge corresponding to this solution

$$\frac{8\pi^2}{g^2} G_{\mu\nu}^a \tilde{G}^{a\mu\nu} = \partial_\mu \left[\frac{8\pi^2}{g^2} 2\epsilon^{\mu\nu\alpha\beta} \left(A_\nu^a \partial_\alpha A_\beta^a + \frac{g}{3} f^{abc} A_\nu^a A_\alpha^b A_\beta^c \right) \right] = \frac{8\pi^2}{g^2} \partial_\mu K^\mu. \quad (1.95)$$

The topological charge Q is simply given as the integrated zero component

$$Q = \int d^3x K^0 . \quad (1.96)$$

As for the topological soliton, this charge corresponds to a winding number labeling the non-trivial homotopy class of the theory

$$\pi_3(SU(2)) = \mathbb{Z} . \quad (1.97)$$

We now have everything in place to define the true vacuum state in pure Yang-Mills. It is given as a superposition of the prevacua of topological charge n . The vacuum $|\Psi_\theta\rangle$ is called θ -vacuum, since it contains an additional free parameter,

$$|\Psi_\theta\rangle = \sum_n e^{in\theta} |\Psi\rangle_n . \quad (1.98)$$

In particular, the θ angle is crucial for the question of strong CP violation [77] and is correspondingly linked with the axion [78, 79, 80]. Note, however, that an instanton is an object which allows to switch from one prevacuum to another. Therefore, it is always a topological charge attributed to the instanton given by the difference of the charges of the prevacua.

The action of the instanton (1.94) is critical if the BPS condition $G = \tilde{G}$ is fulfilled. This leads to the classical profile of the self-dual BPST instanton

$$A_{a\mu} = \frac{2}{g} \eta_{a\mu\nu} \frac{x_\nu}{x^2 + \rho^2} , \quad (1.99)$$

$$G_{\mu\nu}^a = -\frac{4}{g} \eta_{a\mu\nu} \frac{\rho^2}{(x^2 + \rho^2)^2} , \quad (1.100)$$

where the 't Hooft symbols $\eta_{a\mu\nu}$ are defined in [67]. The instanton has eight moduli in total. Four moduli are given by the position of the center in Euclidean space x_0 we set to zero. Furthermore, the instanton possesses a size modulus ρ and three moduli reflect the orientation in $SU(2)$ space. The action of the critical instanton with charge $Q = 1$ is then simply given as

$$S_{inst} = \frac{8\pi^2}{g^2} . \quad (1.101)$$

The BPST instanton is one of the very few situations, where we actually know the exact solution for the profile of a topological object.

1.6 AdS/CFT Correspondence

To conclude this chapter, we review the main features of the AdS/CFT Correspondence [10, 11]. In general, the AdS/CFT conjecture states that certain conformal field theories on

the boundary of AdS space-times are dual to superstring theories on the AdS background in the bulk. This general concept is known as holography, since bulk physics can completely be captured by its boundary degrees of freedom. In particular, Maldacena conjectured in [10] that $\mathcal{N} = 4$ Super Yang-Mills theory (SYM) in $3 + 1$ dimensions is dual to type IIB superstring theory on the product space $AdS_5 \times S_5$, where S_5 simply means that five dimensions are compactified on a circle. The reason for this compactification is simply that type IIB superstring theory is 10 dimensional. Note that the gauge group of SYM is given by $SU(N)$ in this case.

First, let us answer the question how Maldacena came to his conjecture. For that purpose, consider N marginally separated $D3$ branes embedded in the $(9 + 1)$ dimensional space-time of superstring theory. In type IIB superstring theory, we can excite closed strings on empty space, while open strings always have to end on the $D3$ branes. If we take the low energy limit (energies far below the string scale $1/l_s$), only massless degrees of freedom can be excited. The effective open string theory reduces to $\mathcal{N} = 4$ $U(N)$ SYM, while the low energy effective theory for the closed strings corresponds to IIB supergravity.

This can be understood in the following way. On the one hand, open strings with both ends on one brane are massless excitations exhibiting a $U(1)$ symmetry. On the other hand, open strings which end on two different branes have a finite mass given by the separation of both branes. However, when we consider the low energy limit, where all N branes coincide, the symmetry group is enhanced to an $U(N)$ group. In other words, in the low energy limit all the strings which were massive become massless because the separation of the $D3$ branes vanishes. Note that finally the gauge group of the boundary field is $SU(N)$, since one $U(1)$ group corresponds to moving the whole set of branes.

On the contrary, the situation for closed massless strings is different. As already mentioned, their theory reduces to supergravity in the low energy limit. The background metric is dominated by the N $D3$ brane set-up leading to the line element

$$ds^2 = \frac{1}{\sqrt{1 + \frac{R_{AdS}^4}{y^4}}} \eta_{ij} dx^i dx^j + \sqrt{1 + \frac{R_{AdS}^4}{y^4}} (dy^2 + y^2 d\Omega_5^2). \quad (1.102)$$

Here $d\Omega_5^2$ is the five dimensional solid angle of the compactified extra dimensions, while y denotes the non-Minkowskian direction and the radius is simply expressed in terms of the string coupling $R_{AdS}^4 = 4\pi g_s N \alpha'^2$. Here α' denotes the Regge slope. Now the crucial point is simply that surprisingly, for the near horizon limit $y \ll R_{AdS}$ (corresponding to the low energy limit), we recover the AdS space-time from this metric

$$ds^2 = \frac{R_{AdS}^2}{z^2} (\eta_{ij} dx^i dx^j + dz^2) + R_{AdS}^2 d\Omega_5^2, \quad (1.103)$$

where we used the redefinition $z = R_{AdS}^2/y$. In other words, in the low energy limit the closed string theory reduces to supergravity on the background geometry $AdS_5 \times S^5$ in the bulk. In the same limit the open string theory leads to a conformal field theory with a gauge group $SU(N)$ confined on a $3 + 1$ dimensional brane. In principle, the AdS/CFT-

duality can be summarized as

$$\mathcal{N} = 4 \text{ SYM in } 3 + 1 \text{ } d = \text{Type II B Superstring Theory on } AdS_5 \times S_5 . \quad (1.104)$$

Let us now discuss the different parameters on both sides of the duality. On the one hand, the gauge theory is characterized by the gauge coupling g_{YM} and N . On the other hand, the supergravity contains the string coupling g_s and N as well. Note, however, that N has a different interpretation on the supergravity side as the number of coincident branes. The couplings are connected via

$$g_s = \frac{g_{YM}^2}{4\pi} . \quad (1.105)$$

In addition, we can express the gravity parameters in terms of the ratio of AdS radius and string length

$$\frac{R_{AdS}^4}{l_s^4} = \left(\frac{R_{AdS}^2}{\alpha'} \right)^2 = 4\pi g_s N = \lambda_{tH} . \quad (1.106)$$

where we introduced the 't Hooft coupling

$$\lambda_{tH} = g_{YM}^2 N . \quad (1.107)$$

We are mostly interested in the weakly coupled limit. As can be seen from

$$\left(\frac{R_{AdS}}{L_P^{(10)}} \right)^4 \sim N , \quad (1.108)$$

this is the case when the number of fields behaves as $N \rightarrow \infty$. Note that the ten dimensional Planck length is given as $L_P^{(10)} = g_s^{1/4} \alpha'^{1/2}$.

The crucial reason for this phenomenon to be a duality is connected to the coupling regimes. As it turns out, the strongly coupled gravity theory is dual to the weakly coupled field theory and vice versa. To clarify this statement, consider the Maldacena limit, where we take, additionally to $N \gg 1$, the 't Hooft coupling $\lambda_{tH} \gg 1$. Correspondingly, the CFT is strongly coupled in this regime. Additionally, it directly follows that $\frac{R^2}{\alpha'} \gg 1$. As a consequence, in this limit the gravity is not only weakly coupled, but additionally in the low energy regime. Thus, the duality connects a strongly coupled gauge theory with a weakly coupled classical gravity. This is an extremely useful feature as it allows to make predictions on strongly coupled regimes by investigating weakly coupled physics.

In order for both theories to be equivalent, their partition functions must be the same. For that purpose, let us investigate how the correspondence can occur and follow the work of Witten [11]. First of all, we make the observation that AdS in 5 dimensions and a CFT on Minkowski exhibit the same symmetry group. The boundary of AdS_5 is simply four dimensional Minkowski space-time M_4 . However, the symmetry group of AdS_5 is $SO(2, 4)$ which corresponds to the conformal group for M_4 . Consequently, a dual field theory on the boundary must be conformal.

To investigate the partition functions on both sides of the duality, let us consider a massless scalar field ϕ obeying the classical equations of motions in AdS_5 . We denote ϕ_0

as the non-normalizable restriction of ϕ to the boundary. If the correspondence is true, ϕ_0 should act as a source for conformal operators on the boundary. In other words, on the one hand the theory on the boundary is defined by the generating functional

$$\langle e^{\int \phi_0 \mathcal{O}} \rangle_{CFT} , \quad (1.109)$$

where \mathcal{O} denotes an operator of the CFT. Note that in the massless scalar case the conformal dimension of \mathcal{O} is d . On the other hand, we can of course compute the partition function of classical supergravity

$$Z_{sugra}(\phi) = e^{-S_{sugra}(\phi)} , \quad (1.110)$$

where S_{sugra} is the classical supergravity action. Therefore, the conjecture simply means that both partition functions are equivalent,

$$Z_{sugra}(\phi_0) = \langle e^{\int \phi_0 \mathcal{O}} \rangle_{CFT} . \quad (1.111)$$

Let us stress at this point, that this is true in the limit of strongly coupled conformal field theory, while supergravity is weakly coupled. In particular, it allows to solve strongly coupled conformal theory by solving weakly coupled supergravity which is, of course, much simpler.

We can also generalize this logic to massive scalar fields. Solving the classical equations of motion for ϕ in this case, we find no solution which smoothly goes to a constant at the boundary. This of course makes sense, since the boundary is conformal. Thus, no massive particles should reach the boundary to spoil scale invariance.

Additionally, this has implications for \mathcal{O} on the boundary. Its conformal dimension is changed to

$$\Delta = \frac{1}{2} \left(d + \sqrt{d^2 + 4m^2 R_{AdS}^2} \right) . \quad (1.112)$$

Correspondingly, the conformal dimension of the operators which are sourced by ϕ_0 is affected. Another interesting feature of the correspondence is related to the fact that it correlates a gravity theory in $4 + 1$ dimensions with a field theory in $3 + 1$ dimensions. We usually refer to this property as holography. Obviously, this is related to the Bekenstein bound of the entropy $S = Area/4G_N$, where G_N is the Newton constant. In fact, it was shown [81, 82] that AdS exactly saturates this bound,

$$\frac{Area}{4G_N} = S \sim N^2 \delta^{-2} . \quad (1.113)$$

In particular, Susskind and Witten counted the degrees of freedom on the field theory side with the UV cut-off δ and found that it matched to the number of degrees of freedom of the boundary of AdS with an IR cut-off δ .

This concludes this small review of the AdS/CFT correspondence.

Chapter 2

Resolution of the Black Hole Bound State in Scattering Experiments

In classical general relativity it is impossible for an external observer to extract information about the black hole interior. According to the no hair theorem [55], the Schwarzschild black hole is solely characterized by its mass M_B . As a consequence, we can describe the black hole exterior completely in terms of geometry as was done in section 1.1. However, it was shown by Duff [83] that the same result is obtained by taking a field theory perspective. In order to obtain the full non-linear general relativity, an infinite amount of tree-level scattering processes of weakly coupled gravitons has to be resummed. In other words, we can understand the black hole exterior in terms of geometry as well as in a quantum-mechanical S -matrix description. Since only tree-level diagrams are involved in the computation of Duff, it is purely classical, but it can easily be generalized to include \hbar quantum contributions as well. We simply have to take quantum loops into account.

Now let us turn to the black hole interior. In the usual geometric description, there exists an event horizon, since inside the black hole the role of time and radial distance are interchanged such that we cannot construct a globally defined time-like Killing vector. This was already described in the beginning of section 1.1.2. From the QFT point of view, this violates the fundamental law of unitary time evolution. Thus, we cannot find a QFT description for the black hole interior leading to the same results as the geometric description. As was already pointed out in section 1.2, this ultimately leads to the information paradox when we consider QFT in curved space-time as the non-unitary time evolution inevitably leads to the evolution of pure states into mixed states.

However, the black hole interior has never been tested. We have a priori no reason to trust the geometrical description inside the black hole because it obviously leads to inconsistencies. Therefore, we want to take a different perspective. Since nature is fundamentally quantum, we assume that an unitary time evolution should be granted everywhere such that we can work in a usual QFT description. This perspective was already discussed in the introduction and is basically the starting assumption of the black hole portrait [4] presented in section 1.3 and of the auxiliary current description of black holes [7]. It states that there must be some bound state description of black holes in terms of N microscopic

degrees of freedom. As was explained in section 1.3, such a microscopic description of black holes inevitably leads to quantum corrections due to the compositeness which scale as \hbar/N . Note that this does not mean that the results of QFT on curved space-time are never valid. Instead, since Hawking considers the semi-classical limit $N \propto M_B \rightarrow \infty$, he neglects these quantum effects which are responsible for the purification of Hawking radiation. We can always obtain the semi-classical limit if we consider $N \rightarrow \infty$. As a remark, let us stress that in this description the only fundamental space-time is given by Minkowski space, while all the other space-times can be viewed as quantum-mechanical bound states.

In some sense, we can compare the reasoning to QCD. First, protons were viewed as elementary particles characterized by its Casimir invariants of the Poincaré group, i. e. spin and mass. However, experiments implied that there should exist a proton substructure. In particular, this means that hadrons are only a suitable descriptions for low energies, while for high energies we have to take their constituents into account.

As was already pointed out in the introduction, Dvali and Gomez recently proposed the black hole portrait [4] to describe black holes as bound states of gravitons. Furthermore, Hofmann and Rug took first steps in [7] to put these ideas in a more formal context by using auxiliary currents to construct a proper black hole bound state. In this chapter we are not interested in the concrete model to construct a black hole bound state $|B\rangle$. Rather, we start from the assumption that QFT is fundamental. Therefore, unitary time evolution is always granted. This directly implies that the black hole should consist of some quantum degrees of freedom. The main goal of this chapter will be to give a concrete example of embedding a microscopically resolved black hole in a high energy scattering process. Clearly, we expect that the outcome of scatterings on the resolved black hole depends on the occupation number of constituents. More explicitly, we are interested in relating the momentum distribution of black hole constituents with the scattering cross-section.

Obviously, the bound state resolution is very closely related to similar questions in QCD. In particular, bound states constructed from a large number of constituents N were first introduced by 't Hooft. In [51] he considered the large N limit of a $SU(N)$ gauge theory which gives rise to planar dominance and $1/N$ as a suitable expansion parameter. Furthermore, Witten investigated baryons consisting of N quarks from this point of view [52]. Assuming that $SU(\infty)$ is still confining, he showed that the baryon mass scales as $M \propto N$. Note that the black hole portrait gets to the same result, since $M_B = Nr_g^{-1}$ as in (1.40).

In the QCD context one usually considers scattering processes of leptons on protons to obtain information about the interior of the proton. In particular, in deep inelastic scattering leptons emit photons of high virtuality which are absorbed by the proton [15]. Measuring the recoil of the lepton allows to reconstruct the structure functions of the proton. These structure functions contain all the non-perturbative bound state information about the proton's interior. This is only possible because the high energetic photon can probe the interior of the proton. Therefore, it can encode the non-perturbative information leading to color confinement in the cross-section. Let us stress that the lepton can still be treated perturbatively as an asymptotic particle. Notice that the scattering amplitude

factorizes in a perturbative part containing the lepton kinematic and a non-perturbative part. Since Shifman et al. [84, 85] showed how the internal structure of hadrons can be described in a mean-field language, one can explicitly identify the non-perturbative contributions in this context.

The purpose of this chapter is to provide a consistency check that assuming there is a microscopic description of black holes, the occupation number of constituents appears in scattering amplitudes. More explicitly, we want to scatter on a black hole with a scalar field in order to obtain non-perturbative information about the black hole encoded in the black hole structure functions. In order to probe the black hole interior, we consider processes where a graviton of high virtuality is exchanged. As soon as we assume that QFT is also valid inside the black hole, there must be some microscopic degrees of freedom absorbing the graviton. In other words, the black hole has to be a bound state of constituents. Note that we treat the Schwarzschild radius of the black hole in this context as the charge radius of the proton. This means that it sets the length scale for the confinement of the black hole constituents. Furthermore, let us remark that there are, clearly, some differences between GR and QCD. First of all, QCD is asymptotically free, while GR is not. As a consequence, we cannot consider the limit of infinite virtuality for the graviton because this would violate perturbative unitarity in the exterior. However, in the energy regime far below the Planck mass we can still resolve large black holes. Secondly, the black hole constituents are individually weakly coupled as well as was, for instance, shown in [4]. Nevertheless, they get confined due to large collective effects. Note that the work presented in this chapter is closely related to the original work [86].

First, in section 2.1 we describe the set-up of a black hole absorbing gravitons of high virtuality emitted from a scalar particle scattering on the black hole. Secondly, in section 2.2 we show how we can represent the absorption part of the scattering amplitude in terms of the time ordered forward Compton scattering amplitude. Finally, in sections 2.3 and 2.4 we present a method how we can use the operator product expansion to reexpress the forward scattering in terms of derivatives of the momentum distribution of black hole constituents.

2.1 Microscopic Structure of the Black Hole

As the aim of this chapter is to present how the microscopic substructure of a black hole emerges in scattering experiments, let us embed it in a certain S -matrix process. In the S -matrix framework, Duff [83] showed how we can reconstruct the geometrical features of gravitational objects from the quantum mechanical point of view. However, this treatment is semi-classical. In particular, the black hole is introduced as a classical external source. Since we are interested in the resolution of the black hole, let us not consider scatterings on the black hole introduced as an external source, but as an internal source with its own Hilbert space.

Let us briefly comment on the black hole Hilbert space. We can distinguish the Hilbert space \mathcal{H}_1 for elementary particles like gravitons in our case and an additional one \mathcal{H}_2

describing composite objects like, for instance, the black hole. These Hilbert spaces can be split up in a part containing asymptotic scattering states and one containing bound states,

$$\begin{aligned}\mathcal{H}_1 &= \mathcal{H}_1^s \oplus \mathcal{H}_1^b, \\ \mathcal{H}_2 &= \mathcal{H}_2^s \oplus \mathcal{H}_2^b.\end{aligned}$$

The crucial point is simply that we can describe bound states of elementary particles in \mathcal{H}_1^b as scattering states of composite particles in \mathcal{H}_2^s at the kinematical level. As was argued above, the quantum mechanical description ensures a unitary time evolution everywhere. Clearly, in such a description the black hole described in Hilbert space \mathcal{H}_2^s is a quantum bound state with constituents given in \mathcal{H}_1^b .

In principle, the microscopic structure can be resolved for large virtual momenta. Note, again, that the event horizon of the black hole in this description is a semi-classical artefact. It is similar to the charge radius of a proton in QCD. Thus, information can leave the black in this quantum resolution treatment. Nevertheless, taking the limit $N \rightarrow \infty$ we simply recover all the semi-classical features of the usual black hole [4, 7]. In this case, all the microscopic quantum effects which affect scattering experiments and Hawking radiation vanish leading to the assumption that no information can leave the black hole¹.

Obviously, for energy scales below the inverse length scale of the bound state it behaves effectively as an external source where geometrical concepts emerge from resumming tree-level diagrams of gravitons [83]. This leads to the geodesic motion in the background of a Schwarzschild source. In other words, for $r > r_g$ we simply observe a classical $1/r$ -potential. However, it is worth mentioning that such a low energy observer can never distinguish a black hole from any other object of the same mass due to Birkhoff's theorem [24].

On the contrary, if the black hole is not classical, but a quantum object, while Minkowski metric is the only fundamental space-time, we should be able to probe its interior by measuring the outcome of high energy scattering processes. This means that we consider processes of sufficiently high exchanged virtual momentum q . Of course, the energy bound for the resolution is simply given by the inverse size of the black hole,

$$-q^2 > r_g^{-2}. \quad (2.1)$$

It is crucial to notice that we do not need to include new gravitational degrees of freedom for such scattering experiments as long as we stay below the Planck scale. Correspondingly, we obtain the upper bound

$$-q^2 < M_P^2 \quad (2.2)$$

for the virtuality. For small black holes the microscopic description breaks down when $M_P \sim r_g^{-1}$. At these scales, new degrees have to be taken into account. However, for large black holes our description should be completely sensible.

¹As was already pointed out, Hawking exactly considers this limit in his computation ($M_B \rightarrow \infty$).

Now let us discuss a certain experimental set-up to microscopically resolve the black hole. For that purpose, we consider a massless scalar field ϕ as a probe particle. This scalar field is simply coupled to pure linearized Einstein gravity corresponding to the action

$$S = \int d^4x \left[\frac{1}{2} h_{\mu\nu} \epsilon_{\alpha\beta}^{\mu\nu} h^{\alpha\beta} + \frac{1}{M_P} h_{\mu\nu} T^{\mu\nu} \right]. \quad (2.3)$$

Here $\epsilon_{\alpha\beta}^{\mu\nu}$ is the linearized kinetic term of the graviton in Minkowski space-time² as in equation (1.8). The energy-momentum tensor of the scalar field is given as

$$T^{\mu\nu} = \frac{1}{2} S^{\mu\nu\alpha\beta} \partial_\alpha \phi \partial_\beta \phi, \quad (2.4)$$

where $S^{\mu\nu\alpha\beta} = \eta^{\mu\alpha} \eta^{\nu\beta} + \eta^{\mu\beta} \eta^{\nu\alpha} - \eta^{\mu\nu} \eta^{\alpha\beta}$. In order to probe the black hole, we consider an ingoing field ϕ scattering on an individual constituent of the black hole by emitting a virtual graviton which is interchanged between ϕ and the constituent (figure 2.1). If the virtuality of the graviton is in the desired energy regime, one can in principle measure the black hole interior.

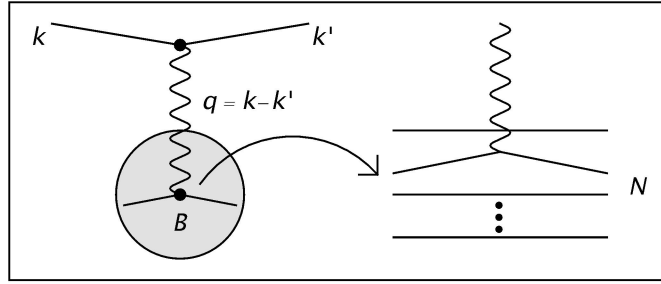


Figure 2.1: The left figure shows the tree-level diagram for the scattering experiment we consider in this chapter. A scalar field scatters on a black hole bound state with constituent degrees of freedom. As usual, the wiggly line denotes the propagator of the virtual graviton which is exchanged between the scalar field and the black hole. In the right figure, the black hole is resolved into N constituents to properly visualize the scattering on individual constituents.

The one-graviton exchange amplitude on tree-level can be achieved by expanding the interaction Lagrangian to second order. If we do not truncate the external legs using the LSZ reduction formula, this amplitude simply reads

$$\mathcal{A}^{(2)}(x_1, x_2) = \frac{i^2}{M_P^4} \int d^4z_1 d^4z_2 \mathcal{P}^{\mu\nu}(z_1, z_2; x_1, x_2) \mathcal{N}_{\mu\nu}(z_2).$$

Here we split the amplitude into a perturbative part \mathcal{P} containing the kinematics of the probe particle and the exchanged graviton and a non-perturbative part \mathcal{N} which carries

²Since Minkowski is the only fundamental space-time from our point of view, this is the logical choice.

all the non-trivial information about the black hole interior. In particular, the \mathcal{N} part is evaluated in the black hole state $|B\rangle$, while \mathcal{P} is evaluated in the usual Minkowski vacuum $|0\rangle$. The black hole state $|B\rangle$ contains all the non-perturbative bound state information. As was already mentioned, there are several approaches to describe black holes in terms of bound states [4, 7]. However, we are only interested in extracting bound state information under the assumption that QFT and unitary time evolution is fundamental. Note that the perturbative and the non-perturbative part of the amplitude are defined as

$$\begin{aligned}\mathcal{P}^{\mu\nu} &= \langle 0|T\phi(x_2)T_{\alpha\beta}(z_1)\phi(x_1)|0\rangle \Delta^{\alpha\beta\mu\nu}(z_1, z_2), \\ \mathcal{N}_{\mu\nu} &= \langle B'|:\mathcal{T}_{\mu\nu}:(z_2)|B\rangle\end{aligned}\tag{2.5}$$

with $|B'\rangle$ denoting the black hole state after the absorption of a virtual graviton. Furthermore, $\Delta^{\alpha\beta\mu\nu}$ is the free graviton propagator. $\mathcal{T}_{\mu\nu}$ is the energy momentum tensor of the individual constituent of the black hole and must not be confused with the energy-momentum tensor $T_{\alpha\beta}$ of the scalar field. In other words, we consider a process where the probe scalar field directly interacts with an individual bound state graviton (see also figure 2.1). As was pointed out above, this is only a suitable approximation in the energy regime given by equations (2.1) and (2.2).

Note that we would obtain the semi-classical scattering results when $\mathcal{N}_{\mu\nu}$ is given as the classical energy-momentum tensor of the black hole. Accordingly, the black hole would simply be treated as an external source. However, we will follow the logic that there is some black hole substructure encoded in $|B\rangle$.

Using similarity transformations on the black hole state, we can bring the non-perturbative part to the form

$$\mathcal{N}(z_2) \approx e^{-i(P'-P)\cdot z_2} \langle B'|:\mathcal{T}: (0)|B\rangle, \tag{2.6}$$

where P' and P denote the black hole momentum after and before the graviton absorption, respectively. Now we truncate the external ϕ legs to obtain the scattering amplitude

$$\begin{aligned}\langle B'\phi'|B\phi\rangle^{(2)} &= -i(2\pi)^4 \delta(k' + P' - k - P) \alpha_g^2 \\ &\times \langle B'|:\mathcal{T}_{\mu\nu}: (0)|B\rangle \Delta^{\mu\nu\alpha\beta}(k' - k) S_{\alpha\beta\rho\sigma} \frac{k'^\rho k^\sigma}{k'^0 k^0}.\end{aligned}\tag{2.7}$$

with the coupling $\alpha_g \equiv 1/(4\pi M_P^2)$.

In order to obtain the total cross section $\sigma(B'\phi' \leftarrow B\phi)$, we have to compute the absolute square of the truncated amplitude. Additionally, we integrate over the whole set of intermediate bound states in the theory leading to

$$k'^0 \frac{d\sigma}{d^3 k'} = \frac{2}{\mathcal{F}(\phi)} |\alpha_g \Delta(k' - k)|^2 \mathcal{E}^{\alpha\beta\mu\nu}(k, k') \mathcal{A}_{\alpha\beta\mu\nu}(B; k, k'). \tag{2.8}$$

where $\mathcal{F}(\phi)$ is simply the ingoing flux of ϕ particles and Δ now refers to the scalar part of the graviton propagator. On the one hand, the emission tensor $\mathcal{E}^{\mu\nu\alpha\beta}$ contains the

kinematic information about the asymptotic scalar field and the virtual gravitons. It is simply given as $\mathcal{E}^{\mu\nu\alpha\beta} = Q^{\mu\nu}Q^{\alpha\beta}$ with

$$Q^{\mu\nu} = 4\pi^2 \Pi^{\mu\nu\alpha\beta}(k' - k) S_{\alpha\beta\rho\sigma} \frac{k'^\rho k^\sigma}{k'^0 k^0}. \quad (2.9)$$

Here we introduced the graviton polarization tensor

$$\Pi_{\mu\nu\alpha\beta}(q) \equiv \pi_{\mu(\alpha}\pi_{\beta)\nu} - \pi_{\mu\nu}\pi_{\alpha\beta} \quad (2.10)$$

$$\pi_{\mu\nu}(q) \equiv \eta_{\mu\nu} - \frac{q_\mu q_\nu}{q^2}, \quad (2.11)$$

where k, k' denote the on-shell asymptotic momenta of the ingoing and outgoing scalar field, respectively. On the other hand, the absorption part is defined as

$$\mathcal{A}_{\alpha\beta\mu\nu} = \frac{1}{2\pi} \int d^4x e^{-i(k'-k)\cdot x} \langle B | \mathcal{T}_{\alpha\beta}(x) \mathcal{T}_{\mu\nu}(0) | B \rangle. \quad (2.12)$$

This part of the amplitude contains the non-trivial information about the resolved black hole. In particular, this information is encoded in the non-perturbative effects which govern this part of the amplitude. Notice that the amplitude completely factorizes in a perturbative part containing the probing scalar field and a non-perturbative part.

The agenda of the next sections will be to represent the absorption part in terms of the constituent occupation number.

2.2 Time Ordering

Since the non-perturbative contribution given by the absorption tensor $\mathcal{A}_{\alpha\beta\mu\nu}$ is not ordered in time, we will proceed in this section to represent the absorption tensor in terms of causal correlation functions. The procedure we use is analogous to similar methods in QCD in the framework of DIS, where the microscopic structure of hadrons is probed [15]. Correspondingly, we closely follow the DIS line of thought and start by expressing the absorption tensor in terms of the forward scattering Compton amplitude which contains a time ordered product.

First of all, we search for a relation between $\mathcal{A}_{\alpha\beta\mu\nu}$ and a tensor built from $\mathcal{T}_{\alpha\beta}(x)\mathcal{T}_{\mu\nu}(0)$. Inserting a complete set of physical states (including bound states) in between the energy-momentum tensors at x and 0 in (2.12) and additionally using space-time translations we arrive at

$$\mathcal{A}_{\alpha\beta\mu\nu} = \frac{1}{2\pi} \sum_{B'} (2\pi)^4 \delta(q + P - P') \langle B | \mathcal{T}_{\alpha\beta}(0) | B' \rangle \langle B' | \mathcal{T}_{\mu\nu}(0) | B \rangle.$$

Here the exchanged momentum is $q \equiv k - k'$, while P and P' denote the momenta of the wave packets representing the ingoing and outgoing black hole, respectively. Note that we used here the translational invariance of the black hole state $|B\rangle$ to show that

$\langle B|\mathcal{T}_{\alpha\beta}(x)|B'\rangle = \langle B|e^{iPx}\mathcal{T}_{\alpha\beta}(0)e^{-iPx}|B'\rangle = \langle B|\mathcal{T}_{\alpha\beta}(0)|B'\rangle$. Accordingly, we can bring the absorption tensor to the form

$$\mathcal{A}_{\alpha\beta\mu\nu} = \frac{1}{2\pi} \int d^4x e^{iq\cdot x} \langle B|[\mathcal{T}_{\alpha\beta}(x), \mathcal{T}_{\mu\nu}(0)]|B\rangle. \quad (2.13)$$

As in deep inelastic scattering, we define the absorptive part of the Compton amplitude $\mathcal{C}_{\alpha\beta\mu\nu}$. In particular, it describes the forward scattering of a virtual graviton off a black hole,

$$\mathcal{C}_{\alpha\beta\mu\nu} = i \int d^4x e^{iq\cdot x} \langle B|\mathbb{T} \mathcal{T}_{\alpha\beta}(x)\mathcal{T}_{\mu\nu}(0)|B\rangle. \quad (2.14)$$

$\mathcal{C}_{\alpha\beta\mu\nu}$ exhibits the wanted time ordering. However, we still have to find the concrete representation of $\mathcal{A}_{\alpha\beta\mu\nu}$ in terms of the forward scattering amplitude. Therefore, we insert again a complete set of states in equation (2.14) leading to

$$\mathcal{C}_{\alpha\beta\mu\nu} = \sum_{B'} \frac{(2\pi)^3 \delta(\mathbf{P}' - \mathbf{P} - \mathbf{q})}{P'^0 - P^0 - q^0 - i\varepsilon} \langle B|\mathcal{T}_{\alpha\beta}|B'\rangle \langle B'|\mathcal{T}_{\mu\nu}(0)|B\rangle. \quad (2.15)$$

At this point, it is convenient to define the Abs function as

$$\text{Abs } \omega^{-1} \equiv [(\omega - i\varepsilon)^{-1} - (\omega + i\varepsilon)^{-1}]/(2i)$$

leading to $\text{Abs}(P'^0 - P^0 - q^0 - i\varepsilon)^{-1} = \pi\delta(P'^0 - P^0 - q^0)$. As the final result of this subsection it follows

$$\pi\mathcal{A}_{\alpha\beta\mu\nu}(B; q) = \text{Abs } \mathcal{C}_{\alpha\beta\mu\nu}(B; q). \quad (2.16)$$

Thus, we can always express the absorption tensor in terms of the time ordered forward Compton scattering amplitude in this way. Notice that this derivation is completely general, since we did not use any specifics about $|B\rangle$, $\mathcal{T}_{\alpha\beta}$ or GR in order to derive the result.

2.3 Operator Product Expansion of the Absorption Tensor \mathcal{A}

Having established the time-ordering for the energy-momentum operators, let us now discuss how we can extract the non-perturbative bound state information in this framework.

Interestingly, the method presented here is extremely general in the sense that we do not have to specify $|B\rangle$ in order to show that the correlator $\langle B|\mathbb{T} \mathcal{T}_{\alpha\beta}(x)\mathcal{T}_{\mu\nu}(0)|B\rangle$ occurring in (2.14) can be represented in terms of the occupation number of bound state constituents. As mentioned above, we only have to assume that $|B\rangle$ represents a bound state with some non-trivial substructure. In general, there is no reason why normal ordered products of constituents or in other words condensates should vanish in this state. These condensates contain all the non-perturbative physics leading to the confinement of the gravitons in the

black hole. In a concrete calculation it follows that normal ordered products occurring when we use Wick's theorem do not vanish when evaluated in the bound state. More explicitly, we can always represent the time ordered product of the constituent energy-momentum tensors in terms of the normal ordered bi-local operator $\mathcal{O}_{\mu\nu}(x, 0) \equiv : \partial_\mu h(x) \partial_\nu h(0) :$, where $h(x)$ represents the constituent field,

$$\text{T } \mathcal{T}_{\alpha\beta}(x) \mathcal{T}_{\mu\nu}(0) = \frac{1}{4} S_{\alpha\beta}^{\rho\sigma} S_{\mu\nu}^{\lambda\pi} C_{\sigma\lambda}(x) \mathcal{O}_{\rho\pi}(x, 0) .$$

The black hole state expectation value of $\mathcal{O}_{\rho\pi}(x, 0)$ contains all the non-perturbative bound state information we want to extract, while $C_{\alpha\beta}(x) \equiv 4 \langle 0 | \text{T} \partial_\alpha h(x) \partial_\beta h(0) | 0 \rangle$ denotes the correlation with respect to the perturbative vacuum, given as

$$C_{\alpha\beta}(x) = -\frac{2}{\pi^2} \frac{x^2 \eta_{\alpha\beta} - 4x_\alpha x_\beta}{(x^2)^3} . \quad (2.17)$$

In other words, this part simply corresponds to the perturbative propagation of the bound state constituent. To extract the bound state information encoded in $\mathcal{O}(x, 0)$, we simply expand it in terms of local operators. This is equivalent to employing a operator product expansion. In particular, we Laurent expand the corresponding propagator. Hence, the Taylor part of the series can be written as

$$h(x) = \exp(x \cdot \partial_z) h(z) |_{z=0} . \quad (2.18)$$

In this chapter we are solely interested in parton level results. Nevertheless, it is easy to introduce gauge interactions between the constituents if we use the covariant derivative instead of the partial derivative. However, using equation (2.18), we can express $\mathcal{O}_{\mu\nu}(x, 0)$ in terms of an infinite series,

$$\mathcal{O}_{\mu\nu}(x, 0) = \sum_{j=0}^{\infty} \frac{1}{j!} \mathcal{O}_{\mu\nu}^{[j]}(0) , \quad (2.19)$$

$$\mathcal{O}_{\mu\nu}^{[j]}(0) \equiv : (x \cdot \partial_z)^j \partial_\mu h(0) \partial_\nu h(0) : \quad (2.20)$$

Note that this procedure is analogous to the operator product expansion performed in DIS. To relate the local expansion operators to the forward scattering amplitude, we have to evaluate them in the black hole state,

$$\langle B | \mathcal{O}_{\mu\nu}^{[j]}(0) | B \rangle = \kappa (x_\alpha P^\alpha)^j \langle B | h(r) h(0) | B \rangle P_\mu P_\nu , \quad (2.21)$$

where κ denotes a combinatoric factor. Here a simple point-split regularisation has been employed ($r^2 \rightarrow 0$).

Clearly, the local operator on the right hand of (2.21) accounts for the occupation number density. In fact, this means that the forward scattering amplitude and correspondingly the absorption is directly related to a sum over the graviton occupation number in the black hole and its higher derivatives. Of course, this result is not surprising when we assume that the black hole has a microscopic substructure.

2.4 Analytic properties of the Forward Scattering Amplitude \mathcal{C}

Now let us directly relate the absorption tensor with the occupation number density using the analytic properties of the Compton scattering amplitude. As a first step, we employ the Ward-Takahashi identity corresponding to diffeomorphism invariance to determine the tensorial structure of the Compton amplitude $\mathcal{C}_{\alpha\beta\mu\nu}(q, P)$. It is fixed to be $\mathcal{C}_{\alpha\beta\mu\nu}(q, P) \sim \theta_{\alpha\beta\mu\nu}(q, P) \equiv \Pi_{\alpha\beta}^{ab} \Pi_{\mu\nu}^{mn} \eta_{bm} P_a P_n$ which, of course, makes the source conservation manifest. Secondly, we Laurent expand the non-perturbative operators $\mathcal{O}_{\mu\nu}(x, 0)$ to leading order up to $\mathcal{O}(q_\alpha P^\alpha / P^2)$. Thus, we arrive at

$$\mathcal{C}_{\alpha\beta\mu\nu}(q, P) = \langle B|h(r)h(0)|B\rangle \theta(q, P)_{\alpha\beta\mu\nu} \frac{-i}{2\pi^2} \sum_{j=-\infty}^{\infty} C_j(q) w^j. \quad (2.22)$$

Here, the coefficients C_j are calculable and turn out to be momentum independent. Furthermore, we introduce the expansion parameter $u \equiv -P^2/q^2 \gg 1$. This parameter is the gravitational analog of the inverse Bjorken scaling variable occurring in deep inelastic scattering experiments. However, the obvious difference between those parameters is related to asymptotic freedom. In contrast to QCD, we cannot consider the infinite momentum limit, since gravity becomes strongly coupled at Planckian scales. Nevertheless, the large black hole mass M_B provides us with a natural expansion parameter. More explicitly, for virtual momenta $-q^2 \ll M_B^2$ it is clear that $u = -P^2/q^2 = -M_B^2/q^2$ becomes an extremely good expansion parameter. Note that it is still possible to resolve the black hole substructure as long as $-q^2 > 1/r_g$.

Fixing the virtual momentum $q^2 = -Q^2$, $\mathcal{C}_{\alpha\beta\mu\nu}$ exhibits similar to hadrons in QCD a discontinuity at

$$u_* = \frac{M_B}{2(M'_B - M_B)} \left(1 - \frac{M_B'^2 - M_B^2}{Q^2} \right) \gg 1. \quad (2.23)$$

Correspondingly, \mathcal{C} has a single, isolated pole at $u_* \gg 1$. In contrast to QCD, no branch cut occurs to leading order in M_B . This is simply reminiscent of the fact that we work in the limit $M'_B/M_B - 1 \approx 0$. Obviously, when we do not suppress these $1/N$ -type effects, we obtain a continuum of black holes with slightly different quantum numbers leading to the usual branch cut.

On the one hand, we are interested in the parameter space $u > 1$, since $u \in [-1, 1]$ is the unphysical region (see figure 2.2). On the other hand, the radius of convergence covers only the region $u \in [-1, 1]$. Thus, we use the analytic properties of the scattering amplitude to directly project onto all the different Laurent-coefficients by a contour deformation of an intergration path in the complex u plane which, in particular, should enclose the discontinuity points $-u_*$, u_* . It follows

$$\int_0^1 d\zeta \zeta^{k-2} \mathcal{A}_{\alpha\beta\mu\nu}(q, P, \zeta) = \frac{C_{k-1}}{4\pi^2} \langle B|h(r)h(0)|B\rangle \theta_{\alpha\beta\mu\nu}(q, P) \quad (2.24)$$

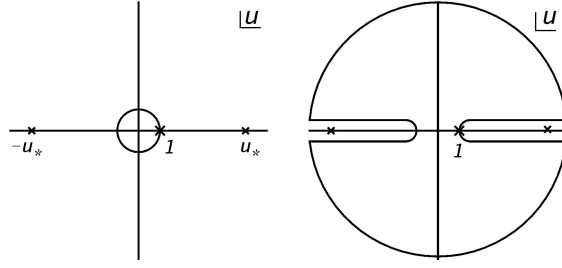


Figure 2.2: The integration contour in the complex u -plane is depicted. While the left figure shows the integration contour given by the radius of convergence, the right figure displays the physical parameter u -region ($P^2 > Q^2$). Sending the radius of the circle to infinity, we can relate the physical and the unphysical region by performing a contour deformation.

with $\zeta \equiv 1/u$ denoting the graviton virtuality relative to the black hole target mass.

In other words, all moments of the absorption tensor with respect to ζ are directly proportional to the constituent distribution inside the black hole. This implies that the cross-section satisfies

$$d\sigma/d^3k' \propto \langle B|h(r)h(0)|B \rangle, \quad (2.25)$$

which is exactly the desired result of this chapter. It simply means that we can determine the black hole bound state information encoded in the constituent occupation number $\langle B|h(r)h(0)|B \rangle$ by measuring the cross-section in high energy scatterings on the black hole. Note that this result is, of course, not surprising, but seems to be completely generic for all bound states.

2.5 Conclusions and Summary

Finally, let us draw a conclusion. This chapter was dedicated to give a concrete example of embedding a microscopically resolved black hole in a high energy scattering process. The starting assumption of this chapter was to assume that QFT is fundamental everywhere such that a unitary time evolution is always granted. As a consequence, it inevitably follows that we can extract information about the black interior when we consider the scattering regime $-q^2 > 1/r_g^{-2}$. As we would expect by default, the bound state information given by the occupation number directly appears in scattering experiments. In particular, we adopted the DIS techniques of QCD to high energy scatterings on black holes. For $-q^2 < M_p^2$, we do not need to introduce new physics to obtain these results. If it is possible in the future to perform such high energy scatterings on large black holes, we could in principle obtain information about the black hole constituent occupation number $\langle B|h(r)h(0)|B \rangle$ from the cross-section. Note that the results obtained in this chapter are independent of a special choice of bound state construction.

Chapter 3

Coherent State Picture for Solitons

In section 1.3 we reviewed the method of Dvali and Gomez [4] to represent black holes in terms of bound states of gravitons. Following the philosophy that nature is fundamentally quantum, one can ask the question if it is possible to apply a bound state description to other classical objects in different theories. The answer is, of course, that there is no reason why it should be unique to gravity that we should represent classical entities as quantum bound states. In fact, we know of many examples like the proton, where experimental results suggested that a bound state description should be employed.

In this chapter we want to address solitons from the bound state perspective. In particular, we want to present a concrete technique to represent solitons as a quantum bound state of microscopic degrees of freedom. To achieve this task, we will present a method to represent the soliton as a quantum coherent state.

As already mentioned in the introduction, coherent states are a quite effective method to describe laser beams in quantum terms. In some sense, coherent states are the most classical quantum states, since coherent state expectation values of one point functions are equal to the classical field values. Therefore, Barnich [87] used coherent states to describe the classical Coulomb field of an electric charge in terms of quantum constituents. Naturally, these constituents were given as longitudinally polarized photons. Since solitons and instantons behave classical as well, it is a logical perspective that we can represent them using coherent states. We will discuss this in more detail below.

Although the philosophy is similar to the black hole case, one can still argue that we are not forced to implement a constituent quantum picture for solitons. In contrast to the black hole, we do not obtain obvious inconsistencies (like the information paradox) by maintaining a classical soliton. Therefore, one could in principle ask why it should be necessary to represent solitons as bound states. However, it seems unnatural that this is the case, since all the experiments imply that nature is fundamentally quantum.

Thus, to summarize the purpose of this chapter will be the following. We want to represent the classical soliton solution of various examples in terms of the proper quantum degrees of freedom. In other words, instead of the semi-classical description of solitons where the solitonic background is classical, we want to present a full quantum picture for the soliton. Of course, the model has to satisfy certain requirements. Namely, by

consistency we should be able to obtain all the classical results at least to leading order.

Let us briefly clarify, semi-classicality in this context. As for the black model discussed in section 1.3, we can distinguish two different kinds of quantum contributions. The usual semi-classical treatment only considers \hbar quantum corrections on top of a fixed, classical background. In this chapter we are interested in a full quantum picture of the background which in particular takes quantum mechanical back-reactions on the soliton into account. These effects usually are of the order \hbar/N , where N is the total number of solitonic constituents.

In the first section of this chapter, we apply the constituent picture to different types of solitons. Then we discuss supersymmetric solitons from this point of view in section 3.2.

3.1 Corpuscular Soliton

Before starting to discuss the soliton, let us refer to the original work [16] on which this section is based.

The basic idea is, as it was extensively mentioned before, to write down a framework to represent the classical solitons as a coherent state of N constituents. These constituents should not be confused with usual asymptotic particles. On the contrary, they exist only confined in the soliton. Obviously, the constituents are interacting in order for them to stay confined in the soliton. The resulting potential leads to a dispersion relation which is, in general, different from a free one. To make this manifest, we will refer to the constituents as corpuscles. Note that the corpuscles can never be viewed as free asymptotic particles. We will further clarify the nature of the corpuscles in section 3.1.3.

The only way we can usually make sense of a particle in physics is if it is weakly coupled. For instance, in QCD quarks are only useful degrees of freedom to describe physics when they are in the weak regime. In the strong regime (large distances), hadrons are the sensible object. Correspondingly, the coherent state picture for solitons makes only sense in the regime where the corpuscles are individually weakly coupled. Additionally, we have to mention that usually the occupation number of bound states scales like the inverse relevant dimensionless coupling of the constituents. Subsequently, the weak coupling regime automatically corresponds to a large occupation number of corpuscles meaning that solitons become fundamental in the strong coupling regime because $N \sim 1$. According to [4], in the black hole case we can consider bound states of arbitrary size¹, since due to the derivative self coupling of gravitons the individual energy of the constituents enters in the dimensionless coupling. On the contrary, the occupation number for solitons is fixed by the parameters of the theory.

As a remark, let us mention that the resolution into bosonic corpuscles should not be confused with the well known phenomenon of Sine-Gordon solitons which can be described in terms of fermions. In [88, 89] it was shown that there is a one-to-one correspondence between strongly coupled fermions in the Thirring model and usual Sine-Gordon solitons

¹Of course, this is only true as long as $M_B > M_P$.

[88, 89] when we identify the strongly coupled fermion number with the topological charge of the soliton.

Let us briefly comment on the different aspects we want to discuss in this section. First of all, we will show that we obtain consistently all classical results for various types of solitons in this new framework. Secondly, we want to give a new understanding for the topological charge of topological solitons in the corpuscular picture. Usually, the topological charge is defined purely classical. In particular, it is always conserved and cannot decay via any quantum process. The coherent state formalism allows us to distinguish between two types of quanta. Since we can determine the momentum distribution of the quanta, we can distinguish quanta which contribute to the mass of the soliton and quanta which are solely responsible for the topological charge of the soliton. The first type occurs in every bound state we know of. Their momentum distribution has a maximum at the inverse length scale we can attribute to the bound state. However, the corpuscles forming the topological charge are a completely new concept in the soliton coherent state description. It is possible to express the quantum mechanically resolved soliton as a convolution of the topological and the energetical sector. To illustrate this further, we can denote this statement as

$$\text{soliton} = (\text{topology}) \times (\text{energy}). \quad (3.1)$$

Similarly, we can express the soliton state $|sol\rangle$ as a tensor product of the energetic $|E\rangle$ and the topological state $|t\rangle$ leading to

$$|sol\rangle = |t\rangle \otimes |E\rangle. \quad (3.2)$$

Of course, such a split becomes trivial for the non-topological soliton we discuss in section 3.1.1 simply because their topological sector is trivial.

To really identify the topological quanta of the soliton it is helpful to first compare the topological and the non-topological soliton. Note that the coherent state philosophy allows to easily extract the occupation number in each mode N_k of the constituents by using Fourier techniques. Using the knowledge about N_k , we can now compare both. The crucial difference is the fact that for the topological soliton the occupation number of the infinite wavelength quanta N_0 diverges due to a $1/k$ -type pole. However, these quanta do not contribute to the mass of the soliton.

To understand this behavior, we need to simply remind us of the fact that topology is a feature usually attributed to the boundary of the theory. Consequently, only the extremely long wavelength modes can account for topological properties, since exactly these modes can contain asymptotical information. In this sense, we can view topology as a Bose sea of zero momentum modes.

Quantum mechanically, it is exactly this divergence of the total occupation number N which reveals why the topological charge is conserved. Correspondingly, the topological soliton cannot decay into the topologically trivial vacuum $|0\rangle$. To understand this more properly, let us take a closer look at the corresponding decay amplitude

$$\langle sol|0\rangle \sim e^{-N}. \quad (3.3)$$

Here we used some coherent state properties we will explain below. Since $N \rightarrow \infty$, in particular due to the N_0 modes, this amplitude vanishes in the topological case. On the contrary, the non-topological soliton is not protected by such a divergence such that it is unstable. This phenomenon is usually known as false vacuum decay.

In the first subsections we use the coherent state picture to describe non-topological solitons and topological solitons. Then we will make the topology-energy split manifest. Finally we address the soliton-anti-soliton interaction. Notice that we will not be interested in computing $1/N$ type quantum corrections in this section, but we will consider them when we discuss the corpuscular supersymmetry breaking in section 3.2.

3.1.1 Coherent State Picture of the Non-Topological Soliton

We start our discussion on the resolution of solitons in terms of corpuscles with the non-topological soliton. The analysis presented here will be similar to the original work [16]. The main purpose of this subsection is to show how classical results emerge in the quantum treatment.

We will consider here the non-topological soliton in 1+1 dimensions. The corresponding model was already introduced in section 1.4.1. As already mentioned there, we consider the Lagrangian

$$\mathcal{L} = (\partial_\mu \phi)^2 - m^2 \phi^2 + g^2 \phi^4, \quad (3.4)$$

where for the mass and the coupling holds m^2 and $g^2 > 0$, respectively. As mentioned in section 1.4.1, this theory has a classical stable vacuum $\phi = 0$ at $x = \pm\infty$, while the solution

$$\phi_{non-top}(x) = \frac{m}{\sqrt{2g}} \text{sech}(mx) \quad (3.5)$$

describes the motion of the field from the vacuum value to the unstable value $\phi = m/\sqrt{2g}$ and back. Of course, the energy of this soliton can be computed when we use (3.4) and (3.5),

$$E_{non-top} = \int dx [(\partial_x \phi_{non-top}(x))^2 + m^2 \phi_{non-top}^2 - g^2 \phi_{non-top}^4] = \frac{2m^3}{3g^2}. \quad (3.6)$$

Let us now briefly discuss the semi-classical picture to make the difference to the full quantum corpuscular treatment of solitons manifest. Usually, one introduces small quantum fluctuations around this background. We denote the corresponding annihilation and creation operators in momentum mode k by \hat{b}_k and \hat{b}_k^\dagger . Notice that the non-trivial soliton background state $|sol\rangle$ is the vacuum for these operators,

$$\hat{b}_k |sol\rangle = 0. \quad (3.7)$$

This treatment allows to compute \hbar -type quantum corrections when we evaluate the corresponding loops, but it does not take back-reactions on the soliton background into account.

The crucial part of this thesis is that we want to do something completely different. We want to understand the background state $|sol\rangle$ itself as a bound state made out of a

totally new type of constituents or corpuscles. In other words, we consider a different type of quantum effect related to the quantum nature of the background. Of course, we could always consider the usual semi-classical treatment on top of the constituent framework. As already mentioned, we refer to these quanta as corpuscles and denote their creation and annihilation algebra as \hat{a}_k and \hat{a}_k^\dagger . These corpuscles behave totally different than the usual particles. In contrast to usual quanta as are given by \hat{b}_k and \hat{b}_k^\dagger , corpuscles do not exist as asymptotic S -matrix states. Furthermore, we can distinguish both classes of quanta by their vacuum

$$\hat{a}_k|0\rangle = 0 \quad (3.8)$$

$$\hat{b}_k|sol\rangle = 0, \quad (3.9)$$

where $|0\rangle$ is the true Minkowski vacuum. In principle, these corpuscles should be governed by a fundamental Hamiltonian such that solitons emerge from the corresponding low energy effective theory. However, since we are not powerful enough to determine the true microscopic theory, we will use a different approach.

The basic idea is that the soliton bound state $|sol\rangle$ can be represented as a coherent state of these corpuscles. This seems natural because the coherent state is the most classical quantum state. Every other quantum state would simply exhibit even more severe quantum effects than the ones we are uncovering when using the coherent state formalism. First of all, we have to identify the Fock space which the \hat{a}_k and \hat{a}_k^\dagger span. For that purpose, we Fourier Transform the classical field,

$$\phi_{non-top}(x) = \sqrt{l} \int \frac{dk}{\sqrt{4\pi|k|}} (e^{ikx} \alpha_k + e^{-ikx} \alpha_k^*), \quad (3.10)$$

where the α_k and α_k^* are the corresponding Fourier coefficients depending on momentum k and $2\pi l$ is the regularized volume of space. These coefficients are just complex functions given by

$$\alpha_k^* \alpha_k = \pi \frac{|k|}{2l} \frac{1}{g^2} \operatorname{sech}^2 \left(\frac{\pi k}{2m} \right). \quad (3.11)$$

Correspondingly, we can reexpress the mass of the soliton given in (3.6) simply in momentum space

$$E_{non-top} = \int_k |k| \alpha_k^* \alpha_k, \quad (3.12)$$

where we introduced $\int_k \equiv l \int dk$.

To implement the corpuscular resolution, we promote the classical Fourier coefficients to the corpuscular annihilation and creation operators $\hat{a}_k, \hat{a}_k^\dagger$. These still fulfill the usual creation-annihilation algebra

$$[\hat{a}_k, \hat{a}_{k'}^\dagger] = \frac{1}{l} \delta(k - k'), \quad (3.13)$$

for momenta k, k' . Consistency requires that we have to obtain the classical results to leading order. For that purpose, consider the field operator resulting from promoting the Fourier coefficients

$$\hat{\phi}(x) = \sqrt{l} \int \frac{dk}{\sqrt{4\pi|k|}} (e^{ikx} \hat{a}_k + e^{-ikx} \hat{a}_k^\dagger). \quad (3.14)$$

Let us stress at this point that this is not a free wave expansion. In particular, since we simply Fourier transformed the classical result (3.5) which is time independent, no time component is occurring in the argument of the exponential functions. This is, of course, only possible because these corpuscles can only exist in the presence of a bound state, but not as asymptotic S -matrix states pointing out that the corpuscles are interaction eigenstates. Nevertheless, the dispersion to leading order is $\omega_k = |k|$. We will comment on this below. Matching with the classical solution implies the condition

$$\langle sol | \hat{\phi}(x) | sol \rangle = \phi_{non-top}(x). \quad (3.15)$$

Note that this is a matching condition solely on the level of the one point function. Correspondingly, only higher n -point functions can lead to corpuscular ($1/N$ type) corrections. Obviously, this implies the condition

$$\langle sol | \hat{a}_k | sol \rangle = \alpha_k \quad (3.16)$$

for the corpuscular Fock state operators. Representing the soliton in terms of coherent states constructed from the corpuscular annihilation and creation operators $\hat{a}_k, \hat{a}_k^\dagger$, the situation is extremely simplified because the coherent state is an eigenvector for the annihilation operator.

Having established a way to achieve the classical results from the quantum perspective, we can now construct the coherent state $|sol\rangle$. Since we need an eigenvector for each \hat{a}_k , the total coherent state can be expressed as a product state over coherent states $|\alpha_k\rangle$ each satisfying $\hat{a}_k |\alpha_k\rangle = \alpha_k |\alpha_k\rangle$,

$$|sol\rangle = \prod_{\otimes k} |\alpha_k\rangle. \quad (3.17)$$

The expression for the $|\alpha_k\rangle$ is well known in the literature [14]:

$$|\alpha_k\rangle = e^{-\frac{1}{2}|\alpha_k|^2} e^{\alpha_k \hat{a}_k^\dagger} |0\rangle = e^{-\frac{1}{2}|\alpha_k|^2} \sum_{n_k=0}^{\infty} \frac{\alpha_k^{n_k}}{\sqrt{n_k!}} |n_k\rangle. \quad (3.18)$$

Here the $|n_k\rangle$ are the number eigenstates in a given mode, where n_k is the corresponding occupation number. In particular, this means that

$$|n_k\rangle \sim (\hat{a}_k^\dagger)^{n_k} |0\rangle. \quad (3.19)$$

As mentioned above, we want to understand the soliton as a coherent bound state of N constituents. Therefore, we have to answer the question where N arises in our framework. For that purpose, note that we normalized the Fourier transform in equation (3.10) in such a way that the Fourier coefficients are dimensionless. Correspondingly, the creation and annihilation operators are dimensionless as well. We have to normalize the operators with the dispersion relation of the corresponding constituents. Otherwise, we would not get the desired creation and annihilation algebra given in equation (3.13). Here the dispersion relation is to leading order given as

$$\omega(k) = |k|. \quad (3.20)$$

We will come back to the implications of the dispersion relation in a moment. Since the operators are dimensionless, we can explicitly interpret their expectation values as occupation numbers N_k in a momentum mode k for the coherent state $|\alpha_k\rangle$. This simply amounts to

$$N_k \equiv \langle sol | \hat{a}_k^\dagger \hat{a}_k | sol \rangle = \alpha_k^* \alpha_k. \quad (3.21)$$

Using this and equation (3.11), we notice that the $k \lesssim m$ modes are mostly occupied. These are exactly the modes which give the main contribution to the energy as (3.12) suggests. Hence, the dominating modes are exactly given by the size of the soliton as one would expect for any bound state.

Now everything is in place to compute the total number of constituents N . For that purpose, we simply have to integrate over all modes

$$N \equiv \int_k N_k = \int_k \alpha_k^* \alpha_k. \quad (3.22)$$

Let us comment on the dispersion relation and the special meaning of the Fock space operators in this case. The $\hat{a}_k^\dagger, \hat{a}_k$ should not be confused with creation and annihilation operators of asymptotic propagating quanta of the theory as, for instance, the $\hat{b}_k^\dagger, \hat{b}_k$ operators introduced above. Rather, they span a Fock space for a totally new type of quanta. In particular, this statement is reflected in the dispersion relation of the quanta.

Naively one could interpret the dispersion in equation (3.20) as the dispersion of a free asymptotic particle, but the constituents are strongly interacting collectively. In fact, classically the potential term is of the same order as the kinetic term due to the special form of the solution. Correspondingly, the total classical energy of the profile is given as twice its kinetical energy. Thus, to leading order in $1/N$, we can represent the energy of the soliton as

$$E_{non-top} = \int_k |k| N_k = \frac{2m^3}{3g^2}. \quad (3.23)$$

Note that in the full quantum treatment the dispersion gets corrected. In particular, the equivalence of kinetical and potential term only holds on the classical level. The higher order operators in the potential term

$$-m^2 \hat{\phi}^2 + g^2 \hat{\phi}^4 \quad (3.24)$$

automatically lead to $1/N$ -type corrections to the dispersion relation. In this subsection we neglect those effects, since we want to show how the classical results are obtained in the new framework to leading order. How to compute corrections is shown explicitly in section 3.2.

To conclude this subsection, we evaluate the stability of the non-topological soliton in the quantum picture. For that purpose, we compute the total occupation number using (3.11) and (3.22),

$$N = \frac{m^2}{g^2} \left(4 \frac{\log(2)}{\pi} \right). \quad (3.25)$$

Notice that this finiteness of the total occupation number (3.25) explicitly reflects the instability of the vacuum $\phi = 0$. As presented in [68, 69], the vacuum $\phi = 0$ is not the true vacuum, but can decay. This phenomenon occurs, since this kind of soliton has no conserved topological charge to protect it. The decay process occurs via bubble nucleation. As the classical vacuum is a zero energy state, the critical bubble is a zero energy configuration interpolating between $\phi = 0$ and $\phi > m/g$.

We can obtain the same result in our formalism and it is directly connected to the finiteness of the total occupation number N . In general, the overlap of a coherent state $|sol\rangle$ with occupation number N and the Minkowski vacuum is given by

$$\langle 0|sol\rangle \propto e^{-N/2}. \quad (3.26)$$

This can easily be derived from our coherent state representation (3.17), but is also known from the original literature [14]. Combining (3.25) and (3.26) while restoring \hbar , we can express the overlap in terms of the parameters of the theory

$$\langle 0|sol\rangle = e^{-\frac{(\frac{\log(2)}{\pi})m^2}{\hbar g^2}}. \quad (3.27)$$

This is clearly not suppressed such that such a decay, in general, is possible. Note, however, that the overlap does, in fact, vanish in the classical limit, where we send $\hbar \rightarrow 0$ while keeping the mass and the coupling finite.

This sheds a new light on the bubble nucleation process in the classical picture. From the quantum mechanical point of view, the false vacuum decay appears due to intermediate coherent states which have non-zero overlap with the classical vacuum. This simply corresponds to the fact that coherent states are not energy eigenstates. Only for the classical $N \rightarrow \infty$ limit we recover an energy eigenstate such that the overlap becomes zero again.

In the next subsection we shall discuss the topological soliton which is, on the contrary, stabilized by its topological charge.

3.1.2 Coherent State Picture of the Topological Soliton

As already advertised, we want to discuss the topological soliton in this subsection. Like in the non-topological case, we want to recover the classical results from the quantum picture.

Therefore, we consider only leading order effects in the first part of the section. In section 3.1.4 we will discuss quantum implications and the topology-energy split. Note that this section is closely related to the original work [16].

The Lagrangian of the classical topological soliton is given as in section 1.4.1,

$$\mathcal{L} = (\partial_\mu \phi)^2 - g^2(\phi^2 - m^2/g^2)^2. \quad (3.28)$$

The main difference to the non-topological case is the non-trivial vacuum structure of the theory at hand. In particular, ϕ acquires two different vacuum expectation values $\phi = \pm m/g$ at $x \rightarrow \pm\infty$. The corresponding solution is known as 'kink' and interpolates between both vacua

$$\phi_{top}(x) = \pm \frac{m}{g} \tanh(xm). \quad (3.29)$$

Essentially, the philosophy we want to follow is the same as in section 3.1.1. We want to understand the classical profile as an emergent effect of a resolved quantum bound state. For that purpose, we assume that the topological soliton can be represented as a coherent state $|sol\rangle$ of corpuscles.

In accordance with the non-topological case, we claim that there exists a corpuscular Fock space spanned by \hat{a}_k and \hat{a}_k^\dagger satisfying the same algebra as in equation (3.13). To obtain the correct classical limit, their expectation values are again simply identified with the Fourier coefficients of the classical profile. Thus, we can define the occupation number in each mode as

$$N_k = \langle sol | \hat{a}_k^\dagger \hat{a}_k | sol \rangle = \alpha_k^* \alpha_k = \pi \frac{|k|}{l} \frac{1}{g^2} \text{csch}^2 \left(\frac{\pi k}{2m} \right). \quad (3.30)$$

Here we can see that the dispersion relation is again given as $\omega = |k|$. We will comment on this in the next subsection.

As for the non-topological case, we can determine the energy of the topological soliton by integrating over the occupation number times the energy in each mode

$$E_{top} = \int_k |k| N_k = \frac{8m^3}{3g^2}, \quad (3.31)$$

which is the well known classical result. Since we used the property that the potential term is classically the same as the kinetical term, this is an approximation up to leading order in $1/N$.

3.1.3 Corpuscular Algebra vs. Asymptotic Algebra

As already mentioned, the corpuscles cannot exist as asymptotic S -matrix states. In particular, they are interaction eigenstates. To understand this more properly, let us consider for the moment usual asymptotic S -matrix particles with Fock state operators $\hat{b}_k, \hat{b}_k^\dagger$. The time evolution of these quanta is governed by the free Hamiltonian for these particles with

some interaction potential $V(\hat{b}_k, \hat{b}_k^\dagger)$ added. Correspondingly, the total Hamiltonian is given as

$$\hat{H}_S(\hat{b}_k, \hat{b}_k^\dagger) = \int dk \omega_{free} \hat{b}_k^\dagger \hat{b}_k + V(\hat{b}_k, \hat{b}_k^\dagger), \quad (3.32)$$

where ω_{free} is the free dispersion relation of these quanta. As long as the interaction terms are small we can use usual perturbation theory to compute amplitudes for the asymptotic quanta. Note that \hat{H}_S is diagonal on the perturbative vacuum.

Now let us consider the corpuscles from this point of view. Classically, the topological soliton corresponds to the critical solution of minimized energy. This simply means that the soliton satisfies the BPS condition

$$\partial_x \phi_{top} = g \left(\phi_{top} - \frac{m}{g} \right)^2. \quad (3.33)$$

Of course, this is far from a slight correction to the free propagation, since the potential term and the kinetical term are of the same order. Non-perturbative physics dominate the solitonic bound state. Accordingly, the Hamiltonian for the asymptotic quanta \hat{H}_S is not diagonal on the soliton state.

Therefore, we introduce the corpuscles $\hat{a}_k, \hat{a}_k^\dagger$ as a new type of non-asymptotic quanta to circumvent these problems. Using these corpuscles, we can build up the coherent soliton state in such a way that we obtain the classical results by matching the one-point function. Correspondingly, these quanta have nothing in common with the S -matrix objects.

On the contrary, they are much more similar to quarks which are the constituents of baryons in QCD. The corpuscles can only exist in a bound state and have a typical wavelength given by the size of the soliton (QCD scale for the Baryon). Using the matching condition

$$\langle sol | \hat{\phi}(x) | sol \rangle = \phi_{top}(x). \quad (3.34)$$

we can construct the coherent soliton state and express the soliton energy in terms of the corpuscles

$$E = \int_k \omega(k) \langle sol | \hat{a}_k^\dagger \hat{a}_k | sol \rangle, \quad (3.35)$$

where $\omega(k) = |k|$ is the corpuscular dispersion. This dispersion looks like the free one of the S -matrix quanta only because the BPS condition basically allows to diagonalize the Hamiltonian classically. However, this is only true to leading order. If we want to consider the true quantum theory, we must not use the classical BPS condition to diagonalize the Hamiltonian, but we have to consider the corpuscular Hamiltonian

$$\hat{H}_{corp} = \frac{1}{2} \int_k \omega(k) \hat{a}_k^\dagger \hat{a}_k + V(\hat{\phi}), \quad (3.36)$$

where $V(\hat{\phi})$ denotes the potential for the scalar field. From this form of the Hamiltonian, we can now compute $1/N$ -type quantum corrections by simply considering commutation relations. This will be done explicitly in section 3.2. However, it is important to stress

that, in contrast to the asymptotic Hamiltonian, the corpuscular Hamiltonian is diagonal on the soliton state to leading order in $1/N$

$$\langle sol | \hat{H}_{corp} | sol \rangle = \int_k \omega(k) \langle sol | \hat{a}_k^\dagger \hat{a}_k | sol \rangle + \mathcal{O}(1/N). \quad (3.37)$$

Of course, we can relate the corpuscular quanta with the S -matrix quanta, since we know that the energies in both sets up have to match. This means that the expectation value of the corpuscular and S -matrix Hamiltonian has to fulfill

$$\langle sol | \hat{H}_S(\hat{b}_k, \hat{b}_k^\dagger) | sol \rangle = \langle sol | \hat{H}_{corp}(\hat{a}_k, \hat{a}_k^\dagger) | sol \rangle. \quad (3.38)$$

To solve this for an explicit relation between $\hat{a}_k, \hat{a}_k^\dagger$ and $\hat{b}_k, \hat{b}_k^\dagger$ is an extremely hard task. Additionally, notice that the corpuscular vacuum is different from the S -matrix vacuum. This is reminiscent of the fact that both Hamiltonians are diagonal on different states.

As a final remark, let us mention that the dispersion relation occurring for the corpuscles is non-trivial when we take corpuscular $1/N$ corrections into account. The corpuscles can never be viewed as free particles as they are interaction eigenstates. In fact, the corpuscles have zero frequencies. This property is usually attributed to tachyons with momentum equal to the absolute value of their mass corresponding to an infinite tachyon speed.

Since tachyons cannot exist as asymptotic states, but only in certain bound states, it makes totally sense to view the corpuscles in such a way. However, note that this is only a way to interpret the soliton constituents which does not change any physically measurable result.

3.1.4 Topology-Energy decomposition of Solitons

In the corpuscular approach, it is possible to get a completely new understanding of the emergence of energy and topology of the soliton. To make this statement manifest, we compute the total occupation number N of the topological soliton,

$$N = \int_{k_0} dk N_k \sim -\log(k_0)|_{k_0 \rightarrow 0} \rightarrow \infty. \quad (3.39)$$

Naively, one could think that this divergence tells us that the quantum approach makes no sense in this case. To clarify this, let us investigate why this divergence arises. The occurrence of the divergence is related to the non-trivial topological charge of the soliton. Notice that the charge is associated with the boundary properties of the theory. In total accordance, this divergence occurs due to a $1/k$ -type singularity in the occupation number N_k . Clearly, only these infinite wavelength modes can reach the boundary as exactly these modes can be associated with the topological charge.

Since it is the crucial point of this section, let us be even more explicit. We know that the non-trivial vacuum structure at $x \rightarrow \pm\infty$ is responsible for the topology. Therefore, only the infinite wavelength modes $k = 0$ can account for this effect.

One could ask, why there is an infinite number of zero momentum corpuscles responsible for the creation of the topology of the solution, but this is even a necessary condition due to the fact that the topological charge is conserved. No quantum process can change an infinite occupation number in a measurable way. Consequently, the charge stays untouched with respect to quantum fluctuations.

Now we can understand why the topological soliton is stable and cannot decay via bubble nucleation as the non-topological soliton. The amplitude for a decay to the Minkowski vacuum is given as

$$\langle 0|sol\rangle \propto e^{-N/\hbar} = e^{-\frac{1}{\hbar}\infty}, \quad (3.40)$$

where we used equations (3.26) and (3.39). The divergence is, in some sense, the quantum mechanical manifestation of the stability of the topological soliton. As we would expect, the amplitude even vanishes for the non-topological soliton (finite N) in the purely classical regime $\hbar \rightarrow 0$.

These results naturally lead to the question how the classical energy can be finite when the number of corpuscles diverges. The answer is simply that the $1/k$ -pole is canceled, since each corpuscle contributes an energy of order k . Most of the energy in equation (3.31) is contributed by the quanta with wavelength of the order $1/m$ ($N_m \sim \frac{m^2}{\hbar g^2}$), while the zero momentum modes do not contribute at all to the energy. Correspondingly, although the total number of quanta N diverges, non vanishing quantum processes affecting the energy exist, since the local occupation number of quanta contributing to the energy is finite.

Due to this observation, it makes totally sense to make the split of quanta contributing to the energy and the topology manifest. For that purpose, we can represent the soliton as the convolution of an energy and a topology profile

$$\text{soliton} = (\text{ topology }) \star (\text{ energy }) \quad .$$

One could ask why we use a convolution to connect both profiles. The reason is connected to the method we use to quantize the theory. The occupation number N_k is simply given by the squared Fourier coefficient of the classical profile. To represent the soliton profile as a topological and an energy profile, we thus use the fundamental theorem of convolution.

In particular, we can split the soliton state in a part which is the eigenvector of the annihilation operator accounting for energetical quanta $|E\rangle$ and its topological counterpart $|t\rangle$

$$|sol\rangle = |t\rangle \otimes |E\rangle.$$

Let us now split the kink soliton profile (3.29) in two parts. First of all, we identify the sign function with the property

$$\text{sign}(x) \star f(x) = +\frac{1}{2} \int_{-\infty}^x f(x') dx' - \frac{1}{2} \int_x^{\infty} f(x') dx', \quad (3.41)$$

as being responsible for the topology. We have two reasons for this claim. First, it accounts for the right topology in configuration space. Namely, $\phi = \pm m/g$ at $x \rightarrow \pm\infty$. Secondly,

when we go to Fourier space it exhibits a $1/k$ -pole which is responsible for the topology. Hence, we can represent the classical soliton profile as

$$\phi_{top}(x) = \frac{m}{g} \left(\text{sign} \star \text{sech}^2 \right) (mx). \quad (3.42)$$

Here the sech^2 function corresponds to the energy part of the profile. At this point, we can make an intriguing observation. The part of the profile purely contributing to the energy of the topological soliton is equivalent to the total profile of the non-topological profile squared.

In order to use the convolution theorem in full glory, we define the Fourier transform of the scalar soliton field given in (3.29) in terms of dimensionless integrals

$$\phi_{top}(mx) = \frac{1}{2} \int \frac{d(\frac{k}{m})}{\sqrt{4\pi(\frac{k}{m})}} \left(\alpha_k e^{i(\frac{k}{m})xm} + \text{h.c.} \right). \quad (3.43)$$

To make the split explicit, we express α_k as

$$\alpha_k = t_k(k/m) c_k(k/m), \quad (3.44)$$

where the t_k and the c_k are the Fourier coefficients of the the sign profile and the energetic profile, respectively. These are given as

$$t_k = \frac{i}{\sqrt{k}}, \quad (3.45)$$

and

$$c_k = \sqrt{\pi m} \frac{k}{g} \text{csch} \left(\frac{\pi k}{2m} \right) \quad (3.46)$$

when we normalize them properly. Let us discuss the behavior of these functions. We can make the observation that the t_k exhibit a $1/k$ -type pole which we associated to the topology from the quantum point of view.

The c_k do not possess such a pole, but they account exactly for the total energy of the profile. Namely, the $k \sim m$ modes which have a wavelength of the order of the extension of the profile are dominant in this expression. Typically, this is a usual behavior of bound state constituents. For instance, according to [4] the occupation number of gravitons in the black hole has its dominant contribution from quanta of wavelength given by the Schwarzschild radius.

Following our standard procedure, we want to view these coefficients as expectation values of the corresponding creation and annihilation operators $\hat{t}_k^\dagger, \hat{t}_k$ and $\hat{c}_k^\dagger, \hat{c}_k$ evaluated in the states $|t\rangle$ and $|E\rangle$, respectively. Consequently, they satisfy the eigenvalue equations

$$\hat{c}_k |c_k\rangle = c_k |c_k\rangle \quad (3.47)$$

and

$$\hat{t}_k |t\rangle = t_k |t\rangle. \quad (3.48)$$

In order to establish the quantum framework properly, the operators have to satisfy the commutation algebra

$$\begin{aligned} [\hat{t}_k, \hat{t}_{k'}^\dagger] &= \delta(k - k') \\ [\hat{c}_k, \hat{c}_{k'}^\dagger] &= m^2 \delta(k - k'). \end{aligned}$$

Notice that both operators act on different Fock spaces. Correspondingly, they create two different sets of states $|t_k\rangle$ and $|c_k\rangle$. We can compute them simply by using equation (3.17) and substitute \hat{a}_k^\dagger for $\hat{t}_{k'}^\dagger$ and $\hat{c}_{k'}^\dagger$, respectively. The corresponding product states can be identified with $|t\rangle$ and $|E\rangle$,

$$|t\rangle \equiv \prod_k |t_k\rangle, \quad (3.49)$$

$$|E\rangle \equiv \prod_k |c_k\rangle. \quad (3.50)$$

Let us consider the overlap between the soliton state and the Minkowski vacuum

$$|\langle 0|sol\rangle|^2 = e^{-\int dk |\alpha_k|^2}. \quad (3.51)$$

Now we can use the split and try to evaluate the amplitude simply for the topological part $|t\rangle$ of the soliton state. Accordingly, we find simply

$$|\langle 0|t\rangle|^2 = e^{-\int dk t_k^* t_k} = e^{-\int dk/|k|} = 0. \quad (3.52)$$

Indeed, $|t\rangle$ correctly accounts for the topological features of the soliton. Any other state with a different topological coherent state $|t'\rangle$ will have a zero overlap with $|t\rangle$. Therefore, we can always view the vacuum of a topological Hilbert space as a Bose sea explicitly given by the infinite wavelength corpuscles.

Let us recapitulate what we learned. We can split the Fock state operators for the corpuscles of the topological soliton in two parts. The non-trivial topology of the kink is constructed via an infinite occupation number of topological quanta corresponding to the operators \hat{t}_k^\dagger and \hat{t}_k . In particular, we can construct the coherent state $|t\rangle$ representing the topological sector from this quanta.

The second type of corpuscles \hat{c}_k^\dagger and \hat{c}_k accounts for the energy of the kink. These quanta have a finite occupation number peaked around the wavelength of the order of the length scale associated to the the kink. However, this occupation number is of the same order as for the non-topological soliton.

Clearly, if we define the creation and annihilation operators via $\hat{a}_k = \hat{t}_k \hat{c}_k$, they can no longer satisfy the standard algebra for Fock state operators. However, this does not mean that we cannot make sense of the corpuscles. As extensively mentioned above, they are quite different from usual S -matrix quanta. In particular, they have zero frequencies which is related to the fact that the corpuscles can only occur in a bound state. Therefore, the corpuscles do not necessarily need to satisfy the same requirements as standard asymptotic quanta.

In principle, we could try to apply the same split to the topologically trivial soliton. For that purpose, notice that we can represent its profile as

$$(\delta \star \text{sech})(x), \quad (3.53)$$

where the δ function is responsible for the topology. Of course, this split is trivial and accordingly the energy coherent state we would construct is equivalent to the soliton state we constructed in the previous section. In particular, the eigenvalue of the topological operators is simply ~ 1 . As mentioned before, this means that the occupation number of topological quanta is finite. Thus, the non-topological soliton is not protected against decay.

Topological Charge and Energy in the Decomposition Picture

We observed that the expectation values of the topological quanta \hat{t}_k exhibit a pole at $k = 0$ which is tied to the conservation of the topological charge of the soliton. One can ask the question how we have to explicitly define the topological charge Q in this context. Naturally, one would expect that it is determined by the order of the pole at hand. We can extract it using the Cauchy principal value

$$|Q| = \frac{1}{\pi} \text{ImPV} \int dk \langle t | \hat{t}_k^\dagger \hat{t}_k | t \rangle. \quad (3.54)$$

The general strategy to extract the topological charge for a given classical solution is to identify the infrared divergence in Fourier space responsible for the Bose sea of topological quanta. Obviously, we can always reexpress the Fourier coefficients as the infrared divergent part multiplied by the rest. This naturally leads to the convolution in position space.

In the decomposition picture, the energy of the soliton is an emergent effect of many quanta each contributing an energy given by the dispersion relation. Thus, to leading order the energy is simply given as

$$E_s = \int d(k/m) \langle E | \hat{c}_k^\dagger \hat{c}_k | E \rangle. \quad (3.55)$$

Note that the \hat{c}_k^\dagger , \hat{c}_k are dimensionful, since we shifted the $1/k$ pole to the topological quanta. Starting from (3.55), we can now easily prove that most of the quanta have wavelength $\sim 1/m$. Furthermore, the total number of energetic quanta can be obtained as

$$N_E = m^{-1} \int d(k/m) \langle E | \hat{c}_k^\dagger \hat{c}_k | E \rangle = \frac{8m^2}{3g^2}. \quad (3.56)$$

This is of the same order as for the non-topological soliton.

So far we discussed the decomposition picture only to leading order in $1/N$. Obviously, this is justified for the topological quanta whose occupation number diverges which is again connected to the conservation of the topological charge. However, for the energetical part

quantum corrections are measurable, since N_E is finite. To include these effects we have to consider instead of the leading corpuscular Hamiltonian

$$\hat{H}_{corp} = \sum_k \hat{c}_k^\dagger \hat{c}_k, \quad (3.57)$$

the full corpuscular Hamiltonian including all the interaction terms

$$\hat{H}_{corp} = \sum_k \hat{c}'_k \hat{c}'_k + \text{interaction terms}. \quad (3.58)$$

Here the prime indicates that we include quantum corrections. Naively, one could think that it is enough to include the interaction terms, but note that we used the dispersion relation to properly normalize the corpuscles. Obviously, it gets corrected as well when we include quantum effects. However, to explicitly compute the dispersion relation is quite a task, since we would have to find a Bogoliubov transformation which properly diagonalizes the Hamiltonian.

The interaction terms are induced by the $\hat{\phi}^4$ and terms $\hat{\phi}^3$ terms in the original Lagrangian. Correspondingly, they should be of the form

$$\sum_{k_1, k_2, k_3} \hat{c}'_{k_1} \hat{c}'_{k_2} \hat{c}'_{k_3} \hat{c}'_{k_1+k_2-k_3} + \dots \quad (3.59)$$

As mentioned earlier, the classical soliton has a zero mode corresponding to shifting the kink center. In other words, it is the Goldstone mode which occurs due to the breaking of the continuous translation invariance. A shift y of the profile corresponds to the phase factor for the energetical Fourier coefficients² of the form

$$\hat{c}_k \rightarrow e^{iyk} \hat{c}_k. \quad (3.60)$$

We easily see that (3.57) and (3.59) are invariant under such a shift. Therefore, the corpuscular resolution does not affect the zero mode of the kink.

3.1.5 Quantum meaning of the Soliton-Anti-Soliton interaction

The quantum reasoning can also be applied to interactions between soliton and anti-solitons. In this case, we have to be careful, since we do not know the exact classical solution to the equations of motion. Due to the non-trivial interaction between both solitons the solution should, in principle, be time dependent. Therefore, let us consider the case of a small interaction between a widely separated soliton and an anti-soliton. In this limit we can basically define the corpuscular picture for the complete configuration. This allows for a corpuscular representation of the interaction energy.

²In principle, the shift could also be seen as acting on the topological quanta.

Given a soliton-anti-soliton configuration separated by the distance a , the small interaction limit amounts to $a \gg m^{-1}$, where $1/m$ is the typical length scale associated to the individual solitons. The corresponding static solution is given as

$$\phi_{s,\bar{s}} = \frac{m}{g} \left(\tanh(m(x+a/2)) - \tanh(m(x-a/2)) - 1 \right). \quad (3.61)$$

Note that this configuration can be visualized as the one dimensional analog of a 'bubble', where the vacuum inside the 'bubble' is $\frac{m}{g}$ and outside it is simply $-\frac{m}{g}$.

To implement the quantum picture, we follow our procedure and define the expectation values of the corpuscular creation and annihilation operators in the soliton-anti-soliton coherent state $|s, \bar{s}\rangle$ simply as the Fourier coefficients of $\phi_{s,\bar{s}}$

$$\alpha_k = \sqrt{\pi m i} \frac{\sqrt{k}}{g} \operatorname{csch}\left(\frac{\pi k}{2m}\right) (1 - e^{-iak}). \quad (3.62)$$

At this point, we have to mention that the classical soliton-anti-soliton configuration is topologically trivially. The topological charge of the separated soliton and the anti-soliton add up to 0. Correspondingly, we observe no pole at $k = 0$ for the α_k we would associate to a topological charge. This means that we can restrict our analysis to the energetical corpuscles.

From this point, let us now try to evaluate the interaction energy explicitly. In general, there are two alternative ways to proceed. On the one hand, we can simply define energetic quanta $\hat{c}_k, \hat{c}_k^\dagger$ and $\hat{\bar{c}}_k, \hat{\bar{c}}_k^\dagger$ we discussed in section 3.1.4 for the separate soliton and anti-soliton, respectively. Notice that both profiles have the same individual energy. They are only shifted by a distance a . Thus, the operators and correspondingly the Fourier coefficients are simply related via a phase factor

$$\hat{\bar{c}}_k \rightarrow e^{iak} \hat{c}_k. \quad (3.63)$$

We still consider the limit of small interaction energy. Therefore, the soliton and the anti-soliton coherent states we can construct from these Fock state operators are approximately eigenstates of the Hamiltonian. Denoting them as $|E\rangle$ and $|E\rangle_a$ for the shifted soliton, the interaction energy is simply

$$E_{int} = \langle E | H | E \rangle_a. \quad (3.64)$$

The overlap amplitude between both solitons only depends on the energetical quanta, since the topological sector is trivial. There is a direct link between the overlap and the interaction energy which corresponds to a non-trivial mixing of both solitons. More concretely, we can evaluate

$$|\langle E | E \rangle_a|^2 = \left| \prod_k \langle c_k | e^{iak} c_k \rangle \right|^2 = e^{-2 \int dk |c_k|^2 (1 - \cos(ak))}. \quad (3.65)$$

Using the known expression for the c_k and the soliton energy E_s given in equation (3.55), this amounts to

$$\left| \prod_k \langle c_k | e^{iak} c_k \rangle \right|^2 = \exp\left(-2E_s + 32 \frac{m^3}{g^2} (am) e^{-2am}\right). \quad (3.66)$$

Here the second part in the exponential corresponds to the interaction energy.

On the other hand, we can use a slightly different strategy which allows to determine the corpuscular Hamiltonian. In a similar way as before, we define the two corpuscular algebras $\hat{c}_k, \hat{c}_k^\dagger$ and $\hat{\tilde{c}}_k, \hat{\tilde{c}}_k^\dagger$ for the soliton and the anti-soliton, respectively. Considering the $a \gg 1/m$ limit, we express the soliton-anti-soliton quantum state as a product state of the individual solitons

$$|s, \bar{s}\rangle = |sol\rangle \otimes |\overline{sol}\rangle. \quad (3.67)$$

Each state can individually be decomposed in a topological and an energetical part. Note that the topological sector of the individual solitons is not trivial. The decomposition is given as

$$\hat{c}_k |s, \bar{s}\rangle = (|t_s\rangle \otimes c_k |E_s\rangle) \otimes (|t_{\bar{s}}\rangle \otimes |E_{\bar{s}}\rangle), \quad (3.68)$$

$$\hat{\tilde{c}}_k |s, \bar{s}\rangle = (|t_s\rangle \otimes |E_s\rangle) \otimes (|t_{\bar{s}}\rangle \otimes \tilde{c}_k |E_{\bar{s}}\rangle). \quad (3.69)$$

The eigenvalues of the energy coherent states are the same as for the separate solitons

$$\hat{c}_k |s, \bar{s}\rangle = e^{iak/2} \sqrt{\frac{m^3}{\pi} \frac{\pi k}{gm}} \operatorname{csch}\left(\frac{\pi k}{2m}\right) |s, \bar{s}\rangle, \quad (3.70)$$

$$\hat{\tilde{c}}_k |s, \bar{s}\rangle = -e^{-iak/2} \sqrt{\frac{m^3}{\pi} \frac{\pi k}{gm}} \operatorname{csch}\left(\frac{\pi k}{2m}\right) |s, \bar{s}\rangle. \quad (3.71)$$

When we represent the quantum field of the full profile $\hat{\phi}$ in terms of the two kinds of energy operators, they mix. To leading order³, the Hamiltonian becomes

$$H = \int d(k/m) \left(\hat{c}_k^\dagger \hat{c}_k + \hat{\tilde{c}}_k^\dagger \hat{\tilde{c}}_k + \hat{c}_k^\dagger \hat{\tilde{c}}_k + \hat{\tilde{c}}_k^\dagger \hat{c}_k \right). \quad (3.72)$$

Obviously, the interaction energy between the soliton and the anti-soliton is represented by the corpuscular mixing term $+\hat{c}_k^\dagger \hat{\tilde{c}}_k$. Evaluating the Hamiltonian in the quantum state $|s, \bar{s}\rangle$, we arrive at

$$H = 2E_s - \frac{8m^3}{g^2} (-1 + (am)\coth(am)) \operatorname{csch}^2(am). \quad (3.73)$$

We have not used the large a limit up to this point. When we apply the $a \gg 1/m$ limit, equation (3.73) reduces to

$$2E_s - 32 \frac{m^3}{g^2} (am) e^{-2am}. \quad (3.74)$$

This is, of course, the same result as in equation (3.66). Note that the interaction becomes order one when $am \sim \log(E_s/m)$ which corresponds to the logarithmic correction investigated in [76, 90].

³As for the single soliton situation, we obtain $1/N$ type quantum corrections to this Hamiltonian we will not consider in this section.

Pseudo-Goldstone mode

As pointed out above, the soliton itself has a zero -mode corresponding to the spontaneously broken translational invariance. In the interaction case, the energy explicitly depends on the position of both kinks. This reflects the dependence of the interaction strength on the separation a of the solitons. From the corpuscular Hamiltonian point of view, this becomes manifest in the mixing terms $\sim \hat{c}_k^\dagger \hat{c}_k$ which are obviously not invariant under transformations of the form

$$\hat{c}_k^\dagger \rightarrow e^{iyk} \hat{c}_k^\dagger, \quad \hat{c}_k \rightarrow e^{-izk} \hat{c}_k. \quad (3.75)$$

Each individual soliton possesses a separate symmetry group $U(1)_S$ corresponding to the zero mode. Since the interaction term obviously only depends on the separation distance, the symmetry breaking pattern becomes

$$U(1)_S \times U(1)_{\bar{S}} \rightarrow U(1)_{diag}. \quad (3.76)$$

Half of the symmetries are conserved because we can always shift both profiles by the same amount b without affecting the interaction energy. This corresponds to the case $y = z = b$. Correspondingly, one Goldstone mode is preserved, while the other one becomes a pseudo-Goldstone mode. Notice that in the limit $a \rightarrow \infty$ the interaction term vanishes such that the full symmetry is restored. Accordingly, a second Goldstone mode occurs.

3.2 Corpuscular SUSY Breaking

So far we presented how to construct a consistent quantum picture for classical solitons. In principle, nothing prevents us from applying this logic to supersymmetric solitons. Correspondingly, this section is dedicated to establish a quantum description for supersymmetric kinks. Note, however, that this is still work in progress as there are still some open questions.

In general, the strategy is analogous to the one presented in the previous section. Fourier transforming the classical solution for the supersymmetric kink, we interpret the corresponding Fourier coefficients as expectation values of quantum corpuscular Fock operators evaluated in a coherent state built from these operators.

To motivate why we should apply the resolution picture to solitons in supersymmetric theories, we take a closer look at the classical story. The usual BPS saturated kink preserves exactly half of the supersymmetries. Accordingly, the usual scalar quantum fluctuations with Fock operators b_k and b_k^\dagger defined on top of the classical background have fermionic superpartners of the same mass.

Now let us turn to the full quantum picture which was introduced in this chapter. In the supersymmetric case, the resolution of the background kink could have dramatic consequences. This was first observed in [91]. In particular, all the supersymmetries seem to be broken in the microscopic description. Physically, we can give a very intuitive explanation for this phenomenon. By establishing a quantum picture for the supersymmetric kink, we

introduce new bosonic constituent degrees of freedom represented by the corpuscular Fock operators \hat{a}_k and \hat{a}_k^\dagger which do not have any fermionic counterpart.

To make this computationally manifest, we investigate the BPS condition, since it has to be satisfied when part of the supersymmetry should be preserved. When the kink is microscopically resolved, we observe that we obtain $1/N$ -type quantum effects which cannot be canceled by loop effects of the usual quantum fluctuations b_k and b_k^\dagger .

Additionally, it turns out that a mass splitting is induced between the fermions and the asymptotic bosons indicating that supersymmetry is completely broken. The complete break-down of supersymmetry on the corpuscular quantum state induces the appearance of a second Goldstino

$$|\psi_2\rangle = Q|sol\rangle \quad (3.77)$$

related to the fact that the second supersymmetry charge does not annihilate the soliton state. In this section we will present how to compute $1/N$ effects in the corpuscular picture in this particular example.

First, we consider the classical picture and afterwards we implement the quantum view. Since it is the first time in this work we are concretely interested in $1/N$ quantum corrections, we will present two different methods to extract them. In section 3.2.2 we show how these corrections to the BPS equation arise in the commutator method. Secondly, in section 3.2.3 we will consider the Bogoliubov method.

3.2.1 Coherent state picture for the supersymmetric kink

As explained in section 1.4.2, there are certain supersymmetric models where solitonic solutions occur. In particular, we discuss the classical kink solution in the 1+1 dimensional Wess-Zumino model which saturates the BPS condition in equation (1.72). Accordingly, half of the supersymmetries are semi-classically preserved on the non-trivial background state $|sol\rangle$. For completeness let us write down the corresponding classical Lagrangian already given in (1.69),

$$\mathcal{L} = \frac{1}{2} \left[\partial_\mu \phi \partial^\mu \phi + \bar{\psi} i \gamma^\mu \partial_\mu \psi - \left(\frac{\partial \mathcal{W}}{\partial \phi} \right)^2 - \left(\frac{\partial^2 \mathcal{W}}{\partial^2 \phi} \right) \bar{\psi} \psi \right] \quad (3.78)$$

with the superpotential

$$W(\phi) = \frac{m^2}{g} \phi - \frac{g}{3} \phi^3. \quad (3.79)$$

As in section 1.4.2, ψ is a two-component Majorana spinor. Correspondingly, it is the fermionic superpartner of the bosonic scalar field ϕ . For $m, g > 0$ this Lagrangian has a classical kink solution

$$\phi_{sol}(x) = \frac{m}{g} \tanh(xm). \quad (3.80)$$

The crucial point of this model is given by the fact that the kink satisfies the BPS equation

$$\mathcal{O}_{BPS} \equiv \partial_x \phi_{sol} \pm \left(m^2/g - g\phi_{sol}^2 \right) = 0 \quad (3.81)$$

such that half of the supersymmetries are preserved. We do not expect that usual quantum corrections spoil the supersymmetry, since the non-renormalization theorem protects the superpotential on the semi-classical level against quantum corrections. We can understand this theorem when we consider bosonic and fermionic fluctuations around the classical background. Since the corresponding quantum loops always have opposite signs, these contributions always cancel due to same mass of both particles.

We can introduce the corpuscular quantum picture in an analog way as in section 3.1.2. First, we Fourier transform the classical solution ϕ_{sol} like in equation (3.10) and promote the Fourier coefficients α_k to corpuscular annihilation and creation operators \hat{a}_k and \hat{a}_k^\dagger . To obtain the correct classical result to leading order in $1/N$, the expectation values of the operators in the soliton state have to be equivalent to α_k .

Let us stress that these corpuscular Fock operators are completely different from the quantum fluctuations around the supersymmetric kink whose Fock space is spanned by \hat{b}_k and \hat{b}_k^\dagger . In contrast to the usual asymptotic algebra \hat{b}_k and \hat{b}_k^\dagger , the \hat{a}_k and \hat{a}_k^\dagger can only exist inside the bound state and not as asymptotic quanta. In particular, they are interaction eigenstates. Subsequently, they have in general a non-trivial dispersion relation. There also exist fermionic fluctuations around the background, but it is important to note that the soliton is solely created out of bosonic corpuscles.

Defining a coherent kink state with these quanta as in equations (3.17) and (3.18) we can match the expectation value of the \hat{a}_k and \hat{a}_k^\dagger with the classical Fourier coefficients. Correspondingly, we can determine the occupation number as in equation (3.30). The mass of the supersymmetric kink is as well defined as in equation (3.31) (for $\psi = 0$).

Although equation (3.31) looks like a theory of a free scalar field, it contains highly non-linear dynamics. On the semi-classical level, the potential term is of the same order as the kinetical term as can be seen from the BPS condition (3.81). Since the Hamiltonian satisfies the BPS condition on this level, it is approximately diagonalized up to corrections of order $1/N$. As a consequence, we can use the diagonal Hamiltonian

$$H = (\partial_x \phi)^2 \quad (3.82)$$

to extract the dispersion $\omega(k) = |k|$ for the corpuscles to leading order. If we take the full corpuscular picture into account, we would obtain $1/N$ corrections to the dispersion. As a remark, let us mention that no factor $1/2$ occurs in the Hamiltonian in equation (3.82). This is reminiscent of the fact, that the potential and the kinetical term are of the same order. In other words, this is not simply the kinetic term, but the sum of kinetic and potential term.

Analogous to section 3.1.4, we can split the corpuscles in energetical quanta c_k and topological quanta t_k , where t_k and c_k are defined as in (3.45) and (3.46), respectively. Accordingly, the supersymmetric kink state amounts to

$$|sol\rangle = |t\rangle \otimes |E\rangle \quad (3.83)$$

with $|E\rangle$ and $|t\rangle$ satisfying equations (3.47) and (3.48), respectively. Subsequently, the topological charge which is equivalent to the central charge can be written in terms of topological quanta as in (3.54). Note that the number of topological quanta diverges due to the corresponding pole structure.

However, the number of energetical quanta is finite and given as

$$N_E = m^{-1} \int d(k/m) \langle E | \hat{c}_k^\dagger \hat{c}_k | E \rangle = \frac{8m^2}{3g^2}. \quad (3.84)$$

This fact will become important when we consider $1/N$ corrections in the next step.

3.2.2 Corpuscular Corrections: Commutator Method

Let us now try to determine how non-vanishing $1/N$ type corrections to the BPS equation arise in the corpuscular picture. Obviously, this would automatically imply that all the supersymmetries are broken on the full quantum corpuscular level. We present here two slightly different methods to approach this topic. In this section we discuss the commutator method, while in section 3.2.3 we show how we can achieve the same results using a Bogoliubov approach. However, let us stress at this point that the results presented here are far from complete as some questions regarding the corpuscular dispersion relation remain. We further elaborate on this below.

First of all, consider the BPS equation (3.81) in the corpuscular treatment. In the quantum picture, this classical equation is promoted into an operator statement, since the classical field is given as the expectation value of the corresponding field operator. In other words, every classical field solution in the BPS equation has to be substituted by the corresponding operator given in (3.14). If half of the supersymmetry is still preserved in the corpuscular picture, the BPS operator has to vanish everywhere on the corpuscular coherent kink state,

$$\langle sol | \mathcal{O}_{BPS}^2 | sol \rangle = \langle sol | \left(\partial_x \hat{\phi} \pm \left(m^2/g - g\hat{\phi}^2 \right) \right)^2 | sol \rangle. \quad (3.85)$$

In the following, we will try to show that this condition is violated locally by corpuscular quantum corrections. Before getting into the computation, let us remind ourselves that on the trivial vacuum state $|0\rangle$ the BPS equation should be fulfilled. To achieve this, we have to account for unwanted vacuum effects by properly normal ordering. Correspondingly, we have to investigate quantum corrections to the BPS equation while subtracting vacuum effects,

$$\langle sol | \mathcal{O}_{BPS}^2 | sol \rangle - \langle 0 | \mathcal{O}_{BPS}^2 | 0 \rangle. \quad (3.86)$$

We will come back to this point. For the moment let us start to present the method to compute quantum corrections. It simply amounts to using commutation relations to bring the BPS operator in a normal ordered form. In the vacuum state the normal ordered parts obviously vanish. However, in the non-trivial soliton state the normal ordered products correspond to the Fourier coefficients α_k which can be related to the occupation number and accordingly to the classical field values.

For instance, let us consider the quartic term $\langle sol|\hat{\phi}^4|sol\rangle$ occurring in the BPS condition. Using the commutation algebra for the corpuscular Fock operators $\hat{a}_k, \hat{a}_k^\dagger$, we arrive at

$$\langle sol|\hat{\phi}^4|sol\rangle \sim \phi_{sol}^4 + \hbar\phi_{sol}^2 + \hbar^2. \quad (3.87)$$

Here we restored the corresponding powers of \hbar . Each power of \hbar corresponds to the evaluation of a commutator. The first term in the first line is simply the classical value, but the second term corresponds to an actual $1/N$ -type quantum correction. Note that only operators which are at least of the third order in $\hat{\phi}$ can lead to corpuscular corrections. This can be understood as follows. Only terms which contain commutators as well as normal ordered contributions correspond to corpuscular corrections, since the purely normal ordered terms correspond to the classical profile. Clearly, such a mixing can only occur for terms of at least third order.

We still have to answer how to treat the third term in (3.87). This term only contains commutators. As can be seen from

$$\langle 0|\hat{\phi}^4|0\rangle \sim \hbar^2, \quad (3.88)$$

it would even preexist in the Minkowski vacuum state. We know how to deal with vacuum contributions in quantum field theories. One has to properly normal order the correlator, i. e. subtract the vacuum contributions. Subtracting (3.88) from (3.87), leads to

$$\hat{\phi}^4 \rightarrow \hat{\phi}^4 - \langle 0|\hat{\phi}^4|0\rangle. \quad (3.89)$$

Obviously, the third term in (3.87) vanishes when we redefine the correlator in this way. Thus, in principle, we should renormalize the corpuscular Hamiltonian,

$$\langle sol|H|sol\rangle \rightarrow \langle sol|H|sol\rangle - \langle 0|H|0\rangle. \quad (3.90)$$

Keeping this in mind, let us return to the computation of the $1/N$ corrections. Using the commutation relations and subtracting the vacuum contributions, we can bring the BPS condition to the form

$$\mathcal{G}_{kink} = \langle sol|\mathcal{O}_{BPS}^2|sol\rangle - \langle 0|\mathcal{O}_{BPS}^2|0\rangle = \frac{1}{\pi}(g\partial_x\phi_{sol}(x) + 3g^2\phi_{sol}^2)\log\left(\frac{\Lambda_{UV}}{\mu_{IR}}\right) \quad (3.91)$$

which is depicted in figure 3.1. Here Λ_{UV} and μ_{IR} are UV and IR cut-offs, respectively. Obviously, equation (3.91) reveals that the BPS equation is not satisfied on the coherent state if $\log(\Lambda_{UV}/\mu_{IR})$ does not vanish. However, the value of this logarithm heavily depends on the concrete form of the full corpuscular dispersion which is unknown. We further elaborate on this topic below. Equation (3.91) is explicitly derived in the appendix A.

The new effects emerge from mixing terms of quantum effects and classical field values. The surviving contributions in (3.91) have no analog on a trivial vacuum. In particular, the $1/N$ type corrections explicitly depend on x and cannot be associated with a constant

shift of the vacuum energy. Thus, these corrections, indeed, encode non-trivial information about the resolved background.

The logarithms which appear can be understood in the context of renormalization. The bare classical field values $\phi_{sol}(x)$ are not measurable, but only the corpuscularly renormalized objects which appear in physical correlation functions. In particular, the renormalized field no longer satisfies the BPS condition leading to a complete breaking of supersymmetry on the soliton state. At this point, let us stress again that the corpuscular renormalization is far from completely understood. In particular, the logarithmic term only arises when we approximate the corpuscular dispersion by $|k|$ which itself is only true up to order $1/N$. Therefore, to obtain more quantitative statements we have to better understand the microscopic dynamics of the corpuscles. This is left for future work.

Note that the corrections are not only suppressed by \hbar as usual loop effects. With respect to the classical field ϕ_{sol} the corrections are further suppressed by $1/N$. This becomes manifest in the lower power of classical fields.

In the classical treatment, one observes only one Goldstino arising due to the spontaneous breaking of half of the supersymmetries. Correspondingly, the breaking of all the supersymmetries on the corpuscular kink induces the appearance of a second Goldstino. Its profile is given as

$$|\psi_2\rangle^2 = |\mathcal{O}_{BPS}|_{sol}\rangle^2 . \quad (3.92)$$

Clearly, the second Goldstino only occurs when \mathcal{O}_{BPS}^2 does not vanish on the state $|sol\rangle$ as it is the case in the corpuscular picture. The resulting Goldstino profile is depicted in figure 3.1.

The BPS condition is not violated everywhere, but only on a certain length scale. As we would expect, this length scale is determined by the typical width of the kink $1/m$. Far away from the center of the kink the quantum corrections are exponentially suppressed. This, again, shows that these effects are closely related to the resolution of the soliton, but not to the vacuum.

As extensively mentioned throughout the thesis, the corpuscular resolution leads to $1/N$ type quantum corrections. The supersymmetric kink possesses infinitely many constituents which are responsible for the conservation of the topological charge. Thus, we would naively expect that no corrections would occur. However, from the topology energy split point of view we have to rephrase the statement about $1/N$ type quantum corrections. More explicitly, the corpuscular corrections are of the $1/N_E$ type, where the number of energetic quanta N_E is finite and given in (3.84). In other words, only the energetical quanta participate in local quantum processes leading to non-vanishing corrections to the BPS condition⁴. Of course, the infinite wavelength corpuscles responsible for topology are not involved in local measurements, since it takes an infinite amount of time for them to participate in local processes. Therefore, the violation of the BPS condition implies that $\langle sol|\hat{H} - Z|sol\rangle$ does not vanish anymore because the central charge, in contrast to H , is

⁴In the following, $1/N$ always means $1/N_E$.

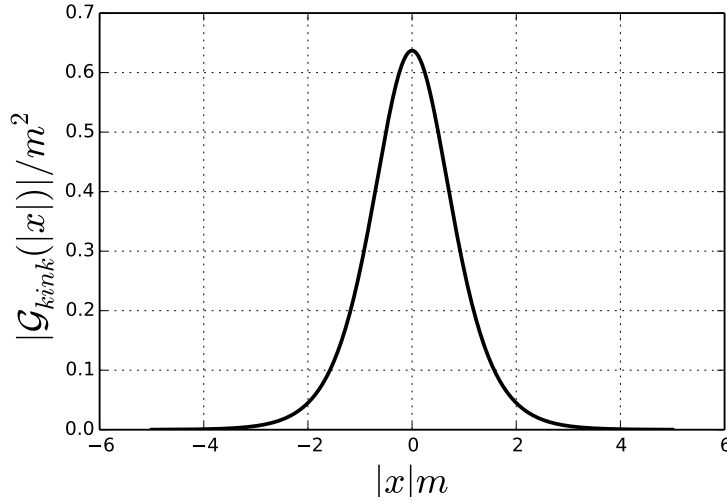


Figure 3.1: The function \mathcal{G}_{kink}/m^2 is depicted versus the normalized spatial coordinate xm . Note that in this figure the logarithm is normalized to $\log(\Lambda_{UV}/\mu_{IR}) = 1$. \mathcal{G}_{kink}/m^2 directly measures the violation of the BPS condition and, furthermore, it exactly corresponds to the profile of the second Goldstino.

not affected by quantum processes. The reason for this is the infinite amount of topological quanta from which the topological charge emerges as shown in (3.54).

In general, one could ask if the fermion quantum fluctuations around the soliton background could account for the bosonic corpuscular fluctuations as it is the case in the semi-classical treatment due to Fermi-Bose degeneracy to all order in perturbation theory in the usual description. Therefore, let us explicitly restore the fermionic and bosonic fields in the Hamiltonian and determine the quantity $\langle sol|\hat{H} - Z|sol\rangle$. As explained above, we subtract, again, the Minkowski vacuum contribution $\langle 0|\hat{H} - Z|0\rangle$ in order to account for the vacuum effects.

Expanding \hat{H} in the three different types of field, i. e. the corpuscular field operator $\hat{\phi}$, the usual bosonic fluctuations $\hat{\phi}_b$ and fermionic fluctuations ψ , we obtain the full quantum corpuscular Hamiltonian

$$\hat{H} = \frac{1}{2} \left[\partial_\mu(\hat{\phi} + \hat{\phi}_b)\partial^\mu(\hat{\phi} + \hat{\phi}_b) + \bar{\psi}i\gamma^\mu\partial_\mu\psi + \left(\frac{\partial\mathcal{W}}{\partial(\hat{\phi} + \hat{\phi}_b)}\right)^2 + \left(\frac{\partial^2\mathcal{W}}{\partial(\hat{\phi} + \hat{\phi}_b)^2}\right)\bar{\psi}\psi \right] \quad (3.93)$$

with

$$W = \frac{m^2}{g}(\hat{\phi} + \hat{\phi}_b) - \frac{g}{3}(\hat{\phi} + \hat{\phi}_b)^3. \quad (3.94)$$

Obviously, we can express the corpuscular, bosonic operator in terms of its creation and annihilation algebra \hat{a}_k and \hat{a}_k^\dagger . Since the quantum fluctuations correspond to asymptotic

particles, they can be expanded in terms of free waves as usual:

$$\begin{aligned}\psi &= \sum_s \int \frac{dp}{\sqrt{(2\pi)2\omega_f}} \left(\hat{g}_p^s u_p^s e^{-ipx} + \hat{h}_p^{s\dagger} \bar{v}_p^s e^{ipx} \right), \\ \phi_b &= \int \frac{dp}{\sqrt{(2\pi)2\omega_b}} \left(\hat{b}_p e^{-ipx} + \hat{b}_p^\dagger e^{ipx} \right),\end{aligned}$$

where \hat{b}_p , \hat{g}_p^s and \hat{h}_p^s are the annihilation operators for bosons, fermions of spin s and anti-fermions of spin s , respectively. As usual, the v_p^s and u_p^s are the spinor polarization vectors [92]. In generic situations, the dispersion relation for fermions ω_f and bosons ω_b are different. For supersymmetric theories they obviously have to coincide, since the fermion mass has to be equivalent to the boson mass even when one takes loop corrections into account. Using the commutation relations of the different sets of Fock operators, we can determine

$$\begin{aligned}\langle sol | \hat{H} - Z | sol \rangle &= \frac{1}{2} \int dx \left(I(2g\phi'_{sol} + 6g^2\phi_{sol}^2 - 2m^2 + g^2I) \right. \\ &\quad \left. + 2g\partial_x\phi_{sol}J + 6g^2\phi_{sol}^2J - 2m^2J \right. \\ &\quad \left. - 4g^2\phi_{sol}^2K \right),\end{aligned}\tag{3.95}$$

where we used the classical solution for the spinor u_p^s for the Dirac equation on the soliton background, $\bar{u}_p^s u_p^s = 2g\phi_{sol}$. The functions I and J correspond to divergent integrals arising from commutators of corpuscles and bosonic fluctuations, respectively. Similarly, the K function denotes the integral arising from anticommutators of fermionic fluctuations. The derivation for (3.95) is analogous to the computation of \mathcal{G}_{kink} in the appendix A.

Additionally, ϕ_{sol} is simply the classical expectation value. Note that we already neglected the normal ordered contributions of ϕ_b and ψ in equation (3.95). Obviously, these terms have to vanish, since the corresponding Fock operator \hat{b}_k , \hat{g}_k^s and \hat{h}_k^s annihilate the soliton state $|sol\rangle$. The integrals are given as

$$\begin{aligned}I &= \int \frac{dk}{4\pi\omega}, \\ J &= \int \frac{dk}{4\pi\omega_b}, \\ K &= \int \frac{dk}{4\pi\omega_f},\end{aligned}$$

where ω is the dispersion relation of the corpuscles. Assuming that the corpuscular dispersion is free everywhere ($\omega = |k|$), we would obtain the logarithmic term $\log(\Lambda_{UV}/\mu_{IR})$ for I as in equation (3.91). However, since the dispersion is only known up to order $1/N$, the exact behavior of I is still an open question. Thus, we can only show that there are breaking terms, but it is so far not possible to compute how strong these effects are. Obviously, this is related to the question of how to corpuscularly renormalize. In the following we assume that I does not vanish and we can make sense of it.

On the one hand, when we do not resolve the soliton, all the terms proportional to I vanish, while the usual bosonic and fermionic parts remain the same such that we recover the usual result. Correspondingly, it follows $\langle sol | \hat{H} - Z | sol \rangle = 0$. On the other hand, taking the corpuscular structure into account the terms proportional to I in (3.95) do not vanish. Even if the usual bosonic and fermionic contributions corresponding to J and K cancel each other exactly, there are simply no fermionic superpartners which could cancel the contributions of I . In other words, by introducing the bosonic corpuscles to resolve the kink we immediately break supersymmetry.

Supersymmetry directly corresponds to having the same mass for bosons and fermions in the theory. Thus, the breaking of supersymmetry should become manifest in a mass splitting between these particles. This leads to corpuscular corrections to the bosonic and fermionic dispersion relation, respectively. In general, it follows $J \neq K$. Nevertheless, let us for the moment assume that $J = K$ which is, of course, only true up to order $1/N$. In this approximation we can use the classical BPS condition $2g\phi'_c J + 2g^2\phi_c^2 J - 2m^2 J = 0$ to bring equation (3.95) to the form

$$\begin{aligned} \langle \phi_c | \hat{H} - Z | \phi_c \rangle &= \frac{1}{2} \int dx \left(4g^2 \phi_c^2 (I + J - K) \right. \\ &\quad \left. + g^2 I^2 + 2g^2 IJ \right). \end{aligned} \quad (3.96)$$

The corpuscular breaking terms are, again, proportional to I . Therefore, they vanish only in the limit $I \rightarrow 0$, where we neglect the corpuscular resolution of the kink. At this point, it is important to note that all the terms proportional to the integral J originated from operators of the form $\hat{\phi}_b^2$. These are exactly the mass terms for the bosonic fluctuations. Taking a closer look at (3.95), we observe that an additional mass term is generated for the bosons which is of the form

$$\Delta m_b = 2g^2 I. \quad (3.97)$$

In other words, corpuscular loop corrections induce an additional mass terms for the bosons, but not for the fermions in this approximation. Accordingly, assuming that I does not vanish this indicates that supersymmetry is broken completely.

Dispersion Relation

At this point, let us comment on the dispersion relation. As we already discussed in section 3.1.3, it is highly non-trivial to determine the corpuscular dispersion relation $\omega(k)$. Usually, the dispersion relation should emerge from the microscopic Lagrangian when we integrate out the high-energy degrees of freedom. However, the corpuscular method presented here only introduces these quanta in the low energy effective theory. We simply do not know the underlying corpuscular physics such that we can determine the corpuscular dispersion only to leading order in $1/N$. Correspondingly, the BPS condition is satisfied as well as the Hamiltonian is diagonal up to this order. Thus, the dispersion is approximately given

as

$$\omega(k) = |k| + \mathcal{O}(1/N) . \quad (3.98)$$

To answer the question how the dispersion relation emerges from a more fundamental level is still an open task in this framework. So far it is not possible to exactly determine the corpuscular loop contribution corresponding to the integral

$$I = \int \frac{dk}{4\pi\omega} .$$

Nevertheless, this contribution will not vanish such that supersymmetry remains broken in any case. In the approximation $\omega_k \approx |k|$ this integral exhibits divergencies. This simply means that we have to properly renormalize the bare couplings and masses in the Lagrangian with respect to the corpuscular loop effects. As was mentioned above, the bosonic corpuscles have no fermionic superpartners which could cancel these loop effect. Accordingly, the superpotential cannot satisfy the non-renormalization theorem anymore on the corpuscular soliton state.

Similarly, it is hard to determine the free dispersion of the bosonic and fermionic fluctuations simply because their mass is renormalized by corpuscular effects. Again, to leading order the bosonic and fermionic dispersions are given as

$$\omega_b = \sqrt{|k|^2 + m^2} + \mathcal{O}(1/N) \quad \text{and} \quad (3.99)$$

$$\omega_f = \sqrt{|k|^2 + m^2} + \mathcal{O}(1/N) , \quad (3.100)$$

respectively. However, the corpuscular corrections are, in principle, not equivalent such that their effective masses are different.

Of course, we can use these dispersions to determine the integrals J and K to leading order. This leads to diverging logarithms which we have to regularize as given in (3.95),

$$\log \left(\frac{\Lambda_{UV}}{m} \right) , \quad (3.101)$$

where Λ_{UV} is a UV cutoff and $1/m$ the extension associated to the profile. As long as we are in the region $\Lambda_{UV} \sim m$ corresponding to length scales of the order of the kink, we effectively do not resolve the soliton and any quantum effects vanish. However, when we start to turn to higher energies $\Lambda_{UV} > m$ we effectively look inside the soliton and quantum effects become important. Let us stress again that we have to know the corpuscular dispersion relation in order to give more quantitative statements.

3.2.3 Corpuscular Corrections: Bogoliubov Method

In this section we will present a slightly different approach to keep track of the corpuscular corrections. We use the mean field split to represent the corpuscular operator in terms of the mean field and fluctuations.

More explicitly, the corpuscular annihilation and creation operators can be represented by

$$\hat{a}_k = \alpha_k + \hat{\delta}_k, \quad (3.102)$$

$$\hat{a}_k^\dagger = \alpha_k + \hat{\delta}_k^\dagger. \quad (3.103)$$

Here $\alpha_k = \sqrt{N_k}$ is, again, the classical Fourier coefficients defined in (3.30). The annihilation and creation operators $\hat{\delta}_k$ and $\hat{\delta}_k^\dagger$ correspond to quantum fluctuations of the mean field $\sqrt{N_k}$. It is crucial to understand that these creation and annihilation operators are different from the full corpuscular operators $\hat{a}_k, \hat{a}_k^\dagger$ we defined earlier in section 3.1.1. In particular, $\hat{\delta}_k, \hat{\delta}_k^\dagger$ correspond to fluctuations of the background itself. Furthermore, they annihilate a different vacuum. In contrast to the corpuscular annihilation operator \hat{a}_k annihilating the Minkowski vacuum, the $\hat{\delta}_k$ have the soliton state $|sol\rangle$ as a vacuum state. Most easily $\hat{\delta}_k, \hat{\delta}_k^\dagger$ can be understood as phonons propagating in a solid state. Using the Bogoliubov approximation that $\hat{\delta}_k$ is small, the Hamiltonian can be written up to bilinear order in $\hat{\delta}_k$

$$\hat{H} = E_{sol} + \mathcal{O}(\hat{\delta}_k^2). \quad (3.104)$$

Usually, we employ a Bogoliubov transformation on the fluctuations $\hat{\delta}_k, \hat{\delta}_k^\dagger$ such that the Hamiltonian is diagonalized. The resulting Bogoliubov modes are given as

$$\delta\hat{a}_k = \sum_i \left(f_{ik} \hat{\delta}_k + \text{h.c.} \right), \quad (3.105)$$

where f_{ik} are the Bogoliubov coefficients. As a consequence, the corpuscular Hamiltonian reduces to

$$\hat{H} = E_{sol} + \sum_k \epsilon_k \delta\hat{a}_k^\dagger \delta\hat{a}_k. \quad (3.106)$$

Here ϵ_k corresponds to the dispersion of Bogoliubov modes and is determined by the diagonalization procedure. To leading order the dispersion of the Bogoliubov modes is the same as for the corpuscles, since classically the Hamiltonian is diagonalized by the kink, $\epsilon_k \approx \omega(k) \approx |k|$. At this point, we observe the same problem as in the commutator method, since the dispersion relation for the Bogoliubov modes is not known.

Note that we have to distinguish the Bogoliubov modes from the usual quantum fluctuations around the background we denoted by \hat{b}_k and \hat{b}_k^\dagger . Although the \hat{b}_k and \hat{b}_k^\dagger have the same vacuum state as the Bogoliubov modes, they do not behave like asymptotic particles. In particular, the Bogoliubov modes are confined to the background bound state and have a different dispersion than the asymptotically free quanta \hat{b}_k and \hat{b}_k^\dagger .

As a remark, let us mention that the diagonalization of the Hamiltonian becomes particularly easy in the soliton case because to leading order the Hamiltonian is already diagonal in the corpuscular Fock operators \hat{a}_k and \hat{a}_k^\dagger . In other words, since to leading order in $1/N$ the BPS condition is satisfied, the diagonalization of the Hamiltonian is trivial.

Reexpressing the corpuscular field $\hat{\phi}$ in terms of the mean field and the background fluctuations, we arrive at

$$\hat{\phi}(x) = \phi_{sol}(x) + \sqrt{l} \int \frac{dk}{\sqrt{(2\pi)2\epsilon_k}} (e^{ikx} \delta \hat{a}_k + e^{-ikx} \delta \hat{a}_k^\dagger), \quad (3.107)$$

where ϕ_{sol} is already defined in (1.73). As explained in the previous subsection, supersymmetry is completely broken on the soliton state when the BPS equation is not satisfied on the corpuscular level. Thus, let us evaluate the BPS equation in the Bogoliubov approach to second order in Bogoliubov modes

$$\begin{aligned} \langle sol | \mathcal{O}_{BPS}^2 | sol \rangle &= \langle sol | \left(\partial_x \hat{\phi} \pm \left(m^2/g - g\hat{\phi}^2 \right) \right)^2 | sol \rangle \\ &= \left(\partial_x \phi_{sol} \pm \left(m^2/g - g\phi_{sol}^2 \right) \right)^2 \\ &\quad + g \left(6g\phi_{sol}^2(x) + 2\partial_x \phi_{sol}(x) \right) \\ &\quad \times \langle sol | \left(\sqrt{l} \int \frac{dk}{\sqrt{(2\pi)2\epsilon_k}} (e^{ikx} \delta \hat{a}_k + e^{-ikx} \delta \hat{a}_k^\dagger) \right)^2 | sol \rangle. \end{aligned} \quad (3.108)$$

Note that we already neglected here all the terms which are vacuum contributions as explained in subsection 3.2.2. The second line corresponds to the classical BPS condition which vanishes. Using the property of the Bogoliubov modes $\delta \hat{a}_k | sol \rangle = 0$, we arrive at

$$\langle sol | \mathcal{O}_{BPS}^2 | sol \rangle = (2g\phi'_{sol} + 6g^2\phi_{sol}^2) \underbrace{\int \frac{dk}{(2\pi)2\epsilon_k}}_{\approx I}. \quad (3.109)$$

Consistently, we obtain the same result as with the previous method. As in equation (3.91), it follows that the BPS condition is not satisfied on the corpuscular level. In particular, the result is the same as the corpuscular contributions in (3.91), but using this method we observe the same problems as before.

Finally, the results show that both approaches to keep track of corpuscular corrections lead to the same results. Unfortunately, in both approaches the corpuscular dispersion can only be determined approximately such that it is formidable task to obtain more quantitative results.

3.3 Conclusions

Let us now review briefly the most interesting results of this section and draw a conclusion. Furthermore, we will comment on future work in this framework.

In the beginning of this chapter we presented an explicit framework to describe solitons in 1+1 dimensions in terms of bound states of constituents. We refer to these constituents as corpuscles to distinguish them for usual asymptotic particles. In particular, the corpuscles can only exist inside the bound state and always interact with each other. To

represent the soliton as a bound state, we constructed a coherent state of these corpuscles. The coherent state is a reasonable choice because it is the most classical quantum state we know of.

This framework allows for a new understanding of several aspects of soliton physics. Namely, it turns out that the occupation number of infinite wavelength modes diverges which we can connect with the conservation of the topological charge. From the corpuscular point of view the overlap between the Minkowski vacuum and the soliton state is given as

$$e^{-N} \rightarrow 0 \text{ for } N \rightarrow \infty .$$

Thus, the divergence of the occupation number can be directly related to the non-trivial topology of the soliton.

Furthermore, this framework allows to distinguish two different types of quanta. The first type are the infinite wavelength topological quanta. The second type of quanta has non-zero energy. Accordingly, it can account for the energy of the profile. The corresponding occupation number of energetical quanta does not diverge. Mathematically, the profiles for the energetical and topological quanta are connected with the soliton profile via convolution.

These energetical quanta automatically lead to $1/N$ -type quantum effects, since they interact on the corpuscular level. This could potentially lead to enormous consequences for supersymmetric kinks. In particular, even the classically BPS saturated kink could break all the supersymmetries due to corpuscular quantum effects. This can be easily understood as we are introducing new bosonic degrees of freedom without a fermionic counterpart. Thus, a mass splitting for the fermions is generated and a second Goldstino occurs.

However, in order to determine the occupation number and the quantum corrections, it is necessary to identify the corpuscular dispersion relation as it encodes all the microscopic interactions. So far it is only possible to determine it up to $1/N$ corrections when classically the BPS condition is satisfied. Thus, we cannot prove that supersymmetry is broken, but we only find strong hints that this is the case in the corpuscular picture. Correspondingly, as a future task it will be necessary to develop methods to determine the corpuscular dispersion relation in generic situations. This could help to further understand how quantum mechanically resolved solitons affect supersymmetry.

Chapter 4

Coherent State Picture for Instantons

Since the coherent state method was quite successful to describe classical solutions like the topological and non-topological soliton, naturally the question arises if we can extend this framework to instantons. Note that the work presented in this whole chapter is in accordance with the original work [93]. An instanton is a classical solution arising as a saddle point in the Euclidean path integral. In contrast to the soliton, it is characterized by a finite action instead of a finite energy. As instantons correspond, in general, to finite action processes in Euclidean time, we naturally associate them with quantum mechanical tunneling processes. For instance, in Yang-Mills theories instantons correspond to processes describing the switching between the different prevacua of the theory. Correspondingly, in this case the instanton is connected with the non-trivial vacuum structure of the theory. Thus, we can attribute a topological charge to the instanton like to the topological soliton before. However, as it turns out it is much harder to develop a quantum understanding for the instanton than it was for the soliton. Since the instanton is a process, it is not similar to a particle like the soliton. This is related to the fact that instantons are saddle points of the path integral in Euclidean time. As a consequence, the instanton solution directly depends on Euclidean time which is very different from the soliton case. Notice that it was crucial in the soliton case that the soliton is static.

To circumvent these obstacles when introducing a corpuscular picture for the instanton, we proceed in a slightly different way than in the soliton case presented in the previous chapter. Instead of directly defining a quantum coherent state $|inst\rangle$ for the instanton, we relate the instanton effect to a usual soliton tunneling through a region which is energetically forbidden in a dimensionally uplifted theory. This mapping on a higher dimensional object is well known in condensed matter physics, where the tunneling of a Cooper pair through a barrier is viewed as an instanton effect by a low energy observer. This tunneling is known as Josephson effect [94].

Let us be more explicit at this point and present the idea of this chapter. We want to understand an instanton in d dimensions as a soliton in $d + 1$ dimensions evolving in Euclidean time. In this chapter we will examine two different aspects of this picture. On the one hand, we show how we can map instantons in various dimensions on a higher dimensional soliton without specifying the embedding. When we consider an instanton

solution in d dimensions $\phi_{inst}(x)$ describing a tunneling process, we can always find a static soliton $\phi_{sol}(x)$ in a $d + 1$ dimensional theory with an equivalent field configuration as the instanton. Of course, this is a trivial statement because the equations of motions which we have to solve in order to obtain the classical solutions are simply the same for the static soliton and the instanton in Euclidean time in one less dimension as was already mentioned in [95].

In order to map the instanton on a soliton evolving in Euclidean time, we have to uplift the instanton theory to $d + 1$ dimensions. Usually a fundamental length scale L is involved in such a procedure simply because the mass dimensions of the couplings and fields depend on the number of dimensions. Therefore, we can relate the corresponding couplings of both theories by

$$\frac{L}{\tilde{g}^2} = \frac{1}{g^2}. \quad (4.1)$$

The classical field values are given as

$$\phi_{inst} = \sqrt{L} \tilde{\phi}_{sol}. \quad (4.2)$$

Obviously, this scale is also involved when we determine the instanton action. It can simply be identified as the action of a soliton propagating a Euclidean distance L

$$S_{inst}^{(d)} = L M_{sol}^{(d+1)}. \quad (4.3)$$

Accordingly, there is a direct mapping of an instanton in d dimensions on a $d+1$ dimensional soliton propagating a Euclidean time L .

When we resolve the uplifted soliton, corpuscular $1/N$ -type quantum effects arise which are inherited by the instanton in the lower dimensional theory. Note that it is still an interesting question how to directly define a coherent instanton state $|inst\rangle$, but we will leave this for future work. If we include the corpuscular picture for the soliton, accordingly the instanton knows about the constituent structure. In this sense, the instanton can be viewed as made out of N corpuscular tunnel processes corresponding to the soliton corpuscles evolving a Euclidean time interval $\tau = L$. This amounts to the Euclidean time evolution

$$\langle sol | e^{iH\tau} | sol \rangle |_{\tau=iL} \propto e^{-S_{inst}}. \quad (4.4)$$

At this point, we have to clarify the action of the time evolution operator on the corpuscular solitonic state. As it turns out, this can most easily be achieved when we turn to a description in terms of Bogoliubov modes we already introduced in section 3.2.3. In particular, performing a Bogoliubov transformation as in (3.105), the Hamiltonian reduces to

$$\hat{H} = E_{sol} + \sum_k \epsilon_k \delta \hat{a}_k^\dagger \delta \hat{a}_k, \quad (4.5)$$

where the Bogoliubov modes $\delta \hat{a}_k$ correspond to small fluctuations usually known as phonons in condensed matter physics. In other words, the time-evolution is mainly governed by the classical energy of the soliton profile E_{sol} such that we can use (4.5) to obtain (4.4).

On the other hand, we can take a slightly different perspective. For instance, we could ask the question if it is possible to dynamically embed the instanton theory in a higher dimensional soliton theory. In other words, is it possible to manufacture a concrete situation where the instanton emerges from the point of view of a low energy observer? We will identify several explicit dynamical mechanisms allowing for a mapping of the instanton on a higher dimensional soliton. The general strategy to achieve this is simply to localize a low energy observer Alice on a barrier or transition region through which the higher dimensional soliton is tunneling. Clearly, a propagation of a soliton with virtual energy is viewed as an instanton for Alice who is not able to resolve the barrier. Note that the barrier width or in other words the Euclidean distance the soliton is propagating is equivalent to the length scale L we introduced earlier in order to connect the couplings of both theories. Thus, in a dynamical embedding L is not a free parameter, but we can derive how L arises from first principles. In general, it depends on the parameters of the higher dimensional theory.

For instance, if we localize a $d+1$ dimensional soliton on a d dimensional brane of width L as is described in [96] the instanton directly occurs on this d dimensional submanifold. Of course, when the soliton is microscopically resolved, the corpuscles are dynamically localized on this layer as well which naturally leads to quantum effects affecting the lower dimensional instanton.

The outline of this chapter is as follows. First, in section 4.1 we explicitly implement the constituent picture for the instanton in $0+1$ dimensional quantum mechanics by mapping it on the $1+1$ dimensional soliton as explained above. In particular, we consider the cases of the topological and the non-topological instanton. As a consequence of the mapping, the instanton inherits the same features as the corpuscular soliton. We can understand the stability of the topological instanton against decay in terms of an infinite occupation number as already presented in sections 3.1.1, 3.1.2 and 3.1.4 for the soliton. Additionally, we can employ the topology-energy split for the instanton. Note that in contrast to the soliton, the instanton is not characterized by a finite energy, but by a finite action. In turn, we can distinguish quanta responsible for the action and those creating the topological charge.

With this framework in mind, it is straightforward to introduce a corpuscular picture for the instanton. However, it is still challenging to construct concrete models of embedding the instanton theory in a higher dimensional theory. In sections 4.1.3 and 4.1.4 we present models where a $1+1$ dimensional soliton is dynamically localized on a region of width L and show how the instanton occurs when restricted to this layer. In addition, we consider the more complicated model of a localized monopole in $3+1$ dimensions between two domain walls in section 4.2. This leads to a localized $2+1$ dimensional $U(1)$ gauge theory. In this lower dimensional theory the tunneling monopole is viewed as an instanton effect by a low energy observer.

Finally in section 4.3.2 we discuss how to implement the quantum picture for the complicated case of Yang-Mills instantons in $3+1$ dimensions by mapping it on an $4+1$ dimensional monopole.

4.1 Instantons in 0 + 1 dimensions as Solitons in 1 + 1 dimensions

4.1.1 Non-topological Instanton

Before establishing a mapping between the non-topological soliton in 1 + 1 dimensions and the non-topological instanton in 0 + 1 dimensions, let us for completeness present, again, the corresponding model. For that purpose, consider the Lagrangian

$$\mathcal{L}_{0+1} = (\partial_t \phi)^2 - m^2 \phi^2 + g^2 \phi^4. \quad (4.6)$$

Here $m^2, g^2 > 0$ are the mass and the coupling, respectively. Note already at this level that it is not surprising that the classical instanton solution in Euclidean time can be mapped on a static non-topological soliton. The structure of the instanton Lagrangian (4.6) simply coincides with the one of the non-topological soliton in (3.4). As a consequence, we observe the same vacuum structure, since

$$\phi = 0 \text{ for } t = \pm\infty \quad (4.7)$$

is the classical stable vacuum. The classical saddle point solution $\phi_{inst}(t)$ we call instanton describes the motion of the field starting in the vacuum at $t = -\infty$ evolving to the unstable field value $\phi = m/\sqrt{2}g$ at $t = 0$, bouncing back and finally condensing to the vacuum at $t = +\infty$ again. In other words, the non-topological instanton describes a tunneling from the vacuum across a barrier and back to the vacuum. Let us point out that the described motion is in total accordance with the non-topological soliton. However, the instanton solution depends on the Euclidean time instead of x . The classical solution interpolating between both vacua is given as

$$\phi_{inst}(t) = \frac{1}{\sqrt{2}} \frac{m}{g} \text{sech}(mt), \quad (4.8)$$

where only x and t are exchanged with respect to the soliton solution in equation (3.5). We can associate an action to this instanton process in Euclidean time, since it is the crucial feature of instantons that they correspond to processes of finite action. Clearly, this is in contrast to solitons which were characterized as finite energy solutions. In the instanton case, we can determine the action simply by inserting the classical solution (4.8) in the Lagrangian (4.6):

$$S_{inst}^{(1)} = \frac{2m^3}{3g^2}. \quad (4.9)$$

The purpose of this chapter is to give a quantum understanding of the classical instanton solution. However, instead of directly defining a quantum coherent instanton state we want to implement the quantum picture by mapping the instanton on a corpuscularly resolved soliton we already presented in the previous chapter. Mainly, the reason why we follow this strategy is connected to the fact that it is not clear how to define a corpuscular algebra for

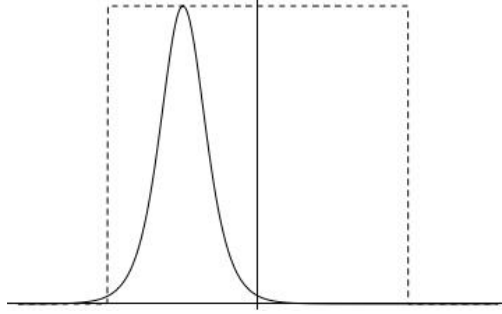


Figure 4.1: Non-topological Soliton evolving an euclidean distance L through a barrier. The dashed box represents the barrier, while the profile corresponds to the soliton. The soliton is created on the left side of the barrier and discharges again on the right side. Correspondingly, this virtual process describes the tunneling through the barrier in terms of the Euclidean motion of a soliton.

operators depending on Euclidean time. To circumvent this obstacle, we thus use a trick and connect the microscopically resolved soliton with the lower dimensional instanton.

At this point, let us discuss how to relate the 1 + 1 dimensional non-topological soliton to the non-topological instanton in 0 + 1 dimensions. Usually, when we downlift a theory to a lower dimensional theory, a certain length scale L is involved. It is basically given as the length scale on which the new theory is localized from the point of view of the higher dimensional theory. In particular, we need such a dimensional parameter because the fields and couplings have different canonical dimensions. In this sense, L allows to connect higher and lower dimensional entities.

In general, the concrete value of L is determined by the embedding procedure we use to localize the higher dimensional theory. This, however, requires to include new interactions in the higher dimensional theory. In this section we are simply interested in the mapping of the instanton on a soliton. Let us simply assume that there is some mechanism which achieves this for us and leads to a new scale L in the theory. In sections 4.1.3 and 4.1.4 we will discuss explicit embeddings and observe that L depends on the parameters of the localization.

Of course, the coupling constants in both theories have to satisfy a certain condition if we want to identify the instanton as a soliton tunneling through a barrier of width L (figure 4.1). Comparing the Lagrangians for the soliton (3.4) and the instanton (4.6), it follows

$$\frac{L}{\tilde{g}^2} = \frac{1}{g^2}, \quad (4.10)$$

in order to get the same profile for solitons and instantons. Note that the coupling of the higher dimensional theory is denoted as \tilde{g} . Consequently, we can relate the instanton and the higher dimensional soliton profile $\tilde{\phi}_{sol}$ via

$$\tilde{\phi}_{sol}(x) = \frac{1}{\sqrt{2}} \frac{m}{\tilde{g}} \operatorname{sech}(mx) = \frac{\phi_{inst}(t=x)}{\sqrt{L}}. \quad (4.11)$$

Similarly, we can relate the energy to the soliton profile with the action of the instanton

$$LE_{sol} = \frac{2m^3}{3\tilde{g}^2} = S_{inst}. \quad (4.12)$$

For reasons of completeness we will repeat the important steps to resolve the non-topological soliton using coherent states. We simply Fourier transform the classical solution

$$\tilde{\phi}_{sol}(x) = \sqrt{l} \int \frac{dk}{\sqrt{(2\pi)2|k|}} (e^{ikx} \alpha_k + e^{-ikx} \alpha_k^*), \quad (4.13)$$

and view the Fourier coefficients as expectation values of annihilation and creation operators $\hat{a}_k, \hat{a}_k^\dagger$ for the soliton corpuscles evaluated in the soliton state represented by a coherent state spanned by these operators. Of course, the Fock operators satisfy the standard algebra

$$[\hat{a}_k, \hat{a}_{k'}^\dagger] = \frac{1}{l} \delta(k - k'), \quad (4.14)$$

while the coherent state is simply given as

$$|sol\rangle = \prod_{\otimes k} e^{-\frac{1}{2}|\alpha_k|^2} e^{\alpha_k \hat{a}_k^\dagger} |0\rangle. \quad (4.15)$$

Defining the occupation number of these quanta in terms of the expectation values of the operators, we obtain

$$N_k = \langle sol | \hat{a}_k^\dagger \hat{a}_k | sol \rangle = \alpha_k^* \alpha_k = \frac{\pi |k|}{2} \frac{1}{g^2} \operatorname{sech}^2 \left(\frac{\pi k}{2m} \right). \quad (4.16)$$

Of course, the $\hat{a}_k, \hat{a}_k^\dagger$ are again Fock state operators for corpuscles and do not create and annihilate asymptotic quanta. This is reflected in the non-trivial dispersion and the zero frequency of the constituents. Correspondingly, these objects only exist inside such a bound state.

As in section 3.1.1, the total number of corpuscles is simply given as

$$N \equiv \int_k N_k = \int_k \alpha_k^* \alpha_k = \frac{m^2}{g^2} \left(\frac{\log(2)4}{2\pi} \right) \quad (4.17)$$

which reveals that most of the constituents have a momentum given by the inverse size of the soliton $k \lesssim m$. The finiteness of N is connected to the fact that the topological charge of this soliton is 0.

As it was advertized in the introduction of this chapter, we can understand the time-evolution of the coherent soliton state when we perform a Bogoliubov transformation of the Hamiltonian. Using the transformation (3.105), we arrive at the diagonal Hamiltonian of the Bogoliubov modes $\delta \hat{a}_k^\dagger$ and $\delta \hat{a}_k$

$$\hat{H} = E_{sol} + \sum_k \epsilon_k \delta \hat{a}_k^\dagger \delta \hat{a}_k. \quad (4.18)$$

Note that in the instanton case the $\hat{\delta}_k$ in equation (3.105) do not mix effectively for large momenta $|k| \gg m$ because in this regime the coefficients α_k are exponentially suppressed as

$$\alpha_k \sim \sqrt{N \frac{|k|}{m}} e^{-\pi \frac{k}{2m}} \ll 1. \quad (4.19)$$

Let us now evaluate how these results affect the classical instanton solution. For that purpose, we identify the soliton state $|sol\rangle$ evolving a Euclidean time interval L with the instanton, where the time evolution is given by the Hamiltonian (4.18). If we choose the time interval $\tau = iL$ to be small enough, we can neglect the second term in (4.18) such that the coherent state approximately evolves like an energy eigenstate. In fact, we can always choose mL to be small, while still keeping $N \sim m^2/\tilde{g}^2$ large. Thus, according to (4.18) to leading order the time evolution of the soliton can simply be computed by

$$\langle sol | e^{iH\tau} | sol \rangle \simeq e^{i \int_k N_k |k| \tau} = e^{iE_{sol}\tau} = e^{-E_{sol}L}. \quad (4.20)$$

Comparing with equation (4.9), this soliton amplitude exactly matches with the one of the instanton

$$\langle sol | e^{iH\tau} | sol \rangle |_{t=iL} = e^{-S_{inst}}. \quad (4.21)$$

Using the matching condition, we can easily reexpress the instanton action in terms of the occupation number of soliton constituents

$$S_{inst} = \int_k N_k L |k| = E_{sol}L. \quad (4.22)$$

As advertised in the introduction of this chapter, this shows how the instanton inherits the corpuscular substructure of the soliton when we establish a mapping between both objects. Similarly, we get $1/N$ -type quantum corrections to the instanton action when we consider the quantum corpuscular Hamiltonian. Nevertheless, the results are consistent with the classical ones to leading order.

As a remark, let us ask the question what happens if we completely downlift the theory meaning that we take the limit $L \rightarrow 0$. In this case, a lower dimensional observer can never detect the extra dimension because this would require an infinite amount of energy $\sim 1/L$. According to equation (4.22), in this limit the energy of the soliton diverges, $E_{sol} \rightarrow \infty$, while the instanton action S_{inst} is kept finite. Subsequently, any finite corpuscular quantum effects vanish because N_k diverges in this limit, even for finite momentum modes.

To summarize, we can only measure quantum corpuscular fluctuations of the instanton background localized in a higher dimensional theory where we could, in principle, detect the extra dimension by going to energies $\sim 1/L$.

4.1.2 Topological Instanton

In the same manner we established a quantum picture for the non-topological instanton, we can resolve the topological instanton by mapping it on a tunneling through topological

soliton. Due to this procedure, all the corpuscular features of the $1 + 1$ dimensional soliton are inherited by the lower dimensional instanton. As a consequence, the topology-energy split of corpuscles in the soliton case translates into two sets of corpuscular processes. One family is responsible for the topology of the instanton, while the other one accounts for the action of the classical instanton profile. In accordance with the soliton, the $k = 0$ pole of the occupation number leads to an infinite occupation number of zero momentum quanta which are responsible for a non-zero topological charge of the profile.

Let us make these statements computationally manifest. For that purpose, consider the $0 + 1$ dimensional theory containing a classical instanton solution

$$\mathcal{L}_{0+1} = (\partial_t \phi)^2 - g^2(\phi^2 - m^2/g^2)^2, \quad (4.23)$$

where $m > 0$ is the mass and $g > 0$ the coupling. Again, it is clear why we can relate this theory with the topological soliton in $1 + 1$ dimensions in section 3.1.2. The instanton Lagrangian (4.23) has the same structure as the one of the topological soliton in equation (3.28). In particular, it has the same interaction terms with equivalent signs leading to the same classical profile. In fact, both theories have the same vacuum structure, since the vacuum expectation values of ϕ are given as

$$\phi = \pm m/g \text{ for } t = \pm\infty. \quad (4.24)$$

In turn, the instanton in $0 + 1$ dimensions describes the tunneling from the vacuum $-m/g$ to the vacuum m/g . Depending on the starting vacuum, one either obtains the kink or the anti-kink solution

$$\phi_{inst}(t) = \pm \frac{m}{g} \tanh(tm), \quad (4.25)$$

which obviously interpolates between both vacua. Note, again, that this profile is basically the same as the one of the kink soliton (3.29). However, the instanton depends on Euclidean time instead of the spatial component x . As instantons are defined to be classical solutions of finite action in Euclidean time, we can associate an action with them:

$$S_{inst} = 8m^3/3g^2. \quad (4.26)$$

Now the reasoning is the same as for the non-topological instanton. It is a priori not clear how to define the corpuscular creation and annihilation algebra in Euclidean time. Therefore, we map the $0 + 1$ dimensional topological instanton on a $1 + 1$ dimensional soliton with a corpuscular resolution tunneling through a barrier of width L . The tunneling automatically implies that this is not a usual propagation, but a virtual process in Euclidean time.

For reasons of completeness, let us briefly present again the corpuscular description of the soliton. The dimensionally uplifted Lagrangian of the topological soliton is the same as in equation (3.28)

$$\mathcal{L}_{1+1} = (\partial_\mu \tilde{\phi})^2 - \tilde{g}^2(\tilde{\phi}^2 - m^2/\tilde{g}^2)^2, \quad (4.27)$$

where as explained above the localization scale L determines the relation between the higher dimensional coupling \tilde{g} and the lower dimensional one g . Obviously, the relation

is the same as in (4.10). Therefore, we can reexpress the classical soliton in terms of the lower dimensional solution when we identify $x = t$,

$$\tilde{\phi}_{sol}(x) = \pm \frac{m}{\tilde{g}} \tanh(xm) = \sqrt{L} \phi_{inst}(t = x). \quad (4.28)$$

Now we can implement the corpuscular philosophy by introducing a Fock algebra $\hat{a}_k, \hat{a}_k^\dagger$ whose expectation values in the standard coherent state $|sol\rangle$ given in (4.15) are identified with the Fourier coefficients α_k given in (3.30). Furthermore, we can decompose the algebra into two sets of annihilation and creation operators responsible for energy and topology of the soliton, respectively. Hence, we define

$$\begin{aligned} \alpha_k &= t_k c_k, \\ c_k &\equiv \sqrt{\pi m} \frac{k}{\tilde{g}} \operatorname{csch}\left(\frac{\pi k}{2m}\right), \\ t_k &\equiv \frac{i}{\sqrt{k}}, \end{aligned} \quad (4.29)$$

where c_k and t_k are the expectation values of the operators for the energetical and topological quanta, respectively. On the one hand, using these definitions we can determine the total energy of the soliton

$$E_{sol} = \int_k k \langle sol | \hat{a}_k^\dagger \hat{a}_k | sol \rangle = \int_k |c_k|^2 = \frac{8m^3}{3\tilde{g}^2}, \quad (4.30)$$

which is solely determined by the number of energetical quanta. On the other hand, the total occupation number diverges due to the presence of an infinite amount of zero momentum quanta

$$N = \int_k dk N_k \sim \int dk |t_k|^2 \sim -\log(k_0)|_{k_0 \rightarrow 0} \rightarrow \infty, \quad (4.31)$$

which is the reason why the topological charge is conserved. This can be seen when one calculates the overlap of the soliton state with the topological trivial vacuum

$$\langle 0 | sol \rangle = e^{-\frac{N}{2}} = 0. \quad (4.32)$$

Let us investigate the implications for the topological instanton viewed as such a soliton tunneling through. Obviously, the action of the instanton is simply given by the energy of the soliton times the distance which the soliton moves in Euclidean time. Subsequently, from equation (4.30) we observe that the action of the instanton can completely be attributed to the energetical quanta of the soliton.

$$S_{inst} = L \int \frac{dk}{m} c_k^* c_k = \frac{L8m^3}{3\tilde{g}^2} = \frac{8m^3}{3g^2}. \quad (4.33)$$

The energetical corpuscles of the higher dimensional soliton correspond to the corpuscles which are responsible for the action from the point of view of the instanton.

However, the topological charge of the instanton is created by an infinite occupation number of zero momentum quanta which do not contribute to the action of the instanton. In turn, from the quantum mechanical point of view the instanton is stable, since the overlap (4.32) vanishes.

As a remark, let us comment on the dispersion of the corpuscles. Since we introduced the resolution of the instanton by mapping it on a corpuscularly resolved soliton, it inherits all the features of the soliton, such as the corpuscular dispersion

$$\omega_k = |k| + \mathcal{O}(1/N) . \quad (4.34)$$

We can determine the corpuscular dispersion relation only to leading order in $1/N$ due to the fact that in the classical limit the BPS condition is satisfied. Nevertheless, we must keep in mind that the corpuscles are not asymptotic particles to whom we can associate a free dispersion. Instead, they only appear as interaction eigenstates inside a bound state.

4.1.3 Explicit Embedding of an Instanton I

Having established a mapping between the $0 + 1$ dimensional instanton and the $1 + 1$ dimensional soliton by introducing a new scale, let us now discuss the second important aspect of this chapter. Namely, how we can dynamically embed the instanton theory in the higher dimensional soliton theory. We will call the observer of the $0 + 1$ dimensional theory Alice. Bob's theory is the $1 + 1$ dimensional one. Note that in this framework we will be able to explicitly determine the length scale L we had to introduce in order to relate the couplings of the instanton and the soliton theory.

As a first example of an explicit embedding, let us consider the action

$$\begin{aligned} \mathcal{L}_{1+1} &= \partial_\mu \chi \partial^\mu \chi + \partial_\mu \tilde{\phi} \partial^\mu \tilde{\phi} - f^2 \chi^2 \left(\chi - 2\frac{\mu}{f} \right)^2 \\ &\quad - \frac{\tilde{g}^2}{2} \tilde{\phi}^4 + M^2 \tilde{\phi}^2 - \beta^2 \chi^2 \tilde{\phi}^2 - \frac{M^4}{2g^2} . \end{aligned} \quad (4.35)$$

Here the different couplings \tilde{g} , f , β and the masses μ and M are positive. For the moment, let us neglect the field $\tilde{\phi}$ which eventually will describe the soliton tunneling through and analyze the background field χ . Clearly, χ has two degenerate minima $\chi = 0$ and $\chi = 2\frac{\mu}{f}$ in this case. We can distinguish two different types of kink solutions interpolating between the vacua given as

$$\chi(x) = \frac{\mu}{f} (1 \pm \tanh(\mu x)) , \quad (4.36)$$

where the $+$ sign corresponds to the solution interpolating between 0 on the left and $2\mu/f$ on the right, while the $-$ sign denotes the solution where the 0 vacuum is on the right hand side. Obviously, the first situation is a kink, while the other one is an anti-kink.

We are interested in creating a barrier of $\chi = 0$ vacuum between the $\chi = 2\mu/f$ vacua as it is depicted in figure 4.2. This set-up generates an energetically forbidden wall for the $\tilde{\phi}$ soliton. Correspondingly, we design a configuration where a kink and an anti-kink are separated by a distance L such that

$$\chi(x < 0) = \chi(x > L) = 2\frac{\mu}{f} \text{ and} \quad (4.37)$$

$$\chi(0 < x < L) = 0. \quad (4.38)$$

As a next step, we investigate the field $\tilde{\phi}$ field in this χ -background. In particular, we study the decoupling limit

$$\beta \rightarrow 0, \quad \frac{\mu}{f} \rightarrow \infty \text{ with } \beta\frac{\mu}{f} \text{ fixed,} \quad (4.39)$$

where we can neglect the back-reaction of the $\tilde{\phi}$ on the χ -configuration. As explained above, we want the $\tilde{\phi}$ soliton solution only to exist inside the barrier in order to describe tunneling, while outside of the barrier the classical vacuum should be $\tilde{\phi} = 0$. Thus, on the one hand we choose $2\beta^2\mu^2/f^2 - M^2 > 0$ such that asymptotically the $\tilde{\phi}$ -quanta have an effective mass $M_{\tilde{\phi}}^2 = 2\beta^2m^2/f^2 - M^2 > 0$.

On the other hand, the $\tilde{\phi}$ quanta should condense in the barrier region $0 < x < L$ such that the effective mass $M_{\tilde{\phi}}$ becomes negative in this region. In other words, $\tilde{\phi}$ exhibits the vacuum expectation values

$$\tilde{\phi} = \pm \frac{M}{\tilde{g}}. \quad (4.40)$$

This means that the \mathbb{Z}_2 symmetry $\tilde{\phi} \rightarrow -\tilde{\phi}$ is broken spontaneously. We can trust these approximations only for $L \gg M^{-1}, M_{\tilde{\phi}}^{-1}$ or in other words when we can neglect the effects of the walls of the layer.

There is a classical kink solution for $\tilde{\phi}$ connecting the two vacua inside the layer. However, we can only determine it analytically in the limit $L \rightarrow \infty$, where it takes the usual form

$$\tilde{\phi}(x) = \pm \frac{M}{\tilde{g}} \tanh(Mx/\sqrt{2}). \quad (4.41)$$

The configuration is topologically stable in this limit. To summarize, only in the region $0 < x < L$ we obtain a classical soliton solution for $\tilde{\phi}$ approximated by (4.41). Outside of the layer for $x < 0$ and $x > L$, $\tilde{\phi}$ vanishes. The topology for $\tilde{\phi}$ is trivial in this region. As a consequence, we can create a kink on the left side of the layer at $x = 0$ and let it evolve to the right side at $x = L$ where it gets discharged. Thus, the global charge which Bob observes is zero. Note that this is a process in Euclidean time, since we need virtual energy to create the soliton. A low energy observer Alice on this layer would observe a vacuum transition $\frac{-M}{\tilde{g}} \rightarrow \frac{M}{\tilde{g}}$ when the soliton passes by. Now the crucial point is simply

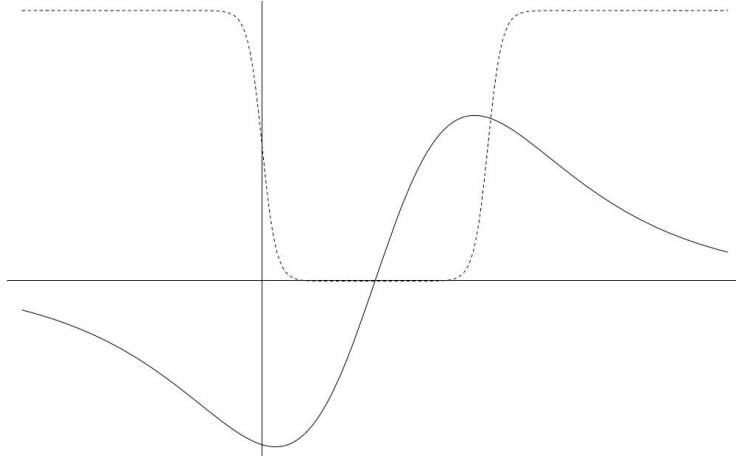


Figure 4.2: The dashed line represents the background kink-anti-kink layer created by the background field χ . The straight line corresponds to the solitonic excitation of $\tilde{\phi}$ on the background. For a large layer thickness L , this configuration is well approximated by a standard kink.

that Alice interprets this effect as an instanton because she cannot resolve the additional spatial dimension.

To make the emergence of the lower dimensional theory manifest, we perform a mode analysis of the $\tilde{\phi}$ -field on the $\chi(x)$ background. Consider the linearized equation of motion for $\tilde{\phi}$,

$$\left(\partial_\mu\partial^\mu + (\beta^2\chi(x)^2 - M^2)\right)\tilde{\phi} = 0. \quad (4.42)$$

If we decompose $\tilde{\phi}(x, t) = \psi(x)\phi(t)$ with $\partial_t^2\phi(t) = -m^2\phi(t)$, the equation for $\psi(x)$ which describes the soliton profile in spatial direction becomes

$$\left(\partial_x^2 - \left(\beta^2\chi(x)^2 - M^2 - m^2\right)\right)\psi(x) = 0. \quad (4.43)$$

Here $\chi(x)$ represents the kink-anti-kink configuration separated by a distance L . If we consider an appropriate range of parameters, we clearly obtain a localized finite norm solution with negative m^2 . Note that $\psi(x)$ is approximately constant inside the region $0 < x < L$ and drops to zero exponentially fast for $x < 0$ and $x > L$. Normalizing it to one, $\int dx \psi(x)^2 = 1$, it follows for large L

$$\psi(x)^2 \simeq 1/L \quad \text{for } 0 < x < L. \quad (4.44)$$

To obtain Alice's effective lower dimensional theory, we have to simply integrate over x ,

$$\mathcal{L}_{0+1} = (\partial_t\phi)^2 - m^2\phi^2 - \frac{g^2}{2}\phi^4. \quad (4.45)$$

Here we used $g^2 = \tilde{g}^2 \int dx \psi(x)^4$. Comparing with equation (4.44) for large L , we now observe how L emerges in this framework. It is given as $1/L = \int dx \psi(x)^4$.

Let us now discuss the physics which are implied by this model. Obviously, the \mathbb{Z}_2 symmetry $\tilde{\phi} \rightarrow -\tilde{\phi}$ is spontaneously broken in Alice's effective theory (4.45) (valid at energies $\ll 1/L$), while from Bob's 1+1 dimensional point this symmetry is restored outside of the barrier. The lower dimensional field ϕ develops two different vacuum expectation values $\phi = \pm \frac{m}{g}$ in the layer as the soliton passes by. This spontaneous transition between the vacua in Euclidean time is described by an instanton from Alice's point of view.

However, for Bob the situation looks different. For him a soliton spontaneously emerges on the left side of the layer, travels through it and discharges on the right side. Thus, this set-up, indeed, allows us to identify the 1+1 dimensional solitonic origin of 0+1 dimensional instantons.

To summarize, the physical situation is the following. On the one hand, outside of the barrier $\tilde{\phi}$ -quanta are not condensed, while from the solitonic point of view there exists a vacuum condensate of $\tilde{\phi}$ -solitons. On the other hand, in the world-volume theory of $\chi = 0$, $\tilde{\phi}$ -quanta are condensed, but solitons are on-shell. Note that the solitons inside the layer are not exactly stable for finite L , since the boundary conditions have to stay trivial. Nevertheless, the solitons can exist as long-lived states. As a consequence, they virtually cross the layer, emerging from the condensate on one side of the layer and discharging in the opposite condensate. This phenomenon is interpreted as an instanton effect switching the vacuum from Alice's lower dimensional point of view. The soliton has to survive at least the Euclidean time interval corresponding to the width of the layer L . In fact, this is the reason why we have to use L to match the couplings on both sides of the mapping. The amplitude of the tunneling is given in equation (4.21).

4.1.4 Explicit Embedding of an Instanton II

To further clarify the subject, let us investigate a slightly different model of dynamical embedding. In contrast to the previous model in section 4.1.3, in this case we will be able to explicitly determine the profile of the soliton tunneling through. In turn, this means that we can express the localization scale L explicitly in terms of the parameter of the uplifted theory.

The strategy we follow is the same as in the previous section. First, we will start from the 1+1 dimensional theory of Bob. Then we will investigate how Alice's 0+1 dimensional theory emerges from this theory in a low energy limit. Consider the model

$$\begin{aligned} \mathcal{L}_{1+1} &= \partial_\mu \chi \partial^\mu \chi + \partial_\mu \tilde{\phi} \partial^\mu \tilde{\phi} - f^2 \left(\chi^2 - \frac{\mu^2}{f^2} \right)^2 \\ &\quad - \frac{\tilde{g}^2}{2} \tilde{\phi}^4 + M^2 \tilde{\phi}^2 - \beta^2 \chi^2 \tilde{\phi}^2 . \end{aligned} \quad (4.46)$$

Here the different masses μ^2 and M^2 are positive as well as the couplings f , β and \tilde{g} . This

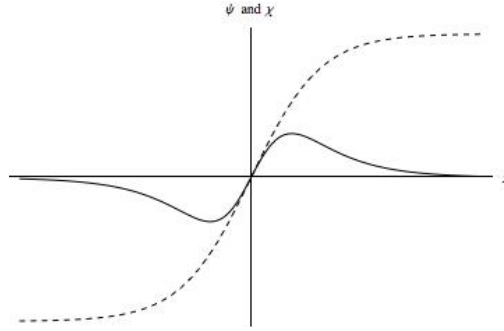


Figure 4.3: The dashed profile corresponds to the background χ . In the transition region of χ the ψ profile representing the $\tilde{\phi}$ soliton is different from 0. In particular, the maxima of ψ are given by $\pm \frac{m}{g}$. As a consequence, Alice observes the transition $-\frac{m}{g} \rightarrow \frac{m}{g}$ when the profile passes her.

theory has a classical background kink solution given by

$$\chi(x) = \pm \frac{\mu}{f} \tanh(\mu x), \quad (4.47)$$

which is not the solitonic kink we want to resolve, but the classical background field we introduce in order to create a barrier where Alice is localized on. Note that the main difference between this model and the previous model in section 4.1.3 is given by the different structure of the background (compare (4.36) with (4.47)). Like in the previous subsection, we introduce the background field to restrict the soliton we are interested in to a certain region of space. Thus, already at this point we would expect that the Euclidean distance should scale as $L \sim 1/\mu$. The situation is depicted in figure 4.3 which makes the difference to the previous model manifest (compare with figure 4.2).

The soliton which is eventually interpreted as an instanton by the low energy observer Alice is the $\tilde{\phi}$ field. Therefore, we chose the notation in accordance with the previous section. As a side remark, let us mention that in principle we could resolve the background kink χ as well, but this would not directly affect the instanton.

Assuming that $\tilde{\phi}$ is only a small correction with respect to χ , we can determine the equation of motion for the soliton to linearized order as

$$\left(\partial_\mu \partial^\mu + (\beta^2 \chi(x)^2 - M^2) \right) \tilde{\phi} = 0. \quad (4.48)$$

To determine the solution for $\tilde{\phi}$, we work in the limit where the back-reaction of $\tilde{\phi}$ on the background kink χ can be neglected. This is achieved by considering, again, the decoupling limit

$$\beta \rightarrow 0, \quad \frac{\mu}{f} \rightarrow \infty \quad \text{with } \beta \frac{\mu}{f} \text{ fixed.} \quad (4.49)$$

Since we want $\tilde{\phi}$ to be localized on the center of the background kink, we have to make sure that it falls off to 0 for $x \rightarrow \pm\infty$. Comparing with the equation of motion (4.48), this

is achieved when the condition

$$\frac{\beta^2}{f^2}\mu^2 - M^2 > 0 \quad (4.50)$$

is satisfied. It follows that the $\tilde{\phi}$ -quanta have positive effective mass $M_{\tilde{\phi}}^2 = \beta^2/f^2\mu^2 - M^2$ far from the kink. As a consequence, $\tilde{\phi}$ has its classical vacuum at $\tilde{\phi} = 0$. Obviously, this means that the soliton is only non-vanishing in the center of the background kink.

Having localized $\tilde{\phi}$ soliton on the kink, we have to choose the remaining parameters in such a way that there is a soliton solution for the field $\tilde{\phi}$ we want to relate to the instanton. In the center of the background kink where the profile interpolates between the two different χ vacua, we cannot approximate $\beta^2\chi(x)^2 - M^2$ anymore by a constant. To solve the differential equation for $\tilde{\phi}$, we separate the variables and decompose

$$\tilde{\phi}(x, t) = \psi(x)\phi(t) , \quad (4.51)$$

with $\partial_t^2\phi(t) = -m^2\phi(t)$. Note that $\phi(t)$ is the scalar field of the lower dimensional theory. The differential equation for the spatial profile of the soliton is given as

$$0 = \left(\partial_x^2 - \left(\beta^2 \frac{\mu^2}{f^2} \tanh^2(\mu x) - M^2 - m^2 \right) \right) \psi(x) . \quad (4.52)$$

In the allowed parameter range there is only one possible solution for ψ in (4.52). It is given as

$$\psi(x) = \sqrt{\frac{3\mu}{2}} \sinh(\mu x) \cosh^{-2}(\mu x) . \quad (4.53)$$

Inserting (4.53) in (4.52), it follows that this is only a valid solution for ψ when $\beta^2/f^2 = 6$ is satisfied. The normalization of ψ is given by $\int dx \psi(x)^2 = 1$.

Let us clarify the meaning of the classical solution $\psi(x)$ for the spatial part of $\tilde{\phi}$. It corresponds to the soliton profile which is passing by from Bobs's point of view. Its mass is given as

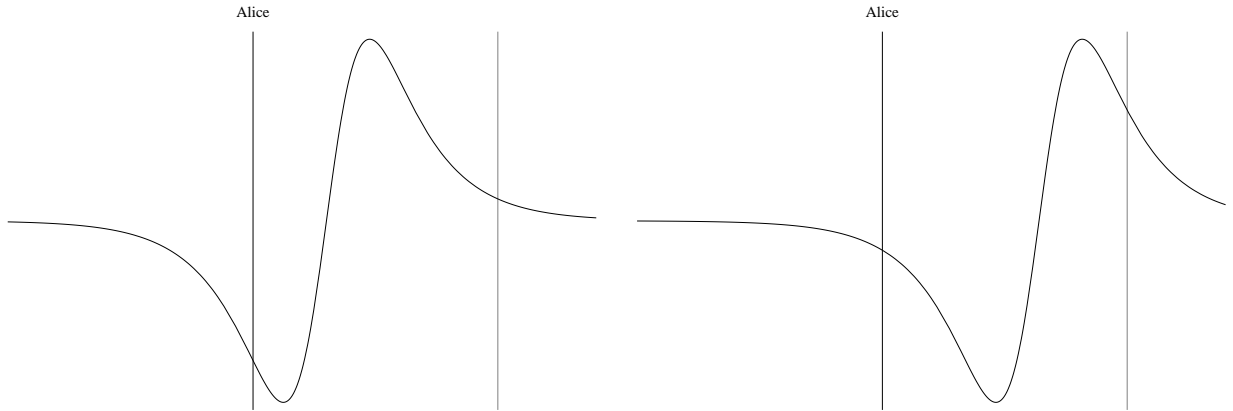
$$m^2 = 5\mu^2 - M^2 . \quad (4.54)$$

To evaluate the situation from Alice's point of view, we need to restrict to one less dimension, since Alice cannot resolve the spatial direction. Integrating the soliton profile ψ along the spatial direction, we arrive at Alice's Lagrangian

$$\mathcal{L}_{0+1} = (\partial_t\phi)^2 - m^2\phi^2 - \frac{g^2}{2}\phi^4 . \quad (4.55)$$

At this point, the length scale L which connects both theories comes into play. L automatically arises when integrating over the soliton profile,

$$\frac{1}{L} = \int dx \psi(x)^4 = \frac{9}{35}\mu . \quad (4.56)$$



(a) The soliton emerges on the left side of the barrier. (b) The soliton propagates through the barrier in Euclidean time.

Figure 4.4: In both figures the ψ profile is depicted, but at different times. The profile moves across the transition region of the χ background kink and passes Alice. Alice measures a vacuum expectation value $\phi = -m/g$ when the minimum of the soliton profile passes her, while she observes $\phi = m/g$ when the maximum is passing by. This means that Alice measures a sign flipping of the vacuum expectation values. Since Alice cannot resolve the spatial extension, she interprets this effect as an instanton.

Accordingly, the lower dimensional coupling is related to the higher dimensional one via the same relation as in (4.1), $g^2 = \tilde{g}^2/L$. In order to obtain a kink instanton solution for ϕ , $m^2 < 0$ has to hold in equation (4.54). Combining this condition with the bound given in equation (4.50) we can determine the allowed parameter range for M^2

$$5\mu^2 < M^2 < 6\mu^2 . \quad (4.57)$$

In other words, in this parameter regime we obtain the wanted soliton solution localized on the kink without destabilizing the $\tilde{\phi} = 0$ -vacuum outside of the center of the χ -kink.

Let us now comment on the physical interpretation of this model. We start presenting the process from Bob's higher dimensional point of view. For him on the left side of the transition area of the background kink the $\tilde{\phi}$ soliton with the profile in spatial direction given by ψ can spontaneously emerge from the $\tilde{\phi} = 0$ vacuum at $x \rightarrow -\infty$. Obviously, this is a process with virtual energy. In fact, this is a necessary condition in order to interpret the propagation of the soliton as an instanton effect. The Euclidean distance the soliton has to travel through is given by the characteristic length scale of the kink $1/\mu \sim L$. After passing this region, the soliton relaxes and condenses to its $\tilde{\phi} = 0$ vacuum expectation value again.

For Alice the situation looks different. She effectively lives in a $0 + 1$ dimensional theory without spatial extension, since she is localized in x -direction on a scale L . Thus, she only has $0 + 1$ dimensional quantum mechanics given by the Lagrangian (4.55) to describe the situation from her point of view. From figure 4.4, we observe that the passing by of a soliton in her theory corresponds to a flip of the field values. When the soliton

is passing the background kink, Alice observes that $\phi \rightarrow -\phi$ spontaneously. Since she does not know about the higher dimensional theory, she naturally interprets this effect as an instanton allowing for a tunneling between the both vacua $\phi = \pm m/g$ of her theory. Correspondingly, she observes that the \mathbb{Z}_2 symmetry of her theory is spontaneously broken due to the non-trivial vacuum structure.

Notice that when we resolve the $\check{\phi}$ field into corpuscles, it directly follows that the instanton $\phi(t)$ knows about the quantum structure as well. Of course, this is exactly what we wanted in order to establish a quantum understanding for instantons.

As a remark, we have to mention that the virtual soliton passing by is not long lived. It condenses to the vacuum after the Euclidean time $\sim iL$.

To summarize this section, we were able to present a concrete $1 + 1$ dimensional model where a soliton configuration passing by is interpreted as an instanton process by a low energy observer Alice. This soliton propagation occurs in Euclidean time, since the process is energetically forbidden from the classical point of view. The amplitude for this transition was determined in equation (4.21).

4.2 Gauge Instanton as Tunneling Monopole

So far we only discussed the rather trivial instanton in $0 + 1$ dimensional quantum mechanics, but of course we can apply the method presented above to more sophisticated objects. Therefore, let us consider in this section a $2 + 1$ dimensional $U(1)$ gauge theory. The purpose of this section is to investigate a concrete model to represent the instanton arising in this theory as a $3 + 1$ dimensional monopole tunneling through a energetically forbidden barrier. The semi-classical magnetic monopole was already discussed in section 1.4.3.

The higher dimensional theory is given as a $SU(2)$ gauge theory coupled to a Higgs triplet Φ^a , $a = 1, 2, 3$ in the adjoint representation. This is the usual setting containing monopoles as described in section 1.4.3. When the scalar field acquires a non-zero expectation value and correspondingly $SU(2)$ breaks spontaneously down to $U(1)$, a non-trivial vacuum structure arises allowing for monopole solutions. As mentioned above, these monopoles should propagate through a barrier as a virtual process in order to be interpreted as an instanton by a low energy observer in the barrier. Thus, in contrast to the usual monopole set-up, we want the monopoles to be localized only in this region of width L . The monopole solution should only exist there, while it should be 0 elsewhere. As a consequence, we need a non-trivial vacuum structure which only breaks $SU(2)$ inside the barrier,

$$\begin{aligned} \langle \Phi^a \rangle &\neq 0 \text{ for } z \in [0, L], \\ \langle \Phi^a \rangle &= 0 \text{ everywhere else.} \end{aligned}$$

We have to extend the usual monopole model in section 1.4.3 in order to arrive at this vacuum structure. This can be done easily by including wall and anti-wall solutions in the theory. According to sections 4.1.3 and 4.1.4, with such a model we can construct a

barrier of width L where the boundaries of the barrier are given by a wall and an anti-wall, respectively.

At this point, let us be more explicit and consider the model studied in [96, 97]¹ with the Higgs potential

$$\mathcal{L}_{SU(2)} = |D_\mu \Phi^a|^2 - G_{\mu\nu}^a G^{a\mu\nu} - \lambda^2 \frac{\Phi^a \Phi^a}{v^2} (\Phi^b \Phi^b - v^2)^2, \quad (4.58)$$

where λ is the scalar self-coupling and v the vacuum expectation value of Φ^a . The field strength $G_{\mu\nu}^a$ and the covariant derivative D_μ are defined as in (1.80) and (1.81), respectively. This model exhibits the wanted vacuum structure $\langle \Phi^a \rangle = \delta_3^a v$ and $\langle \Phi^a \rangle = 0$. We consider solutions where the vacuum region $\langle \Phi^a \rangle = \delta_3^a v$ is restricted to a layer of width L . As a consequence, there should be two domain walls which interpolate between the two different vacua. Note that the layer is infinitely extended in the $x - y$ plane. The corresponding profile for the scalar field is given by

$$\Phi^a = f_\pm(z) \delta_3^a v, \quad (4.59)$$

$$f_\pm(z) = \frac{e^{\pm 2mz}}{1 + e^{\pm 2mz}}, \quad (4.60)$$

where the mass parameter is given as $m \equiv \lambda v$. The (+) solution corresponds to a wall, while (−) denotes the anti-wall. We are interested in manufacturing a set-up where a wall lies at $z = 0$ and an anti-wall at $z = L$ is parallel to the wall. Correspondingly, for $L \gg 1/m$ the solution is of the form

$$\Phi^a = \frac{1}{2} (f_+(z) + f_-(z - L)) \delta_3^a v. \quad (4.61)$$

This profile is depicted in figure 4.5. So far we presented a special wall-anti-wall setting such that Φ^a acquires a non-zero expectation value in a layer of width L . As mentioned above, this leads to a spontaneous breaking of the $SU(2)$ gauge symmetry inside the layer. In other words, the theory is in the confining phase outside this barrier, while it is in the Coulomb phase for $0 < z < L$ leading to monopole solutions inside the layer.

To understand this model more properly, let us discuss its physical implications. Namely, let us consider the $U(1)$ -photon inside the layer. Classically, it can leave the layer and enter the regime $\langle \Phi^a \rangle = 0$. Obviously, this is no longer possible on the quantum level (at the moment by quantum we refer to loop corrections, but not to any microscopic resolution of the background) because in the confining phase outside the barrier a mass gap is dynamically generated for the vector field. Naturally, the gap is given by the QCD scale Λ_{QCD} . As a consequence, the photons can only leave the layer when they form glueballs of this particular mass. Like the magnetic monopoles, the photons are trapped inside the layer formed by the wall and the anti-wall.

Let us turn to the monopole. In the confining phase, the magnetic charge of a monopole would get screened due to the non-abelian self-interaction of the vector fields. In other

¹Similar models are also discussed in [98, 99, 100].

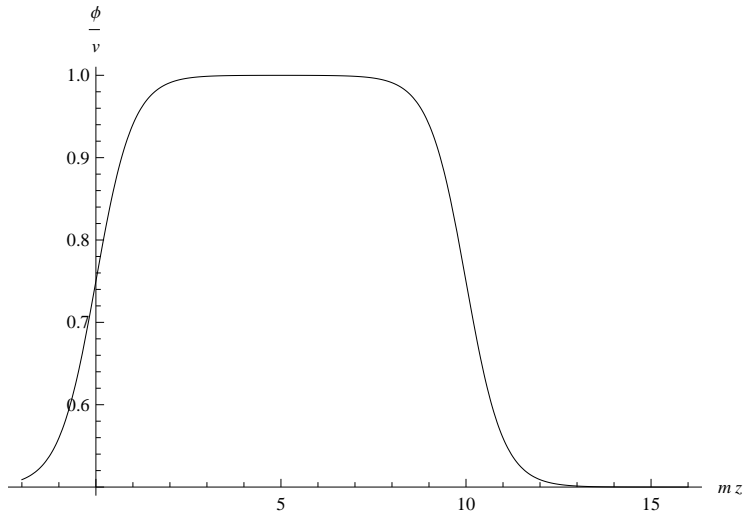


Figure 4.5: Wall-anti-wall profile with $L = 10/m$. $\Phi^a = 0$ outside the layer, while inside the barrier it acquires the expectation value $\Phi^a = \delta_3^a v$.

words, the monopoles condense in the $SU(2)$ phase such that they are not observable. However, inside the layer the situation is completely different. As can be seen in figure 4.6, 't Hooft-Polyakov type monopoles similar to the ones presented in section 1.4.3 can exist inside the wall-anti-wall configuration.

Correspondingly, we observe a similar situation as in the previous section only for two additional transverse dimensions. A soliton given by a magnetic monopole passes through a region of size L and condenses when leaving the layer. Obviously, for a lower dimensional observer Alice which is localized on the layer this situation exactly looks like a Polyakov instanton. Note that this is only true as long as Alice does not resolve the extra dimension by going to energies $E > 1/L$. In particular, we assume the following hierarchy of scales

$$m_W \gg \Lambda_{QCD} \gg L^{-1} \quad (4.62)$$

for which the mass of the W-boson m_W is larger than the glueball mass Λ_{QCD} . With this hierarchy in mind, let us investigate the different energy regimes for Alice. In the case $\Lambda_{QCD} > E > L^{-1}$, Alice can in principle resolve the layer, but the photon still cannot leave because it is simply not energetic enough to form a glueball of sufficient mass. This means that Alice still observes a 3 + 1-dimensional theory. However, in the energy interval $E \ll L^{-1}$ she effectively only observes a 2 + 1-dimensional theory on the layer. As long as we stay in the regime $\Lambda_{QCD} \gg L^{-1}$, where the $U(1)$ photons cannot leave the layer, the gauge couplings for the higher and lower dimensional theory \tilde{g} , g are related by $1/g^2 = L/\tilde{g}^2$ as before.

To understand in which limit we can trust the monopole approximation, we localize for instance a monopole in the middle of the layer at $z = L/2$. It is creating magnetic image charges outside the layer leading to an exponentially decreasing magnetic field for $|x|^2 + |y|^2 \gg L$. Note that this is even the case for the direction parallel to the layer.

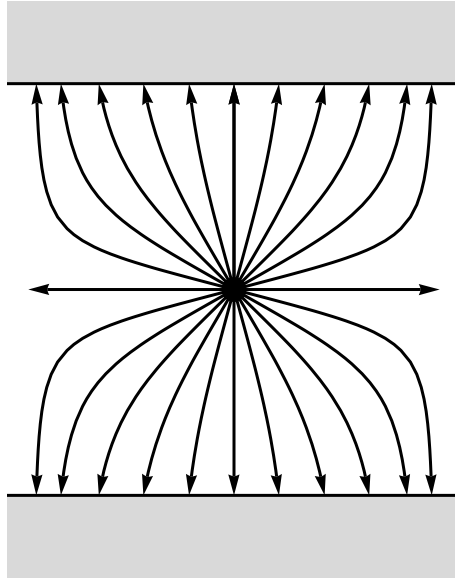


Figure 4.6: The white region depicts the Higgs phase, while the grey regions correspond to the surrounding confining phases. Inside the Higgs phase, magnetic point charges can exist. The magnetic field of these charges is screened at large distances. Since there exist magnetic mirror charges on both sides of the layer, this is even the case in the direction longitudinal to the Higgs phase layer.

The situation is depicted in figure 4.6. Clearly, we can safely trust the 't Hooft-Polyakov monopole solution near the center of the monopole for large L .

Having discussed the different regimes of the model, let us now consider the tunneling process of a virtual monopole through the layer. In the confining phase, where $SU(2)$ is unbroken, monopoles cannot exist. However, they can form at the boundary of the Higgs phase layer. Naively, one could argue that such a process should violate the conservation of the topological charge, but one has to keep in mind that the magnetic charge gets totally screened in the confining phase. The boundaries behave similar to an electric capacitor. They can be discharged and charged with an infinite amount of magnetic charge. Therefore, monopoles can only emerge and condense at the boundaries. Only in the limit $L \rightarrow \infty$ the monopoles have a topological charge and are consequently stable.

Of course, the emergence of a monopole in the layer is a virtual process because the monopole mass can be interpreted as a potential barrier from the confining phase point of view. Correspondingly, we are really describing a monopole tunneling through this potential barrier of width L .

Similar to the $1 + 1$ dimensional example discussed before, a low energetic observer Alice ($E < 1/L$) located inside the layer will not be able to observe the virtual monopole emerging on one side of the layer and discharging on the other. Instead, from Alice's point of view an instanton process in an effective $2 + 1$ -dimensional theory occurs. This instanton describes the tunneling between two different prevacua of the total θ -vacuum.

The Euclidean action Alice associates with this process is to leading order approximated simply as the monopole mass times the Euclidean time interval $\tau = L$ the monopole needs to evolve through the layer. Thus, the action amounts to

$$S = M_{sol}L . \quad (4.63)$$

Of course, this is exactly the instanton action in 2 + 1 dimensions with the usual matching of the coupling constants as in (4.10).

Notice that it is rather surprising that the time evolution of a 3 + 1-dimensional virtual monopole exactly corresponds to a lower dimensional instanton in this special case because both situations are described most accurately in completely opposite limits. On the one hand, in the $L \rightarrow 0$ limit Alice's theory becomes truly 2 + 1 dimensional. On the other hand, the 't Hooft-Polyakov monopole approximation is only valid for $|x|^2 + |y|^2 \ll L$. Therefore, the $L \rightarrow \infty$ limit is working best for the higher dimensional theory. However, we have to be careful, since the 2 + 1 dimensional theory is, in some sense, always 'aware' of its higher dimensional UV completion. In particular, the higher dimensional vector boson mass M_W determines the size of the lower dimensional instanton, while the localization scale is set by $L^{-1} < M_W$. Correspondingly, we cannot simply consider the $L \rightarrow 0$ limit.

4.3 Instantons in 3 + 1 dimensions

4.3.1 3 + 1 dimensional Instanton in a Scalar Field Theory

Before considering the mapping of a BPST instanton in 3+1 dimensional Yang-Mills theory on a higher dimensional monopole, let us turn to a similar, but much simpler scalar model in 3 + 1 dimensions [101]. For that purpose, consider the Lagrangian

$$\mathcal{L} = \partial_\mu \phi \partial^\mu \phi - g^2 \phi^4 . \quad (4.64)$$

Obviously, the theory has a similar classical saddle point solution in Euclidean time like the instanton in Yang-Mills theory. However, since this is still a scalar theory, we circumvent problems which are related to the gauge field in non-abelian gauge theories. In this toy model, we obtain a clearer understanding how the dependence on the size modulus arises for the 3 + 1 dimensional instanton in the quantum corpuscular treatment.

Following our logic, we map the scalar instanton process on a 4 + 1 dimensional soliton tunneling through a localized region of space-time viewed by a low energy observer. The classical instanton solution to (4.64) is given as

$$\phi_{inst}(x) = \frac{2\rho}{g(\rho^2 + x^2)} , \quad (4.65)$$

where we have set the instanton center to $x_0 = 0$. Although the profile depends on the instanton size ρ , the theory nevertheless still exhibits a scale invariance. On the classical level, ρ is simply a modulus of the theory. In other words, the instanton size is arbitrary.

Clearly, this is quite different to the previous models, where the instanton size was set by the mass parameter of the theory. Naturally, one could ask if the scale invariance is preserved when we implement a quantum resolution of the instanton. To investigate this question, we consider a soliton in the $4 + 1$ dimensional uplifted theory

$$\mathcal{L} = \partial_\mu \tilde{\phi} \partial^\mu \tilde{\phi} - \tilde{g}^2 \tilde{\phi}^4, \quad (4.66)$$

where the couplings in equations (4.64) and (4.66) are related via $\frac{1}{g^2} = \frac{l}{\tilde{g}^2}$ to establish the mapping. Fourier expanding the corresponding soliton solution, we obtain

$$\tilde{\phi}_{sol}(x) = \int d^4k \frac{l^2}{\sqrt{(2\pi)^4 2\omega(k)}} \left(\alpha_k e^{-ikx} + \alpha_k^\dagger e^{ikx} \right). \quad (4.67)$$

Here the Fourier coefficients are given as

$$\alpha_k = \frac{\rho^2 \sqrt{2\omega(k)}}{l^2 \tilde{g}} \left(\frac{1}{k} K_1(\rho k) \right) \quad (4.68)$$

with K_1 the modified Bessel function of the first kind. Promoting these coefficients to expectation values of Fock operators $\hat{a}_k^\dagger, \hat{a}_k$ spanning a Hilbert space of soliton corpuscles, we can define the occupation number density in each mode as

$$N_k = \langle sol | \hat{a}_k^\dagger \hat{a}_k | sol \rangle = \frac{\rho^4 2\omega(k)}{l^4 k^2 \tilde{g}^2} [K_1(\rho k)]^2. \quad (4.69)$$

Of course, the soliton state $|sol\rangle$ is defined as in equation (4.15), however, with α_k given in equation (4.68). Defining the dimensionless quantity $u = k\rho$, we can express the total occupation number of this soliton as

$$\begin{aligned} N &= l^4 \int d^4k \langle sol | \hat{a}_k^\dagger \hat{a}_k | sol \rangle = l^4 2\pi^2 \int d|k| |k|^3 |\alpha_k|^2 \\ &= \frac{4\pi^2 \rho}{\tilde{g}^2} \int du u \tilde{\omega}(u) [K_1(u)]^2. \end{aligned} \quad (4.70)$$

For this special case we cannot determine the dispersion relation ω_k as easily as before even to leading order. This is related to the fact that the classical Hamiltonian is not diagonalized by this solution on the classical level. However, from our previous examples it should be clear that the total occupation number should be finite, since this soliton is topologically trivial.

Although we cannot calculate N in this example, we can still determine how it scales with the classical modulus ρ . According to equation (4.70), $N \propto \rho$ which is not surprising. Clearly, the total number of constituents should increase with the size of the corresponding bound state. Consequently, ρ is not a modulus from the quantum point of view. In particular, corpuscular loop corrections to the classical results depend on ρ such that the size invariance is broken on the quantum level. In other words, the symmetry is anomalous

when we introduce a corpuscular resolution. Note that most of the soliton mass is, of course, contributed by corpuscles of wavelength given by the soliton size ρ , while the mass behaves as $M_{sol} \sim N/\rho$.

As in the previous examples, we can map the corresponding 3+1 dimensional instanton on a virtual propagation of this soliton. As a consequence, the instanton inherits the same properties as the soliton.

4.3.2 BPST-Instanton

As advertized in section 4.3.1, we now consider the more complicated situation of a BPST instanton in 3 + 1 dimensional Yang-Mills theories. In contrast to the previous models we considered, the instanton in this theory does not correspond to a scalar profile. Instead, the BPST instanton is a saddle point solution to the Euclidean path integral for a gauge field A_μ^a . Nevertheless, as we will show here we can follow the same strategy as for the scalar instatons. Notice that the BPST instanton describes a tunneling process between the different prevacua of Yang-Mills.

To be more explicit, let us consider the 3 + 1 dimensional $SU(2)$ Yang-Mills theory presented in section 1.5.2. For completeness let us briefly review the main features of this model. The corresponding Euclidean action is similar to equation (1.94),

$$S = \int d^4x \frac{1}{4} G_{\mu\nu}^a G_{\mu\nu}^a = \frac{1}{8} \int d^4x (G_{\mu\nu}^a - \tilde{G}_{\mu\nu}^a)^2 + Q \frac{8\pi^2}{g^2}, \quad (4.71)$$

where $G_{\mu\nu}^a = \partial_\mu A_\nu^a - \partial_\nu A_\mu^a + g f^{abc} A_\mu^b A_\nu^c$ is the non-abelian field strength as given in section 1.5.2, while $\tilde{G}_{\mu\nu}^a = 1/2 \epsilon_{\mu\nu\alpha\beta} G_{\alpha\beta}^a$ is its dual. g is the Yang-Mills coupling and we introduced the topological charge Q .

In contrast to the scalar instanton in 3 + 1 dimensions, the BPST instanton satisfies a BPS condition such that the action (4.71) is minimized. As one can easily see, this is the case if

$$G = \tilde{G} \quad (4.72)$$

is satisfied. As a consequence, on the classical level the euclidean action is completely given by a total derivative, i. e. the topological charge Q of the instanton solution. Note that the topological charge associated with the instanton corresponds to the difference of the charges of the prevacua involved.

The self-dual instanton solution satisfying (4.72) with topological charge $Q = 1$ is given as

$$A_{a\mu} = \frac{2}{g} \eta_{a\mu\nu} \frac{x_\nu}{x^2 + \rho^2}, \quad (4.73)$$

where ρ is again the size modulus of the instanton. Thus, on the classical level the theory remains scale invariant. Additionally, we introduced the 't Hooft symbols $\eta_{a\mu\nu}$ connecting the Lorentz structure with the group indices. Notice that we centered the instanton at

$x_0 = 0$ which is an additional modulus of the theory corresponding to the translation invariance of the instanton.

Let us now turn to the corpuscular resolution of the BPST instanton. To introduce a microscopic quantum structure for the instanton, let us consider a magnetic monopole in an uplifted 4 + 1 dimensional theory. If such a monopole propagates an Euclidean distance L , i. e. it tunnels through a barrier of width L , a low energy observer which cannot resolve this barrier would observe an instanton effect. Of course, the mapping only works if the higher dimensional gauge coupling \tilde{g} satisfies equation (4.1).

The action of such a 4 + 1 dimensional Yang-Mills theory containing monopoles is basically equivalent to (4.71), only that we have to consider the higher dimensional gauge fields $\tilde{A}_{a\mu}$ and coupling constant \tilde{g} instead. Clearly, this is the reason why the solution of the 4 + 1 dimensional theory can have the equivalent structure as the lower dimensional saddle point solution in Euclidean time. The monopole solution is similarly to (4.73) given as

$$\tilde{A}_{a\mu} = \frac{2}{\tilde{g}} \eta_{a\mu\nu} \frac{x_\nu}{x^2 + \rho^2}. \quad (4.74)$$

Using the corresponding Yang-Mills Hamiltonian, we can as usual compute the monopole mass

$$M_{mon} = \frac{8\pi^2}{\tilde{g}^2}. \quad (4.75)$$

Obviously, the action for a tunneling process of the monopole is simply the mass representing the potential barrier times the imaginary time interval $\tau = iL$. Since this action should be equivalent with the instanton action measured by the low dimensional observer, it follows

$$S_{inst} = M_{mon} L = \frac{8\pi^2}{g^2}. \quad (4.76)$$

To implement a quantum understanding for the monopole, we Fourier transform the classical solution (4.74):

$$\tilde{A}_{a\nu} = \int d^4k \frac{l^2}{\sqrt{(2\pi)^4 2\omega(k)}} \left(\eta_{a\nu\alpha} \frac{k_\alpha}{k} \alpha_k e^{-ikx} + \eta_{a\nu\alpha} \frac{k_\alpha}{k} \alpha_k^\dagger e^{ikx} \right). \quad (4.77)$$

The corresponding Fourier coefficients are given as

$$\alpha_k = \frac{\rho^2 \sqrt{2\omega(k)}}{l^2 \tilde{g} k} \left[\frac{1}{2} \left(K_0(\rho k) + K_2(\rho k) \right) + \frac{1}{k\rho} K_1(\rho k) \right] \quad (4.78)$$

with the modified Bessel functions K_m , $m = 0, 1, 2$ and the corpuscular dispersion relation $\omega(k)$. Accordingly, we introduce Fock operators \hat{a}_k , \hat{a}_k^\dagger on a corpuscular Hilbert space creating the quantum constituents of the monopole. Building up a coherent monopole state $|sol\rangle$ (defined as before in equation (4.15)) using these creation and annihilation

operators, the expectation values of \hat{a}_k and \hat{a}_k^\dagger in the coherent state have to be equivalent to the Fourier coefficients. Obviously, the total occupation number amounts to

$$\begin{aligned} N &= l^4 \int d^4k \langle sol | \hat{a}_k^\dagger \hat{a}_k | sol \rangle = l^4 2\pi^2 \int d|k| |k|^3 |\alpha_k|^2 \\ &= \frac{4\pi^2 \rho}{\tilde{g}^2} \int du u \tilde{\omega}(u) \left[\frac{1}{2} (K_0(u) + K_2(u)) + \frac{1}{u} K_1(u) \right]^2, \end{aligned} \quad (4.79)$$

where we introduced the dimensionless function $u = k\rho$ like before. In order to investigate the ρ dependence of N we furthermore introduced the dimensionless dispersion $\tilde{\omega}(u) = \omega(k)\rho$.

As for the scalar soliton, the occupation number of the monopole depends linearly on ρ . Correspondingly, on the quantum level ρ stops to be a modulus of the theory meaning that the higher dimensional theory is not scale invariant. This is not surprising, since we introduced a new scale L to the theory to relate the couplings in 3+1 and 4+1 dimensions. By dimensional analysis, it follows $N \sim \frac{\rho}{\tilde{g}^2}$ simply because N is dimensionless and \tilde{g}^2 is not. This is, of course, reasonable as we expect that the monopole bound state size given by ρ should affect the occupation number. Since the quantum breakdown of scale invariance is triggered by $1/N$ -effects, it is restored in the semi-classical limit $N \rightarrow \infty$. Thus, the monopole mass does not depend on ρ to leading order in $1/N$.

So far we circumvented to clarify the corpuscular dispersion $\tilde{\omega}(u)$. Naively, one should guess that it should be given by $|k|$ because the monopole satisfies the BPS condition on the classical level and thus diagonalizes the Hamiltonian. In general, this is not the case for gauge fields. Regarding this particular example, the Hamiltonian density on the instanton solution is given as

$$H = D_\nu A_\mu^a D^\nu A^{a\mu}. \quad (4.80)$$

Of course, the covariant derivative still contains the self-interaction terms. Subsequently, the Hamiltonian is not diagonal in the corpuscular Fock operators, even in the semi-classical limit. Nevertheless, we can extract some information about the dispersion when we topologically analyze the monopole. Consider the gauge field at the boundary $|x| \rightarrow \infty$ behaving as

$$\tilde{A}_{a\nu}(x) = \frac{2}{\tilde{g}} \eta_{a\mu\nu} \frac{x_\nu}{x^2}. \quad (4.81)$$

Although it drops to zero, it does not vanish fast enough. In particular, the $1/|x|$ -type decay of the angular derivatives correspond to a non vanishing winding we identify as the topological charge. In fact, it is not surprising that the topology is encoded in the angular derivatives, since a non-trivial homotopy class $\pi_3(SU(2))$ is associated with the monopole. From the quantum point of view, we can separate two different types of quanta. Following the analysis in section 3.1.4, we know that topology should in particular be attributed to an infinite amount of zero momentum quanta. For the monopole, these are exactly the quanta creating a pure gauge term $\tilde{A}_{a\nu}(x) = \frac{2}{\tilde{g}} \eta_{a\mu\nu} \frac{x_\nu}{x^2}$ at the asymptotics. Computing the

Fourier transform of the pure gauge term which as we argued previously is connected to the angular derivatives, we can interpret these coefficients as expectation values of the topological Fock \hat{t}_k and \hat{t}_k^\dagger creating the topological charge. Correspondingly, we find the condition

$$\langle sol|\hat{t}_k|sol\rangle = t_k = \frac{1}{k^2}. \quad (4.82)$$

The operators \hat{t}_k are simply the zero momentum part of \hat{a}_k such that $\hat{a}_k = \hat{t}_k\hat{c}_k$. In contrast to the \hat{t}_k operators, the annihilation and creation operators \hat{c}_k and \hat{c}_k^\dagger account for the mass of the monopole. In other words, these operators create corpuscles contributing to the energy, instead of the topology. Splitting up the monopole state in a similar way $|sol\rangle = |t\rangle \otimes |E\rangle$, we find $\hat{c}_k|E\rangle = c_k|E\rangle$ and $\hat{t}_k|t\rangle = t_k|t\rangle$. Using $\alpha_k = t_k c_k$, it follows

$$c_k = \frac{k^2 \rho^2 \sqrt{2\omega(k)}}{l^2 \bar{g}_k} \left[\frac{1}{2} \left(K_0(\rho k) + K_2(\rho k) \right) + \frac{1}{k\rho} K_1(\rho k) \right]. \quad (4.83)$$

Note that we are still not able to determine $\omega(k)$ because the Hamiltonian is not diagonal in the \hat{c}_k , and \hat{c}_k^\dagger . Therefore, we do not know the total number of energetic quanta. However, since the monopole is a finite energy solution, the number should be finite. Nevertheless, due to this procedure we are able to show that, indeed, the number of topological quanta diverges:

$$N^{top} = \int_{k_0} d^4 k N_k^{top} = \int_{k_0} d^4 k t_k^* t_k \sim -\log(k_0)|_{k_0 \rightarrow 0} \rightarrow \infty. \quad (4.84)$$

This guarantees that the topological charge of the 4+1 dimensional monopole is conserved, since the monopole overlap with the vacuum is suppressed as $\langle 0|sol\rangle \sim \exp(-N^{top}) \rightarrow 0$. Furthermore, let us again remark that it is not surprising that the zero momentum modes contain the topological information because only these modes can extract information about spatial infinity where the topology is encoded.

Finally, let us comment on the BPST instanton. In particular, consider again the Euclidean propagation of such a monopole. Obviously, we could create a similar setting like in the different embedding examples in this chapter such that the monopole is only allowed in some barrier of width L . Subsequently, a low energy observer Alice who cannot resolve the perpendicular direction and is located on the barrier would interpret the tunneling of this monopole as an instanton effect. This BPST instanton inherits all the corpuscular features of the monopole. Most notably, scale invariance is broken on the instanton solution on the corpuscular level. In particular, the size of the instanton becomes a physical parameter in the microscopic description and stops to be a modulus. Notice that for $L \rightarrow 0$ we recover conformal invariance. However, in this limit Alice does not observe any corpuscular effects, since the number of corpuscles contributing to the action of the instanton diverges.

4.4 Conclusions

Finally, let us draw a conclusion. We pursue two different goals in this part of the thesis. First of all, we want to understand in concrete examples of embeddings how an instan-

ton effect emerges from the point of view of a lower dimensional observer as a higher dimensional soliton passes by. Secondly, we want to corpuscularly resolve the instanton by mapping it on a soliton with a microscopic substructure.

Regarding the first task, we were able to present two different $1 + 1$ dimensional models of a soliton passing by a low energy observer Alice interpreting this effect as an instanton in $0 + 1$ dimensions, since she cannot resolve the extra dimension. In both examples, we use a background kink to create two distinguishable regions. In the first case, we use a kink-anti-kink set-up to create a barrier where solitons are the classical solution. In the second example, we manufacture a similar situation where solitons are everywhere forbidden, but on the transition region of a background kink. Nevertheless, the outcome in both toy models is the same. The virtual motion of a soliton can interpolate between the forbidden regions. However, an observer confined to the transition region or the barrier clearly observes an instanton as the soliton passes by.

As a second example of explicit embeddings, we considered monopoles in $3 + 1$ dimensions. In particular, we presented a set-up, where monopoles are only allowed in a certain region between two domain walls. If we consider a process, where a monopole is created on one side and travels in Euclidean time to the other wall, a low energy observer Alice confined to this region would experience a different effect. She observes a tunneling to a different vacuum due to a $2 + 1$ dimensional instanton.

In these examples, it becomes very clear how we can understand instantons in terms of higher dimensional solitons. With this in mind, it is straightforward to implement a corpuscular description. As we showed, the instanton which is mapped on a soliton simply inherits the soliton's corpuscular substructure. Correspondingly, we can view the instanton as an effect emerging from many corpuscular processes.

This picture has many consequences. For instance, the low energy observer Alice will measure $1/N$ quantum corrections to the classical instanton solution. It is important to note that these effects are only observable when the Euclidean time the soliton is propagating is finite. For $L \rightarrow 0$, Alice cannot observe any effects because she would need an infinite amount of energy to do so.

There are even more dramatic consequences. Namely, the corpuscularly resolved BPST instanton is not scale invariant anymore. It was shown that the number of corpuscles contributing to the action is proportional to the size of the instanton ρ . As a consequence, we can obtain the size of the instanton by measuring $1/N$ type quantum effects. This is not surprising, since we had to introduce a new scale L in order to relate the instanton to a higher dimensional soliton. Again, in the $L \rightarrow 0$ limit scale invariance is restored because N diverges in this limit.

Chapter 5

Coherent State Picture for Classical Gravitational Backgrounds

In section 1.3 it was argued that black holes should be described in terms of its proper microscopic degrees of freedom which turned out be gravitons. When we assume that quantum field theory is fundamental, not only black holes should be seen as bound states. In fact, every background metric which is introduced on purely classical grounds must have a description in terms of quantum constituents. Following this logic, we want to give such a representation for AdS and Randall-Sundrum (RS) space-times in this chapter as it was originally proposed in [4, 6]. The work presented in this chapter is based on the original articles [102, 103]. Note, however, that this is still work in progress.

In particular, we will adapt the coherent state mechanism to promote classical solutions to bound states of quantum degrees of freedom. As we would expect, we can apply the same procedure to the components of the classical AdS metric as to the soliton and instanton profile presented in chapters 3 and 4. Accordingly, the bound state quanta referred to as corpuscles have similar features in the soliton as well as in the AdS case. Namely, the corpuscles can only exist inside the bound state, but not as asymptotic S -matrix quanta. Accordingly, they are interaction eigenstates. However, there are some differences between the corpuscular AdS and the corpuscular soliton. First of all, the corpuscular dispersion can, in general, be very different in both cases because AdS is not diagonalized on the semi-classical level. Secondly, we observe a divergence of the occupation number of corpuscles of small wavelengths. On the one hand, this can be understood in terms of the infinite blue-shift occurring at the boundary of AdS. On the other hand, from the corpuscular point view this effect directly leads to the stability of AdS with respect to decay into Minkowski space-time. Furthermore, let us remark that in the linear limit of AdS we can develop an interpretation of the AdS constituents in terms of on-shell massive gravitons.

As another application, the corpuscular treatment could shed a new light on the holographic principle in AdS. In particular, we can relate the total number of corpuscles N in the bulk directly with the entropy of the conformal field theory on the boundary. However, we can determine this scaling only in the low energy regime, since the behavior of the corpuscular dispersion is unknown for energy scales above $1/R_{AdS}$. The question how to,

in general, derive the dispersion for the constituents is left for future work. As we will show, we can only approximate the dispersion up to energy scales given by the inverse AdS curvature radius. For higher energies we expect that new unknown physics emerge.

Note that similar techniques are used in [104, 105] to describe de Sitter (dS) in terms of constituents. This framework allows for a completely new understanding of the cosmological constant (CC) problem. Namely, the corpuscular interaction leads to a quantum depletion which questions the stability of dS with a CC.

As a second concrete example for the application of the coherent state formalism in GR, we represent Randall-Sundrum 1 (RS1) space-times in terms of corpuscles. RS1 is closely related to AdS with the difference of a UV and a IR brane on the boundary. The existence of the UV brane acting as a natural cut-off leads to a smooth behavior at the boundary. As a consequence, in contrast to the AdS case the corpuscular occupation number N_k in mode k of RS1 does not diverge at any k and has a maximum at the inverse AdS curvature radius R_{AdS} . In this sense, the RS1 set-up shares more similarities with the soliton as AdS. Additionally, we can define the eigenvolume along the conformal coordinate and relate it with occupation number of corpuscles N .

In this chapter we are not only interested in establishing the quantum framework for AdS, but will additionally discuss how quantum effects emerge due to the compositeness of AdS. Note that these effects are, similar to the black hole case, directly related to the fact that the resolution allows for a back-reaction on the background. More explicitly, when we consider the propagation of a scalar field in a resolved background, we expect that the interaction of the scalar with the individual constituents leads to corrections. As was argued, for instance in section 3.2, these quantum effects are of the form $1/N$. Subsequently, they vanish in the semi-classical limit $N \rightarrow \infty$. These results give strong hints that the spectrum of the Unruh radiation a Rindler observer experiences gets corrected. These deviations lead to a violation of thermality. Accordingly, this means that the radiation should contain information. This result is very interesting regarding Hawking radiation emitted from black holes because the thermality of the Hawking radiation is related with the information paradox.

The outline of this chapter is as follows. In section 5.1 we apply the coherent state formalism to generic gravitational metrics by following and reviewing the steps presented in chapters 3 and 4. Then we apply these findings to the linear version of AdS in a similar way as in [105], where it was done for de Sitter. In particular, linearized AdS allows for an easy visualization of the corpuscles in terms of a sea of gravitons. This allows to understand, for instance, the blue shift of a scalar propagating on AdS as a sequence of many scattering processes on the individual constituents of AdS each increasing the momentum of the scalar. Section 5.3 contains the full non-linear treatment of AdS. Here we determine the full corpuscular occupation number and define the AdS Fock operators. Furthermore, we discuss the issues of the dispersion relation and the holographic principle. Similarly, we present the corpuscular framework for RSI space-time in section 5.4. Finally, in section 5.5 we discuss the $1/N$ type quantum effects arising in this framework. We show how corrections to the propagation of a scalar field through AdS arise when we consider back-reactions. However, in this context it is important to determine the full corpuscular

dispersion to obtain more quantitative statements. These results can then be used to show that the spectrum of the Unruh radiation measured by a Rindler observer is not thermal from the corpuscular point of view. Afterwards we draw a conclusion.

5.1 Corpuscular Resolution of arbitrary gravitational Backgrounds

As a first step towards a corpuscular description of AdS and the Randal-Sundrum set-up, let us discuss the general framework to represent arbitrary background metrics in terms of coherent states. The philosophy presented here is, obviously, similar to the classical soliton and instanton cases we discussed in chapters 3 and 4, respectively. Instead of the classical soliton or instanton profile, we want to understand the background metric $g_{\mu\nu}$ in general relativity as an emergent effect from an underlying quantum theory. As was already mentioned in the introduction of this chapter, this idea is also related to the resolution of the black hole and was first mentioned in [6]. If nature is fundamentally quantum, it follows that the only fundamental space-time is given by Minkowski. Accordingly, every classical metric $g_{\mu\nu}$ is interpreted as a bound state of constituent degrees of freedom. At this point, it should not be surprising that we can employ the coherent state strategy presented in chapter 3 also to the classical field $g_{\mu\nu}$. Fourier expanding the components of the metric $g_{\mu\nu}$ in $d + 1$ dimensions, we arrive at

$$g_{\mu\nu} = \frac{l^d}{M_P^{(d-1)/2}} \int \frac{d^d k}{\sqrt{(2\pi)^d 2\omega(k) l^d}} (\alpha_{k\mu\nu} e^{ikx} + h.c.) . \quad (5.1)$$

Let us briefly comment on this equation. As in the previous chapters, we introduced here the regulating spatial length scale l . Secondly, we use the dispersion relation $\omega(k)$ to ensure that $\alpha(k)_{\mu\nu}$ is properly normalized. Only when the coefficients $\alpha(k)_{\mu\nu}$ are dimensionless, we can relate them to occupation numbers in the mode k as soon as we go to the quantum theory. In contrast to the soliton case, we have to additionally introduce the Planck mass M_P . This is reminiscent of the fact that the background metric has mass dimension zero.

The general strategy is now analogous to the soliton case. Obviously, we can promote the Fourier coefficients $\alpha(k)_{\mu\nu}$ to corpuscular annihilation operators $\hat{a}(k)_{\mu\nu}$. These, of course, satisfy the standard commutation algebra $[\hat{a}_k, \hat{a}_{k'}^\dagger] = \delta^{(d)}(k - k')/l^d$. Consistency requires that these operators evaluated in the quantum background state $|metric\rangle$ should correspond to the classical Fourier coefficients,

$$\hat{a}_{k\mu\nu}|metric\rangle = \epsilon_{\mu\nu}\hat{a}_k|metric\rangle = \epsilon_{\mu\nu}\alpha_k|metric\rangle = \alpha_{k\mu\nu}|metric\rangle , \quad (5.2)$$

where $\epsilon_{\mu\nu}$ is the corresponding polarization tensor. Accordingly, the metric operator is given by

$$\hat{g}_{\mu\nu} = \frac{l^d}{M_P^{(d-1)/2}} \int \frac{d^d k}{\sqrt{(2\pi)^d 2\omega(k) l^d}} (\epsilon_{\mu\nu}\hat{a}_k e^{ikx} + h.c.) . \quad (5.3)$$

A careful reader already knows how we have to construct the quantum state $|metric\rangle$ such that it satisfies $\langle metric|\hat{g}_{\mu\nu}|metric\rangle = g_{\mu\nu}$. Since the coherent state is an eigenstate of the annihilation operator, we simply use the corpuscular creation operators to build it. The corresponding coherent state is then given as in equation (3.18)

$$|metric\rangle = \prod_{\otimes k} e^{-\frac{1}{2}|\alpha_k|^2} e^{\alpha_k \hat{a}_k^\dagger} |0\rangle = \prod_{\otimes k} e^{-\frac{1}{2}|\alpha_k|^2} \sum_{n_k=0}^{\infty} \frac{\alpha_k^{n_k}}{\sqrt{n_k!}} |n_k\rangle, \quad (5.4)$$

where $|n_k\rangle$ are the number eigenstates spanned by the corpuscular algebra. In accordance with the soliton picture, the occupation number of the background metric is defined as

$$N_k = \langle metric|\hat{a}_k^\dagger \hat{a}_k|metric\rangle. \quad (5.5)$$

So far we presented the generic procedure to resolve the classical gravitational background in terms of coherent states of corpuscles. For the rest of this chapter we will consider the special cases of AdS and Randall-Sundrum geometry from the corpuscular point of view.

5.2 Corpuscular Picture for Linearized Anti-de Sitter

As already advertized, we will now consider the AdS space-time from the microscopic point of view. Since the full non-linear treatment of AdS as a bound state of corpuscles is much more complicated, we will first consider the linearized version of AdS as a preliminary step. This will serve as a motivation to consider the full treatment, since many interesting features are already revealed on this level. In fact, the corpuscular effects are even more easily visualized in the linear treatment because we can think of the constituents in terms of on-shell gravitons in this case. For that purpose, let us consider a scalar field propagating through an AdS background metric in the linearized version. Assuming that AdS has a microscopic substructure and using the coherent state formalism to take this into account, we can determine the back-reaction on AdS by computing the scattering of the scalar field on the individual constituents of AdS. These scattering processes are, of course, only possible in the full quantum treatment of the background. In turn, they make the origin of the corpuscular corrections manifest. As a first step, let us expand the global AdS patch around Minkowski

$$g_{\mu\nu} = \eta_{\mu\nu} + h_{\mu\nu}. \quad (5.6)$$

According to [106], we can approximate $h_{\mu\nu}$ in $d+1$ dimensional AdS as

$$\begin{aligned} h_{00} &= \frac{\Lambda}{6} r^2, \\ h_{0i} &= 0, \\ h_{ij} &= \frac{\Lambda}{6} x_i x_j, \end{aligned}$$

where $\Lambda = -d(d-1)/2R_{AdS}^2$ is the cosmological constant associated with the AdS and $r^2 = x_i x_i$. As a next step, we Fourier expand the classical, gravitational background metric

$$h_{\mu\nu}(z) = \frac{l^d}{M_P^{(d-1)/2}} \int \frac{d^d k}{\sqrt{(2\pi)^d 2\omega(k) l^d}} (e^{ikx} \alpha_k \epsilon_{\mu\nu}(k) + \text{h.c.}), \quad (5.7)$$

where the notations stay the same as for equation (5.1). Following our usual strategy, we promote the Fourier coefficients to annihilation and creation operators $\hat{a}_k, \hat{a}_k^\dagger$ in order to quantize the background. In particular, this is the reason why we introduced the dispersion relation in (5.7), since we want the Fock operators to be dimensionless. Clearly, the operators \hat{a}_k and \hat{a}_k^\dagger evaluated in the coherent state have to satisfy a matching condition because to leading order this method should give the classical results. Building up a coherent state from the Fock operators as defined in (5.4), we obtain

$$\langle AdS | \hat{a}_k | AdS \rangle = \alpha_k. \quad (5.8)$$

In the linear picture, we can still give a physical interpretation for the corpuscles in terms of usual gravitons. To make this manifest, we represent the dimensionless field $h_{\mu\nu}$ in (5.7) as a graviton field which we canonically normalize $h_{\mu\nu} \rightarrow h_{\mu\nu}/M_P$. On the one

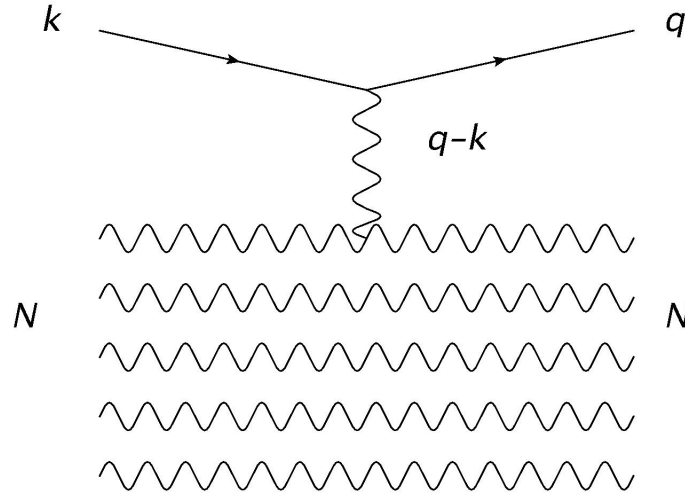


Figure 5.1: The figure depicts a scalar particle of momentum k propagating through a corpuscular resolved AdS. In particular, the scalar scatters on the individual AdS constituents by exchanging off-shell gravitons.

hand, we could interpret the interacting corpuscles represented by $\hat{a}_k^\dagger, \hat{a}_k$ as longitudinal, massless gravitons arising in Einstein's theory expanded around Minkowski. These degrees of freedom are, of course, off-shell and governed by the linear wave equation sourced by the cosmological constant.

On the other hand, the constituents can be viewed as the longitudinal degrees of freedom of on-shell massive gravitons. Deforming the theory at hand by a Fierz-Pauli mass term

for the graviton, we obtain the same solution in the regime $m^2 r^2 \ll 1$. This was explicitly shown for de Sitter space in [106], but can be generalized to AdS space-time as well. A massive graviton propagates five degrees of freedom instead of two. Consequently, we can build up a coherent state of the longitudinal, on-shell gravitons to represent the AdS space-time to leading order. However, their corresponding dispersion relation implies that the constituent gravitons are tachyons.

As was already mentioned, the corpuscular description of AdS inevitably leads to the appearance of $1/N$ type quantum corrections. For instance, these compositeness effects give rise to corrections to the propagation of a scalar evolving through an AdS background. For that purpose, consider a linearized interaction between the scalar field and gravity given by the Lagrangian

$$\mathcal{L}_{int} = \frac{1}{M_p} h_{\mu\nu} T^{\mu\nu}(\phi). \quad (5.9)$$

Here we introduced the scalar energy-momentum tensor

$$T_{\mu\nu}(\phi) = \frac{1}{2} S_{\mu\nu\alpha\beta} \partial^\alpha \phi \partial^\beta \phi - \frac{1}{2} \eta_{\mu\nu} m^2 \phi^2 \quad (5.10)$$

with the tensor structure $S_{\mu\nu\alpha\beta} = \eta_{\mu\alpha} \eta_{\nu\beta} + \eta_{\mu\beta} \eta_{\nu\alpha} - \eta_{\mu\nu} \eta_{\alpha\beta}$. Now let us consider the evolution of this scalar field coupled to the background in accordance with (5.9). Of course, we have to take back-reactions on the AdS space into account to include quantum effects resulting from the resolution of the background. In turn, the quantum AdS state $|\text{AdS}\rangle$ changes in such a process. To make this effect manifest, consider the scattering of the scalar field represented by its annihilation and creation operators \hat{b}_q and \hat{b}_p^\dagger (corresponding to usual asymptotic particles) on the background as in figure 5.1. The scattering amplitude is given by

$$\begin{aligned} \mathcal{A}(q, p) &= i \langle \text{AdS}' | \otimes \langle 0 | \text{T} \hat{b}_q S_{int} \hat{b}_p^\dagger | 0 \rangle \otimes | \text{AdS} \rangle \\ &= \frac{i}{M_p} \int d^{(d+1)}x \langle \text{AdS}' | h_{\mu\nu} | \text{AdS} \rangle \langle 0 | \text{T} \hat{b}_q T^{\mu\nu}(\phi) \hat{b}_p^\dagger | 0 \rangle. \end{aligned} \quad (5.11)$$

Obviously, the correlator $\langle \text{AdS}' | h_{\mu\nu} | \text{AdS} \rangle$ contains the quantum corrections to the classical result. There exists a smooth classical limit when we neglect back-reactions by setting $|\text{AdS}'\rangle = |\text{AdS}\rangle$. By construction, this leads to the classical result. On the contrary, taking corpuscular effects into account the AdS state is affected by such a scattering process such that $|\text{AdS}'\rangle \neq |\text{AdS}\rangle$. In principle, it is not clear if AdS can still be represented in terms of coherent states after such a process. However, coherent states are a legitimate approximation as long as the corpuscular quantum corrections are suppressed. Clearly, this is the case when the curvature radius satisfies $R_{AdS} \gg L_P$. With this assumption, the overlap element between both coherent states is given by

$$\frac{l^d \langle \text{AdS}' | \text{AdS} \rangle}{M_p^{(d-1)/2}} \int \frac{d^d k}{\sqrt{(2\pi)^d 2\omega_k l^d}} \left(e^{ikx} \sqrt{N_k} \epsilon_{\mu\nu}(k) + e^{-ikx} \sqrt{N_k'} \epsilon_{\mu\nu}^*(k) \right). \quad (5.12)$$

In fact, the difference between $|\text{AdS}'\rangle$ and $|\text{AdS}\rangle$ is encoded in the different momentum distributions N'_k and N_k . Consequently, we do not recover the classical field value in equation (5.12), but additionally quantum corrections occur due to the back-reaction. Let us parametrize these effects by introducing δ_k as a measure for the occupation number shift due to the scattering process, $N'_k = (N + \delta)_k$. In the small back-reaction approximation, $|\delta_k| \ll N_k$, the overlap between both coherent states is given by

$$\langle \text{AdS}' | \text{AdS} \rangle = e^{-\frac{1}{2}l^d \int d^d k (N_k + N'_k - 2 \int d^d k \sqrt{N'_k N_k})} \simeq 1 - \frac{1}{4}l^d \int d^d k \frac{\delta_k^2}{N_k}. \quad (5.13)$$

Here we used the expansion $\sqrt{N'_k} \simeq \sqrt{N_k}(1 + \delta_k/(2N_k))$. This result visualizes why we refer to the composite quantum effects as $1/N$. They are always suppressed by the corresponding occupation number. In particular, it is important to note that the quantum effects are not exponentially suppressed as usual corrections to the classical result. Nevertheless, in the semi-classical limit $N \rightarrow \infty$ these effects vanish.

The linear approximation of AdS makes the corpuscular effect emerging from a microscopically resolved AdS background manifest, since we can think in terms of Feynman diagrams. Consider for instance figure 5.1. It depicts the propagation of a scalar through a sea of constituent AdS gravitons. The two-to-two scattering process between the probe scalar and an individual constituent in mode k obviously changes the occupation number N_k , since in such a process the constituent loses energy to the scalar such that N_k is changed. However, the probe scalar absorbs this energy and is blue shifted.

In the next section, we proceed by considering the corpuscular resolution of the the full non-linear AdS.

5.3 Non-Linear Corpuscular AdS

As advertized, we consider full non-linear AdS from the corpuscular point of view in this section. The discussion presented here is closely related to the original work [102, 103]. As will become clear below, we will work in Poincaré coordinates. Note that Poincaré coordinates do not cover the full AdS. In particular, the line element for a D dimensional AdS is given as

$$ds^2 = \frac{R_{AdS}^2}{z^2} (dz^2 + \eta_{\mu\nu} dx^\mu dx^\nu) , \quad (5.14)$$

where z is the conformal coordinate. Correspondingly, the boundary of AdS is a $d = D - 1$ dimensional Minkowski sub-manifold. We use the following conventions for the indices: μ, ν denote the Minkowski coordinates of the boundary, i and j are spatial indices without the conformal coordinate, while M, N correspond to the index structure of the bulk.

To develop a corpuscular understanding of non-linear AdS, we follow the strategy presented in section 5.1 for generic space-times. Taking a closer look at the components of the Poincaré metric g_{MN} , it becomes also clear why we consider the Poincaré patch. The AdS metric is extremely simplified in this case, since it is diagonal and all the components are

equivalent. Subsequently, when we Fourier expand the AdS metric as in equation (5.1), the situation is effectively reduced to only one expansion coefficient α_k ,

$$\alpha_{kMN} = \alpha_k \begin{pmatrix} \eta_{\mu\nu} & 0 \\ 0 & 1 \end{pmatrix}. \quad (5.15)$$

For simplicity we will restrict the following discussion to α_k given as

$$\alpha_k = -l^{-d/2} M_P^{(d-1)/2} \frac{\sqrt{(2\pi)^d 2\omega(k)} |k| R_{AdS}^2}{2} \delta^{d-1}(k_i). \quad (5.16)$$

Note that the delta function $\delta^{d-1}(k_i)$ arises, since the integration along the spatial coordinates is trivial as g_{MN} only depends on z . Furthermore, we observe that the classical coefficients in (5.16) become large for high momenta such that the corpuscular occupation number diverges as well. This reflects the fact that the blue shift at the boundary $z \rightarrow 0$ is infinite.

To implement the quantum picture, we follow the procedure in section 5.1 and promote the classical coefficient α_k to corpuscular Fock operators $\hat{a}_k, \hat{a}_k^\dagger$ satisfying

$$[\hat{a}_k, \hat{a}_{k'}^\dagger] = \frac{\delta^d(k - k')}{l^d}. \quad (5.17)$$

Subsequently, the components of the classical metric are promoted to operators \hat{g}_{MN} . To obtain the right classical limit the operators have to satisfy

$$\langle \text{AdS} | \hat{g}_{MN} | \text{AdS} \rangle = g_{MN}, \quad (5.18)$$

when evaluated in the AdS state. Note that higher order operators of the form \hat{g}_{MN}^n lead to corpuscular quantum corrections of the order $1/N$ as it was the case for the corpuscular soliton. Using the Fock operators, we can build a coherent state $|\text{AdS}\rangle$ of corpuscles as given in equation (5.4) satisfying this requirement. The corpuscular occupation number N_k in mode k is defined by

$$\hat{a}_k |\text{AdS}\rangle = \alpha_k |\text{AdS}\rangle = \sqrt{N_k} |\text{AdS}\rangle. \quad (5.19)$$

In principle, we can determine the total occupation number by integrating over all modes,

$$N = l^d \int d^d k N_k. \quad (5.20)$$

To explicitly evaluate the total occupation number, we have to know the corresponding corpuscular dispersion relation. In the soliton case in chapter 3, we could determine the dispersion approximately, since the classical solution diagonalized the Hamiltonian up to $1/N$ corrections. On the contrary, for AdS the situation is more subtle because we cannot determine the corpuscular dispersion relation from first principles. We already encountered this problem when we discussed the BPST instanton in section 4.3.2. How to determine the corpuscular dispersion relation in generic situations is still an open question. In

general, it arises from the underlying theory which is a priori unknown. The dispersion could be achieved by performing a suitable Bogoliubov transformation which is, however, a formidable task. Therefore, we will leave this for future work. Nevertheless, since the total occupation N is proportional to the spatial Minkowski volume l^{d-1} , $N \rightarrow \infty$ in any case. As a consequence, from the quantum point of view AdS is stable with respect to decay into Minkowski space-time because the overlap is given as

$$\langle AdS|Minkowski \rangle \sim e^{-N} \rightarrow 0 \quad (5.21)$$

Obviously, this reasoning is similar to the topological soliton case, where we encountered a diverging occupation number as well.

In the next two subsections, we will discuss a bound on the dispersion relation and holographic implications of the corpuscular resolution, respectively.

Bound on the Dispersion Relation

Although we cannot compute the dispersion exactly, we can at least determine an upper bound for the scaling of the dispersion. For that purpose, let us define the number of corpuscles per conformal momentum by integrating over spatial Minkowski momenta

$$N_{k_z} = l^{d-1} \int d^{(d-1)}k N_k = \pi l^{d-1} M_P^{d-1} l_z^{-1} k_z^2 R_{AdS}^4 \omega(k_z), \quad (5.22)$$

where l_z is the regulating length scale in the conformal direction. Note that the regulating volume l^d we introduced before is given by $l_z l^{d-1}$ where l^{d-1} denotes the spatial Minkowski volume. As was already mentioned, the corpuscles are only sensible when they are individually weakly coupled. Correspondingly, the number of corpuscles per volume should always be smaller than the Planck density $M_P^{-(d-1)}$. This leads to a bound for the total number of corpuscles in the element $l_z k_z$ per Minkowski volume given as

$$\frac{N_{k_z} l_z k_z}{l^{d-1}} < M_P^{-(d-1)}. \quad (5.23)$$

Subsequently, the upper bound for the scaling of the dispersion relation is given by

$$\pi k_z^3 \omega(k_z) R_{AdS}^4 < 1. \quad (5.24)$$

To understand the implications of this bound, let us discuss certain extremal limits. In the $R_{AdS} \rightarrow \infty$ limit, we are effectively considering a flat space-time composed of corpuscles. Dvali et al. [107] showed that in this limit the corpuscles can be identified as freely propagating gravitons with a dispersion $\omega(k_z) = k_z$. Regarding (5.24), this means that the propagation is close to free up to a cut-off given by $\Lambda_{UV} \sim 1/R_{AdS}$. We expect new physics to emerge at this scale modifying the dispersion relation such that unitarity is not violated. In other words, we can safely approximate the corpuscular dispersion by a free one for $k_z \ll 1/R_{AdS}$. However, $k_z R_{AdS}$ corrections become important for $k_z \sim 1/R_{AdS}$ such that we cannot predict the behavior of the dispersion in this energy regime.

To proceed at this point, we determine the number of corpuscles which behave approximately as free quanta,

$$N \approx (lM_P)^{d-1} . \quad (5.25)$$

Interestingly, this number is equivalent to the famous Bekenstein entropy [62] in generic dimensions. The holographic principle in the semi-classical AdS/CFT treatment is investigated in many papers [108, 109, 110, 111, 112]. Thus, we can identify the number of particles in the bulk below the threshold with the entropy of the dual CFT on a volume l^{d-1}

$$S_{CFT} = (lM_P)^{d-1} = N . \quad (5.26)$$

Correspondingly, the number of microstates on the CFT side coincides with the number of constituents of the bulk background. This is a first hint how we can understand holography from the corpuscular point of view. However, let us stress that this result is only an approximation valid in the low energy regime. So far it is not clear how the dispersion behaves for $|k| > 1/R_{AdS}$.

Equivalence Principle

Naturally, one can ask the question how the principle of equivalence emerges from the corpuscular point of view. In particular, AdS should locally be equivalent to Minkowski. For that purpose, let us define a local occupation number at $z = z'$

$$N_{loc} = l_{loc}^d \int_{1/z'-\delta/2}^{1/z'+\delta/2} dk_z \int d^{(d-1)}k \alpha_k^* \alpha_k = (l_{loc}M_P)^{d-1} z' \delta , \quad (5.27)$$

where l_{loc}^{d-1} is a localized spatial Minkowski volume. Furthermore, δ denotes the small extension in the conformal directions. Accordingly, the local number of corpuscles is small for $l_{loc}^{d-1} \rightarrow 0$ and $\delta \rightarrow 0$. Of course, this means that AdS is locally interpreted as Minkowski. To be more explicit, we can compute the overlap of local AdS with Minkowski,

$$\langle AdS_{loc} | Minkowski \rangle \propto \exp(-N_{loc}) \rightarrow 1 \text{ for } l_{loc}^{d-1} \rightarrow 0 \text{ and } \delta \rightarrow 0 . \quad (5.28)$$

To summarize, from the corpuscular point of view the equivalence principle is reflected in a finite local occupation number.

5.4 Randall-Sundrum Geometry

The Randall-Sundrum (RS) set-up [18, 19] we consider in this section is closely related to AdS space-time. For instance, the RS1 space-time corresponds to usual AdS with two branes placed at the boundaries. The UV brane automatically regularizes the space-time near the boundary. The RS2 space-time considered in [19] only has one brane localized in

the UV. Both set-ups aim to solve the hierarchy problem by introducing extra dimensions. However, in contrast to the well known large extra dimensional models [113], Randall and Sundrum consider warped space-times. The warping factor is the essence of the model in order to resolve the hierarchy problem. When the warping factor is $\ll 1$ on the brane where we place the four dimensional standard model, the weak scale is accordingly decreased with respect to the Planck mass.

As will become clear below, it is interesting to investigate RS1 from the corpuscular point of view although it is similar to AdS. Therefore, we follow our reasoning and build RS1 with a large number of corpuscles on top of Minkowski. Note that the space-time is five dimensional. The corresponding metric is given by

$$ds^2 = g_{MN}dx^M dx^N = e^{-2|y|/R_{AdS}}\eta_{\mu\nu}dx^\mu dx^\nu + dy^2 . \quad (5.29)$$

Here the extra warped direction is y and the indices μ, ν go from 0 to 3. We simply adopt the quantization procedure for the AdS case considered above. Namely, we Fourier transform the components of the metric with the corresponding coefficients given by

$$N_k = l_y^{-1} M_p^3 2\omega_k \frac{4}{\pi} \frac{R_{AdS}^2}{(4 + R_{AdS}^2 k_y^2)^2} \delta^{(3)}(k_i) , \quad (5.30)$$

where l_y is the regualting scale in the y direction. Equation (5.30) makes manifest why it is interesting to consider RS1. Although this space-time shares many of the holographic features of AdS, we do not encounter a divergence in the corpuscular occupation number for small wavelength as long as the dispersion satisfies the bound

$$\omega(k_y)k_y R_{AdS}^2 \leq (4 + R_{AdS}^2 k_y^2)^2 . \quad (5.31)$$

We can determine this bound from a similar analysis as in the previous section. In particular, it is always satisfied when we approximate $\omega(k_y) \approx |k_y|$. As a consequence, we do expect new physics only at scales $k_y \gg 1/R_{AdS}$ such that the RS1 constituents are almost free.

Promoting the expansion coefficients to Fock operators, we can construct a coherent state representing the RS1 space-time as in equation (5.4). Thus, the total number of corpuscles can be written as

$$N = l^3 l_y \int d^4 k \langle RS1 | \hat{a}_k^\dagger \hat{a}_k | RS1 \rangle \approx (M_p l)^3 \quad (5.32)$$

in accordance with the occupation number in the AdS case in equation (5.25). The RS1 model is characterized by its invariant volume of space-time which can be computed to be

$$V_{inv} = \int d^5 x \sqrt{g} = V_M \int dy e^{-4|y|/R_{AdS}} . \quad (5.33)$$

Here $V_M = l^4$ is defined as the transverse volume of the 4 dimensional Minkowski space-time. In the corpuscular description the volume can be represented as

$$V_{inv} = V_M l_z \int \frac{d^4 k}{M_p^3 (2\pi)^d 2\omega(k_y)} \langle RS1 | \hat{a}_k^\dagger \hat{a}_k | RS1 \rangle . \quad (5.34)$$

with the coherent RS1 state $|RS1\rangle$ defined as in equation (5.4).

Note that N is still infinite, since it is proportional to Minkowski space-time. Correspondingly, RS1 is stable with respect to decay into Minkowski. As a remark, let us mention that in some sense RS1 is more similar to a soliton because the occupation number N_k has a maximum at a certain scale $1/R_{AdS}$ setting the size of the bound state.

5.5 Corpuscular Corrections to scalar Propagators in AdS

In general, we expect that the classical propagation of scalar particles through the resolved AdS background is quantum corrected, since the corpuscular picture allows for non-trivial back-reactions on the AdS constituents. For instance, in the supersymmetric soliton case in section 3.2 we observed how these $1/N$ type quantum effects lead to the violation of the BPS equation. Therefore, in this section we are interested in making the quantum effects resulting from the compositeness (\hbar/N effects) computationally manifest. Note that we neglect usual loop quantum effects (\hbar effects) renormalizing the background.

Since these corrections are extremely hard to measure, a second goal of this section will be to determine how these corrections affect the spectrum of Unruh radiation measured by a Rindler observer.

5.5.1 Scalar Propagator

The corpuscular structure of AdS was already introduced in section 5.3. Hence, we can use these results to explicitly compute corpuscular corrections to scalar propagators in the AdS bulk. As was explained, we will consider the Poincaré patch of AdS with the conformally flat metric g_{MN} given in equation (5.14). It suffices to simply consider the metric component g_{zz} , since $g_{zz} = g_{ii} = -g_{tt}$, while all the other metric components vanish. In other words, the classical field we promote to an operator is $g_{zz} \rightarrow \hat{g}_{zz}$. The corresponding expansion coefficient α_k is given in equation (5.17).

With the corpuscular resolution defined in this way and the corpuscular coherent AdS state given in (5.4), we can determine how the quantum back-reaction due to the compositeness of AdS affects the classical motion of a scalar. For that purpose, we have to promote all the metric components in the classical equation of motion of the scalar to operators which can be expressed in terms of creation and annihilation operators. Therefore, we start by expressing the equation of motion

$$\left\{ \frac{1}{\sqrt{-g}} \partial_A (\sqrt{-g} g^{AB} \partial_B) + m^2 \right\} G_c(X, Y) = \frac{1}{\sqrt{-g}} \delta^{(d+1)}(X - Y) \quad (5.35)$$

solely in terms of g_{zz} . Here g denotes the determinant of the metric, $X = \{x_\mu, z\}$ and A, B are $d + 1$ dimensional indices. For simplicity we restrict ourselves now to the $d = 3$ dimensional case in order to make the $1/N$ -type corrections computationally manifest. The

classical scalar propagator $G_c(X, Y)$ is given in the appendix B in equation (B.1). In 3 + 1 dimensions, equation (5.35) simplifies to

$$\mathcal{O}_c(X)G_c(X, Y) = \delta^{(4)}(X, Y), \quad (5.36)$$

where we defined

$$\mathcal{O}_c(X) \equiv -g_{zz}^3 \square_M - 2g_{zz}^2 (\partial^z g_{zz}) \partial^z + g_{zz}^2 m^2 \quad (5.37)$$

with $\square_M = \partial^\mu \partial_\mu + (\partial^z)^2$. As we intended, the only classical field appearing in (5.37) is g_{zz} . Thus, we can straightforwardly enter the quantum picture by replacing $g_{zz} \rightarrow \hat{g}_{zz}$. In other words, we promote g_{zz} in equation (5.37) to an operator represented in terms of the corpuscular annihilation and creation operators introduced in equation (5.19).

As a next step, we evaluate the promoted equation of motion in the coherent AdS state $|\text{AdS}\rangle$ to obtain an observable from the operator equation. To understand the origin of quantum corrections, we have to notice that, in contrast to \hat{a}_k , \hat{a}_k^\dagger has not the coherent state as an eigenvector. Thus, we have to use the commutation relations to bring the Fock operators in a normal ordered form when we want to evaluate the promoted equation of motion in the AdS state. This simply means that in the corpuscular picture the equation of motion is given by

$$\langle \text{AdS} | \mathcal{O}_f(X) | \text{AdS} \rangle G_f(X, Y) = \delta^{(4)}(X - Y), \quad (5.38)$$

where $G_f(X, Y)$ is the full quantum corrected Greens function $G_f(X, Y)$ we are interested in. The $1/N$ type quantum corrections which arise due to the compositeness of the background are explicitly encoded in these non-vanishing commutator terms appearing in the full quantum operator $\mathcal{O}_f(X)$. Note that the normal ordered products eventually reduce to the classical metric. $\mathcal{O}_f(X)$ is obtained by promoting g_{zz} in (5.37) to an operator:

$$\mathcal{O}_f(X) \equiv -\hat{g}_{zz}^3 \square_M - 2\hat{g}_{zz}^2 (\partial^z \hat{g}_{zz}) \partial^z + \hat{g}_{zz}^2 m^2, \quad (5.39)$$

with \hat{g}_{zz} given in equation (5.3). Evaluating $\langle \text{AdS} | \mathcal{O}_f(X) | \text{AdS} \rangle$, we can distinguish the classical contribution \mathcal{O}_c emerging from the normal ordered contributions and the quantum contribution \mathcal{O}_q generated by commutator terms. In particular, it follows that

$$\langle \text{AdS} | \mathcal{O}_f(X) | \text{AdS} \rangle = \mathcal{O}_c + \mathcal{O}_q, \quad (5.40)$$

where we defined

$$\mathcal{O}_q = \frac{1}{4\pi} \left(-2(\partial^z g_{zz}) \partial^z - 3g_{zz} \square_M \right) \int \frac{dk_z}{\omega_k}. \quad (5.41)$$

To summarize, the $1/N$ type quantum corrections to the equation of motion arising due to the compositeness of AdS are encoded in the function \mathcal{O}_q . Subsequently, the Greens function solving the equation of motion is corrected accordingly such that it solves the quantum corrected equation of motion. Note that the computation to determine \mathcal{O}_q simply

amounts to using commutation relations and expressing normal order parts in terms of the classical metric g_{zz} .

A few remarks are in order. First of all, let us stress at this point that the quantum corrections are not the usual vacuum contributions because they are only non-vanishing in the quantum coherent background state. More explicitly, the terms in \mathcal{O}_q arise from mixed expressions of commutators and normal ordered terms vanishing in the trivial vacuum. Secondly, we have to point out that we cannot further evaluate the integral $\int \frac{dk_z}{\omega(k_z)}$, since we do not know the corpuscular dispersion arising from the unknown underlying theory. In particular, the integral suggests that we are actually computing a corpuscular renormalization to the classical propagator. The potentially diverging integral only appears because we are working with the bare classical data N_k characterizing the corpuscular momentum distribution. As commutator terms are equivalent to usual quantum loops, any divergencies we encounter should be absorbed in a redefinition of the classical entities. Since the underlying dynamics leading to the emergence of the bound states are not fully understood up to this moment (i.e. we do not know $\omega(k)$ exactly), we will leave it as a future task to evaluate this part of the quantum corrections. Although we cannot further quantify the strength of the corrections, we at least come to the conclusion that they must exist in this framework. Note that we observed a similar problem when we discussed $1/N$ corrections in the supersymmetric soliton case.

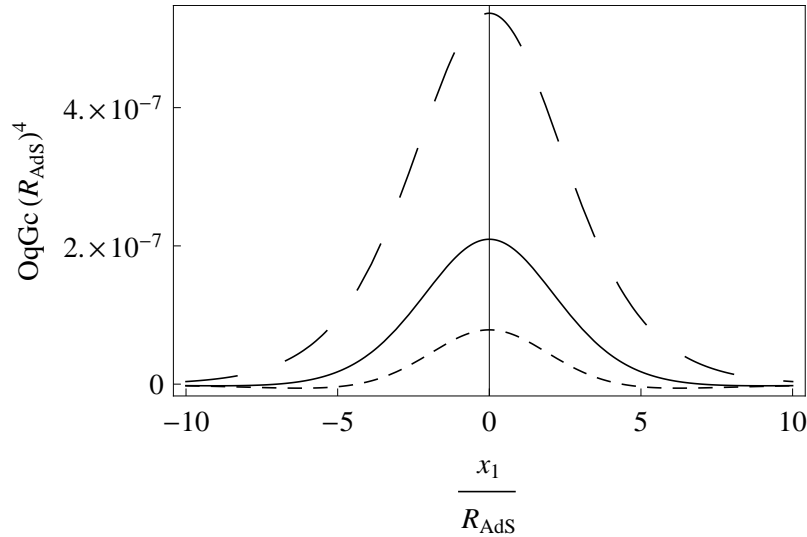


Figure 5.2: This diagram shows the quantum correction to the full propagator given by $\mathcal{O}_q G_c$ as a function of the coordinate x_1 . The other parameters are chosen as $x_2 = y_1 = y_2 = 0$, $z_1 = 7$, $z_2 = 1$, $t_1 = 1$, $t_2 = 0$. We consider three different choices for the scalar mass: $m^2 = -1$ (largely dashed), $m^2 = 0$ (straight) and $m^2 = 1$ (dashed). The unit length scale in this figure is given by R_{AdS} .

Using equations (5.38) and (5.40), we can solve for the full quantum corrected propagator $G_f = G_c + G_q$. Bearing in mind that \mathcal{O}_q is \hbar/N suppressed with respect to \mathcal{O}_c ,

we can solve equation (5.38) iteratively for the quantum correction $G_q = \sum_{j=1}^{\infty} G_{q,j}$ to the propagator at each order. More explicitly, it follows

$$G_f = G_c - \underbrace{G_c \mathcal{O}_q G_c + G_c \mathcal{O}_q G_c \mathcal{O}_q G_c - \dots}_{G_q} \quad (5.42)$$

using $\mathcal{O}_c G_c = 1$. Clearly, (5.42) is simply a Dyson series which can be summed up leading to the full propagator

$$G_f = \frac{G_c}{1 + \mathcal{O}_q G_c}. \quad (5.43)$$

Note that we suppressed here the standard integrals over space-time in equations (5.42) and (5.43). In general, this derivation could have been done for any classical background resolved as a coherent state. Of course, the difference between the backgrounds is always encoded in \mathcal{O}_q . We can return to the semi-classical limit simply by setting $\mathcal{O}_q = 0$. This is the analog of the limit $N \rightarrow \infty$ we employed in section 5.2.

As we expected, the classical scalar propagator gets corrected due to the corpuscular back-reaction when the space-time integral over $\mathcal{O}_q G_c$ is not vanishing. To investigate this, we consider the figures (5.2) - (5.5) where the first order corpuscular corrections to the Green's function are depicted. We normalized all these plots to the so far unknown integral $\int dk_z / \omega_k$. Furthermore, we introduced the following coordinate labels $X = (t_1, x_1, y_1, z_1)$ and $Y = (t_2, x_2, y_2, z_2)$.

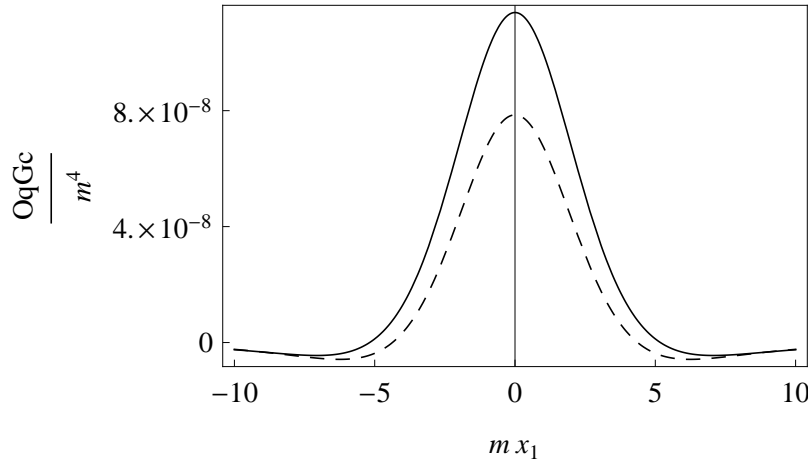


Figure 5.3: This diagram shows the quantum correction to the full propagator given by $\mathcal{O}_q G_c$ as a function of the coordinate x_1 . The other parameters are chosen as $x_2 = y_1 = y_2 = 0$, $z_1 = 7$, $z_2 = 1$, $t_1 = 1$, $t_2 = 0$, $m^2 = 1$. We consider two different choices for the curvature radius R_{AdS} : $R_{AdS} = 0.8$ (straight) and $R_{AdS} = 1$ (dashed). The unit mass scale in this figure is given by m .

Let us now comment on the diagrams. As a first remark, it is worth mentioning that the quantum corrections drop to zero and are well behaved far away from the poles of

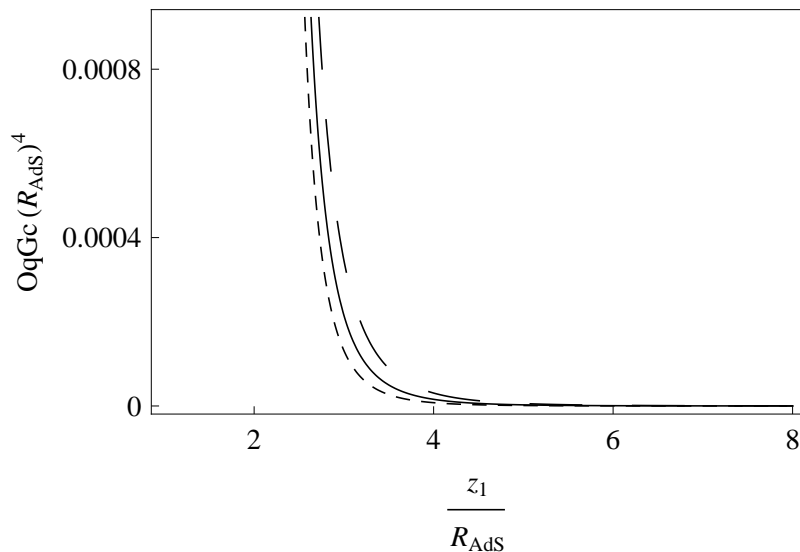


Figure 5.4: This diagram shows the quantum correction to the full propagator given by $\mathcal{O}_q G_c$ as a function of the coordinate z_1 . The other parameters are chosen as $x_1 = x_2 = y_1 = y_2 = 0$, $z_2 = 1$, $t_1 = 1$, $t_2 = 0$. We consider three different choices for the scalar mass: $m^2 = -1$ (largely dashed), $m^2 = 0$ (straight) and $m^2 = 1$ (dashed). The unit length scale in this figure is given by R_{AdS} .

the propagator. For instance, in figure (5.2) the quantum corrections for different scalar masses have a maximum for $x_1 = 0$, but are still well behaved everywhere. In particular, they are suppressed for $x_1 \gg z_1$. We could expect this, since the corpuscular corrections are encoded in the conformal direction of the bulk and not in the boundary. This means that considering a larger portion of the boundary does not affect the quantum corrections heavily.

In figure (5.3) we investigate the dependence of the corrections on the AdS curvature radius R_{AdS} for fixed scalar mass, again as a function of x_1 . In particular, the results show that the corrections decrease for larger curvature radii. This, of course, could be expected from the beginning because as we explained these corrections are of the $1/N$ type. Since the local number of quanta in each mode,

$$N_k = |\alpha(k)|^2 = \frac{M_p^{(d-1)}}{l_z} \pi \omega(k) |k|^2 R_{AdS}^4 (2\pi)^{d-1} \delta^{d-1}(k_i), \quad (5.44)$$

increases with R_{AdS} , the quantum corrections should be more suppressed for larger radii.

In figure (5.4) we investigate the pole structure of $\mathcal{O}_q G_c$ with respect to z_1 for different masses. We observe that the corrections are very small for large z_1 , but diverge when the separation of the two points becomes lightlike.

The last diagram (figure 5.5) depicts $\mathcal{O}_q G_c$ for the radii $R_{AdS} = 1$ (straight curve) and $R_{AdS} = 1.5$ (large dashed curve) versus z_2 . Again, it shows that the corpuscular effects become extremely important when the separation of the points is lightlike.

A few final remarks are in order. First of all, let us mention that the structure of \mathcal{O}_q heavily depends on the number of spatial dimensions. Since the number of powers of the classical field g_{zz} in the classical equation of motion depends on the dimension of space-time, we accordingly obtain higher powers of the operator \hat{g}_{zz} on the quantum level. This means that the outcome of the calculation heavily depends on the dimension of AdS because higher dimensional operators of the form \hat{g}_{zz}^n encode the $1/N$ corrections.

Secondly, let us stress that all the results presented here are only an approximation. They only show that there are corrections, but we cannot determine the strength of these effects as the dispersion relation is not known for every k .

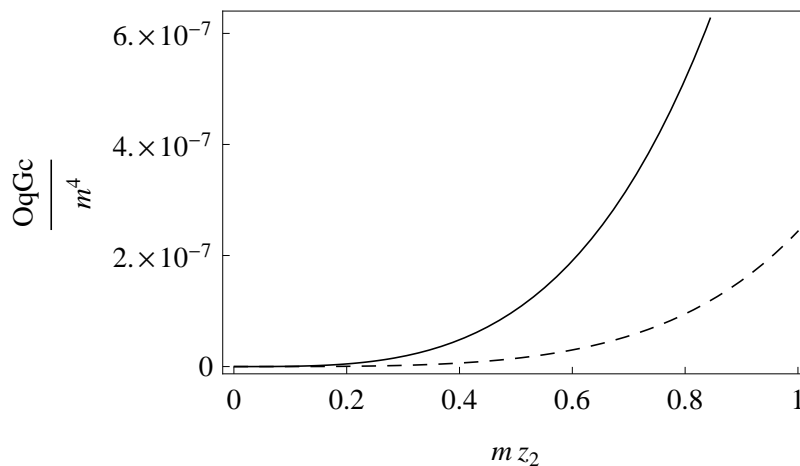


Figure 5.5: This diagram shows the quantum correction to the full propagator given by $\mathcal{O}_q G_c$ as a function of the coordinate z_2 . The other parameters are chosen as $x_1 = x_2 = y_1 = y_2 = 0$, $z_1 = 5$, $t_1 = 1$, $t_2 = 0$, $m^2 = 1$. We consider two different choices for the curvature radius R_{AdS} : $R_{AdS} = 1$ (straight) and $R_{AdS} = 1.5$ (largely dashed). The unit mass scale in this figure is given by m .

5.5.2 Unruh Effect in AdS

This section is dedicated to investigate the impact of these results for the Unruh effect. We apply the very same analysis of section 5.5.1 to the Wightman function instead of the propagator. Since the corrections to Wightman functions are directly translated into corrections to the Unruh effect in AdS, we expect that the corresponding corpuscular effects should be detectable in the spectrum of the radiation. In particular, we show that the thermality of Unruh radiation is violated due to the corpuscular effects.

Semi-Classical Analysis

First, let us briefly review the Unruh effect in the semi-classical treatment. For a more detailed discussion the reader is referred to the literature [20]. In general, an accelerated

observer known as Rindler observer observes a thermal black body spectrum of Unruh temperature T . To derive this effect, we determine the corresponding transition rate $\dot{\mathcal{F}}(E)$ defined as the Fourier transform of the classical Wightman function $W_c(X, Y)$. For a generic quantum state $|\psi\rangle$, the Wightman function is given by $W_c(X, Y) = \langle \psi | \Phi(X) \Phi(Y) | \psi \rangle$. Obviously, this makes the similarity of the propagator and the Wightman function manifest. The Wightman function is a solution to

$$\mathcal{O}_c W_c(X, Y) = 0. \quad (5.45)$$

Restricting to an AdS background in 3 + 1 dimensions in Poincaré coordinates, the Wightman function for a massless scalar reduces to

$$W_c(X, Y) = \frac{1}{8\pi^2 R_{AdS}^2} \left(\frac{1}{\nu - 1} - \frac{1}{\nu + 1} \right). \quad (5.46)$$

Here we introduced

$$\nu = \frac{z_1^2 + z_2^2 + (x_1 - x_2)^2 + (y_1 - y_2)^2 - (t_1 - t_2 - i\epsilon)^2}{2z_1 z_2}. \quad (5.47)$$

Since we are only interested in accelerated trajectories along the $z - t$ plane, we set $x_1 = x_2 = y_1 = y_2 = 0$. Note that in AdS the Unruh radiation is only observable when the acceleration of the observer satisfies the condition $a^2 > R_{AdS}^2$. This is usually called the supercritical regime. Correspondingly, we construct the worldline of an accelerated Rindler observer in accordance with [114],

$$\begin{aligned} t(\tau) &= \frac{a}{\sqrt{a^2 - 1/R_{AdS}^2}} z_o e^{\sqrt{a^2 - 1/R_{AdS}^2} \tau}, \\ z(\tau) &= z_o e^{\sqrt{a^2 - 1/R_{AdS}^2} \tau}. \end{aligned} \quad (5.48)$$

This leads to the transition rate

$$\begin{aligned} \dot{\mathcal{F}}(E) &= \int ds e^{-is} W_c(s) \\ &= \left[\frac{E}{2\pi} - \frac{1}{4\pi a R_{AdS}^2} \sin \left(\frac{2E}{\sqrt{a^2 - 1/R_{AdS}^2}} \operatorname{arcsinh}(R_{AdS} \sqrt{a^2 - 1/R_{AdS}^2}) \right) \right] \\ &\quad \times \frac{1}{\exp(2\pi E / \sqrt{a^2 - 1/R_{AdS}^2}) - 1}, \end{aligned} \quad (5.49)$$

with $s = \tau_1 - \tau_2$ and E the energy. Using equation (5.49), we conclude that the temperature of the flux of particles measured by a supercritical accelerated observer in AdS is given by

$$T = \frac{1}{2\pi} \sqrt{a^2 - 1/R_{AdS}^2}. \quad (5.50)$$

In order to be in thermal equilibrium, the Wightman function in accelerated coordinates has to satisfy the KMS (Kubo-Martin-Schwinger) condition. Thus, if the Wightman function is evaluated in a thermal state $|\psi\rangle$, it has to obey the condition

$$W_c(\tau_1, \tau_2) = W_c(\tau_2, \tau_1 + i\beta). \quad (5.51)$$

Here we omitted the spatial arguments and defined $\beta = 1/T$ as the inverse temperature. Clearly, the classical Wightman function (5.46) satisfies this condition. Thus, we can derive that the observer is in thermal equilibrium simply by testing this condition.

Corpuscular Effects

Turning to the corpuscular picture, the strategy is as follows: In order to show that thermality of the Unruh radiation is violated, we will investigate if the KMS condition (5.51) is violated on a microscopically resolved AdS background.

For that purpose, we first of all have to determine the fully quantum corrected Wightman function $W_f = W_c + W_q$ evaluated for a Rindler observer as in equation (5.48). Note that W_c corresponds to the classical Wightman function and W_q to its quantum correction. Most of the work was, in principle, already done in the previous section, where we determined the quantum corrected equation of motion. Classically, the Wightman function satisfies

$$\mathcal{O}_c W_c = 0. \quad (5.52)$$

Using (5.52) and taking the corpuscular structure of AdS into account, it follows

$$(\mathcal{O}_c + \mathcal{O}_q)W_f = (\mathcal{O}_c + \mathcal{O}_q)(W_c + W_q) = 0, \quad (5.53)$$

where \mathcal{O}_q is given as in equation (5.41). Solving for the full Wightman function using a similar resummation technique as in equation (5.42), we obtain

$$W_f = W_c - G_f \mathcal{O}_q W_c. \quad (5.54)$$

It is, in principle, straightforward to check if W_f satisfies the KMS condition (5.51). However, already at this point it is clear that it must be violated. As can be seen from (5.51), the KMS condition basically states that we can exchange X and Y , but in equation (5.54) only the classical Wightman function depends on both coordinates, while the quantum correction \mathcal{O}_q only depends on X . Subsequently, this term violates the KMS condition.

Nevertheless, let us try to make these considerations computationally manifest. For simplicity, we will set $\tau_2 = 0$ in our analysis implying $\tau_1 = s \equiv \tau$. Since we are more interested in proving deviations from thermality than in the actual form of the Wightman function, we will focus on showing that the first order quantum correction W_{q1} is not thermal. The first order correction is obtained in the approximation $G_f \approx G_c$ leading to $W_{q1} \equiv G_c \mathcal{O}_q W_c$. Instead of presenting the complicated analytical result, we depict the deviations from thermality in figure (5.6).

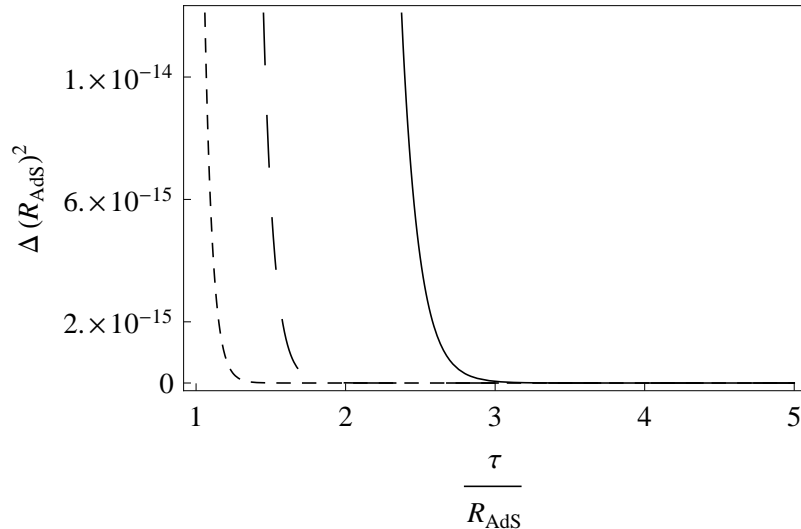


Figure 5.6: This figure shows the quantum derivation from the KMS condition $\Delta \equiv W_{q_1}(\tau, 0) - W_{q_1}(0, \tau + i\beta)$ as a functions of τ . For the additional parameter we choose $z_0 = 1$. We choose three different accelerations for the Rindler observer (all satisfying $a > 1/R_{AdS}$): $a = 2$ (straight), $a = 3$ (largely dashed) and $a = 4$ (dashed). The unit length scale in this figure is given by R_{AdS} .

The KMS condition is violated when $\Delta \equiv W_{q_1}(\tau, 0) - W_{q_1}(0, \tau + i\beta)$ is non-vanishing. Obviously, figure (5.6) reveals that this is, indeed, the case due to the existence of corpuscular corrections to the Wightman function indicating that the Unruh radiation is not exactly thermal.

Let us briefly discuss these results. First of all, it is worth mentioning that the effect becomes more suppressed for large accelerations $a \gg R_{AdS}^{-1}$. Of course, this result is consistent with our expectations, since in this limit the AdS background becomes effectively flat such that the corpuscular effects should be negligible.

Secondly, the quantum corrected Wightman function satisfies the KMS condition for large values of τ . This is in total accordance with the results of the previous subsection where we observed that quantum corrections to the propagator become negligible for large values of $z_1 - z_2$ which corresponds to large values of τ (see equation 5.48). Nevertheless, thermality of AdS is violated due to the interaction with the finite number of corpuscles in the local region of AdS. This local number of constituents is always finite. Therefore, it naturally leads to $1/N$ -type quantum corrections.

To draw a conclusion, Unruh radiation does not exhibit a thermal spectrum in a corpuscular resolved AdS background due to scattering on the individual quanta of the AdS bound state. Note, that these results could be extremely interesting regarding the information paradox occurring for semi-classical black holes. As was explained in section 1.3, we expect that the resolution of the black hole into its microscopic degrees of freedom eventually leads to the deviations from thermality of the Hawking radiation which resolves the information paradox.

5.6 Conclusion

Finally let us draw a conclusion for this chapter. We successfully managed to apply the coherent state method to describe various classical fields as quantum bound states to gravitational background metrics. In a first example, we showed how to explicitly represent linear AdS as a bound state of gravitons. In this description, we can understand the blue shift in AdS as a series of scattering processes on the individual bound state gravitons.

As a next step, we turned to non-linear AdS. In this context, we could obtain a first hint to explain how the holographic principle arises. In particular, the entropy of the CFT is equivalent to the number of corpuscles in the bulk $S_{CFT} = N$ when we consider only the low energetic quanta whose dispersion is well approximated by a free one. Furthermore, we showed that AdS is protected against decay into Minkowski due to the large occupation number, while it locally can be deformed to Minkowski.

As an application of the corpuscular treatment, we computed the corpuscular corrections which a scalar particle observes when it propagates through a resolved AdS. With these results we were able to show that the Unruh radiation measured by a Rindler observer is not thermal. This is an interesting result, since in the black hole portrait we expect similar effects to arise leading to a unitarization of the Hawking radiation.

However, to make more quantitative statements, it is left for future work to determine the corpuscular dispersion relation. Otherwise, we cannot determine the absolute strength of the corrections.

Chapter 6

Summary and Outlook

To conclude this thesis, let us summarize and discuss the results. The main goal we pursued in this thesis was to represent various classical objects in terms of its proper microscopic degrees of freedom. We investigated black holes, solitons, instantons and the AdS space-time from this bound state perspective.

As a first step, we motivated the idea to resolve classical objects in terms of quantum constituents by discussing aspects of black hole physics as this framework allows to easily resolve the information paradox. In particular, based on the ideas of [4] we presented in chapter 2 a set-up how we can probe the microscopic structure of black holes. In this context, the only fundamental space-time is Minkowski, while all other gravitational backgrounds are bound states built on Minkowski. The event horizon in this description is similar to the charge radius of the proton setting the length scale on which the constituents are confined. Since unitarity is preserved in this framework, there must be a globally defined Killing vector everywhere such that we can extract information about the inside of the black hole. Starting from the assumption that QFT and unitarity also preexist inside the classical black hole event horizon, it inevitably follows that we can obtain information about the black hole interior using scattering processes of high virtuality. As a consistency check, we show that the corresponding cross-section for scatterings on the black hole is directly proportional to the occupation number of the black hole constituents. Therefore, we could, in principle, determine the occupation number from experimental data. Clearly, this is interesting, since we expect new scattering data to appear in the near future. For future work, it would be interesting to enhance the different black hole models [4, 7] to predict the outcome of these potential experiments.

In addition to black holes, there are many other classical objects in physics which should be described as bound states of quantum degrees of freedom when QFT is fundamental. For instance, we investigate solitons from the microscopic point of view in chapter 3. We showed how to represent solitons in several examples as coherent states constructed from the soliton constituents. To distinguish these constituents from usual asymptotic S -matrix particles, we refer to them as corpuscles. In contrast to usual particles, the corpuscles are never free, but instead can only exist in the bound state where they feel a large collective potential from the surrounding corpuscles. In order for this bound state construction of

solitons in terms of coherent states to be justified, we clarified how all the classical results can be observed to leading order in the corpuscular occupation number N .

Apart from simply constructing a consistent quantum description, interesting new physics arise from these concepts. First of all, it allows to give a new understanding of the topological charge of the topological soliton. As it turns out, we can relate it to an infinite occupation number of infinite wavelength modes. Clearly, the overlap of a state with an infinite occupation number and the Minkowski vacuum vanishes. Subsequently, the topological soliton is protected against decay into the topological trivial sector. We can even take a step further and distinguish the quanta which are solely responsible for the topological charge and those for the energy. Since the number of energetical quanta is finite, we can still have non-vanishing quantum corrections, although the total number of quanta diverges.

Secondly, we find first indications that in supersymmetric theories where half of the symmetries are preserved on a classical background kink, in fact, all the supersymmetries are broken when we take the microscopic resolution of the kink into account. The compositeness of the kink leads to non-vanishing back-reactions we refer to as $1/N$ effects. These corrections are bosonic in nature spoiling all the supersymmetries. As a consequence, this would lead to the emergence of a second Goldstino and to a mass splitting between the usual fermions and bosons propagating on the background. Note that the $1/N$ corrections are very similar to phonons in a solid state. However, this is still work in progress as many questions like the corpuscular renormalization are not fully understood up to this point.

The most important question we have to answer in future work on solitons is how we can, in general, determine the corpuscular dispersion relation. So far we can determine it approximately in special cases where the Hamiltonian is diagonal on the classical solution (BPS case). Therefore, we can only make quantitative statements for very few classical objects. As a remark, let us mention that it is quite a formidable task to determine the dispersion, since it should arise from the underlying physics of the theory. In general, the strategy would be to perform a Bogoliubov transformation, but this is an extremely hard task. Without such a complete understanding of the microscopic origin of the corpuscular dispersion, it is not possible to make more quantitative statements in the the context of supersymmetric solitons.

In chapter 4, we discussed how to implement the microscopic resolution for the instanton. However, due to its dependence on Euclidean time we followed a slightly different strategy to achieve this goal. Instead of directly defining a coherent instanton state, we mapped the d dimensional instanton on a soliton in a $d + 1$ dimensional theory. Nevertheless, a lower dimensional observer will simply observe an instanton vacuum transition as the soliton passes by in Euclidean time. The finite action of the instanton is identified as the energy of the tunneling soliton times the tunneling distance L . Consequently, the instanton inherits all of the features of the soliton such as the corpuscular structure. To make this computationally manifest, we investigated several concrete models of embedding the instanton in a higher dimensional soliton theory. For instance, we show how we can represent a $2 + 1$ dimensional instanton as a monopole tunneling through an energetically forbidden barrier. Similarly, we discuss the famous BPST instanton. In this case, it turns

out that the corpuscular substructure of the monopole we map on leads to the violation of scale invariance. In particular, the size modulus becomes a physical parameter in the quantum treatment, since the occupation number is proportional to the bound state size. For instantons it is still an open question if it possible to directly define a coherent instanton state without mapping it on a higher dimensional soliton.

Finally, in chapter 5 we discuss GR aspects from the quantum bound state perspective. We show how we can use the coherent state technique to represent classical background metrics in terms of corpuscles. First of all, we observe that in the linear limit of AdS we can interpret the corpuscles as on-shell massive gravitons. This treatment easily visualizes some of the main properties of AdS from the quantum perspective. For example, the blue shift appearing in AdS can be viewed as a sequence of scatterings on the individual gravitons. In each process, the corpuscles convey energy to the probe particle leading to the blue shift.

Similar to the topological soliton, we can show that AdS is stable against decay into Minkowski. As it turns out, the occupation number of corpuscles N diverges, since it is proportional to the spatial volume of Minkowski space-time. Thus, the overlap between Minkowski and AdS scaling as e^{-N} vanishes. Nevertheless, the equivalence principle is still satisfied because the local number of constituents is small. Locally, AdS is equivalent to Minkowski even from the corpuscular point of view.

In addition, the coherent state description gives a hint towards a corpuscular interpretation of the holographic principle. Namely, the number of degrees of freedom in the bulk N scales like the entropy of the lower dimensional CFT on the boundary. Note that is only true for the low energy regime where the corpuscular dispersion is known approximately. It is not clear how in general the corpuscular dispersion can be determined from first principles. In the AdS case, we can determine the scale at which new physics come into play and influence the dispersion, but it is so far left for future work to identify the corresponding dynamics.

As an application of the the coherent state formalism of AdS, we try to determine corpuscular corrections to scalar propagators on AdS. We find strong hints that, indeed, the scalar propagation is corrected by back-reactions.

To draw a conclusion, we successfully established a bound state picture for several classical objects. However, the underlying dynamics of the corpuscles governing the dispersion can in many cases only be determined approximately.

Appendix A

Supersymmetry Breaking

Let us explicitly show how we arrive at equation (3.91). For that purpose, we expand $\mathcal{G}_{kink} = \langle sol | \mathcal{O}_{BPS}^2 | sol \rangle$ in corpuscular annihilation and creation operators \hat{a}_k and \hat{a}_k^\dagger . Note that we will neglect all the terms which are vacuum contributions. As a first step, we compute \mathcal{O}_{BPS} ,

$$\begin{aligned} \mathcal{O}_{BPS} &= \partial_x \hat{\phi} - \left(m^2/g - g\hat{\phi}^2 \right) \\ &= i\sqrt{l} \int \frac{dk}{\sqrt{4\pi|k|}} k \left(e^{ikx} \hat{a}_k - e^{-ikx} \hat{a}_k^\dagger \right) - m^2/g \\ &\quad + gl \int \frac{dkdq}{4\pi\sqrt{|k||q|}} \left(e^{ikx} \hat{a}_k + e^{-ikx} \hat{a}_k^\dagger \right) \left(e^{iqx} \hat{a}_q + e^{-iqx} \hat{a}_q^\dagger \right). \end{aligned} \quad (\text{A.1})$$

When we evaluate \mathcal{O}_{BPS}^2 , obviously, fourth and third order terms in creation and annihilation operators arise which are, in particular, not normal ordered. However, using the standard commutation relation $[\hat{a}_k, \hat{a}_q^\dagger] = \delta(k - q)/l$ for the Fock operators we can bring \mathcal{O}_{BPS}^2 to a normal ordered form,

$$\begin{aligned} \mathcal{O}_{BPS}^2 &=: \left[i\sqrt{l} \int \frac{dk}{\sqrt{4\pi|k|}} k \left(e^{ikx} \hat{a}_k - e^{-ikx} \hat{a}_k^\dagger \right) - m^2/g \right. \\ &\quad \left. + gl \int \frac{dkdq}{4\pi\sqrt{|k||q|}} \left(e^{ikx} \hat{a}_k + e^{-ikx} \hat{a}_k^\dagger \right) \left(e^{iqx} \hat{a}_q + e^{-iqx} \hat{a}_q^\dagger \right) \right]^2 : \\ &\quad + : 6g^2l \int \frac{dkdq}{4\pi\sqrt{|k||q|}} \left(e^{ikx} \hat{a}_k + e^{-ikx} \hat{a}_k^\dagger \right) \left(e^{iqx} \hat{a}_q + e^{-iqx} \hat{a}_q^\dagger \right) \int \frac{dk}{4\pi|k|} : \\ &\quad + 2i\sqrt{l} \int \frac{dk}{\sqrt{4\pi|k|}} k \left(e^{ikx} \hat{a}_k - e^{-ikx} \hat{a}_k^\dagger \right) \int \frac{dk}{4\pi|k|}. \end{aligned} \quad (\text{A.2})$$

This form allows to use the special feature of the coherent state, that it is an eigenvector ($\hat{a}_k | sol \rangle = \sqrt{N_k} | sol \rangle$) of the annihilation operator. As a consequence, the normal ordered products give the classical field value when evaluated in the coherent state. In particular,

the first two lines of (A.2) reduce to the classical BPS equation, while the third and fourth line correspond to corpuscular quantum corrections. In contrast to the vacuum contributions, these effects vanish on the trivial Minkowski vacuum, since they are proportional to normal ordered parts. Furthermore, they contain a divergent part because a δ -function emerges due to the commutation. Thus, we arrive at

$$\begin{aligned} \langle sol | \mathcal{O}_{BPS}^2 | sol \rangle &= \underbrace{\left[\partial_x \phi_{sol} - \left(m^2/g - g\phi_{sol}^2 \right) \right]^2}_{=0 \text{ because this is the classical BPS condition}} \\ &+ \frac{1}{\pi} \left(g\partial_x \phi_{sol}(x) + 3g^2\phi_{sol}^2 \right) \log \left(\frac{\Lambda_{UV}}{\mu_{IR}} \right), \end{aligned} \quad (\text{A.3})$$

which is exactly the wanted result for \mathcal{G}_{kink} as in (3.91).

Appendix B

Corpuscular corrections to the scalar propagator in AdS

As was advertised in chapter 5, we briefly present the important formulas regarding scalar propagators on AdS. In particular, the Green's function solving the classical equation of motion (5.36) is given as

$$G_c(X, Y) = \frac{2}{C_\Delta} \left(\frac{\xi}{2}\right)^\Delta F\left(\frac{\Delta}{2}, \frac{\Delta}{2} + \frac{1}{2}, \sigma + 1, \xi^2\right). \quad (\text{B.1})$$

where F denotes the hypergeometric function, while Δ corresponds to the scaling exponent of the scalar field in $(d + 1)$ dimensional AdS. It can be written as

$$\Delta = \frac{d}{2} + \sigma \text{ with} \quad (\text{B.2})$$

$$\sigma = \sqrt{\frac{d^2}{4} + m^2 R^2}. \quad (\text{B.3})$$

Additionally, the constant C_Δ is defined as

$$C_\Delta = \frac{\Gamma(\Delta)}{\pi^{d/2} \Gamma(\sigma)}. \quad (\text{B.4})$$

Here Γ denotes the gamma-function. The function ξ depends on the coordinates of the start and end point of the propagation,

$$\xi = \frac{2z_1 z_2}{z_1^2 + z_2^2 + (x_1 - x_2)^2}. \quad (\text{B.5})$$

Bibliography

- [1] ATLAS Collaboration, *Observation of a new particle in the search for the Standard Model Higgs boson with the ATLAS detector at the LHC*, Phys. Lett. B 716 (2013) 1-29.
- [2] C. L. Bennett et al. , *First-Year Wilkinson Microwave Anisotropy Probe(WMAP)* Observations: Preliminary Maps and Basic Results*, The Astrophysical Journal Supplement Series (2003) Volume 148 Number 1 .
- [3] B. Abbott et al. (LIGO Scientific Collaboration and Virgo Collaboration), *Observation of Gravitational Waves from a Binary Black Hole Merger*, Phys. Rev. Lett. 116 (2016), 061102.
- [4] G. Dvali and C. Gomez, *Black Hole's Quantum N-Portrait*, (2011) arXiv:1112.3359 [hep-th] .
- [5] G. Dvali and C. Gomez, *Black Hole's 1/N Hair*, Phys. Lett. B719 (2013) 419-423.
- [6] G. Dvali and C. Gomez, *Quantum Compositeness of Gravity: Black Holes, AdS and Inflation*, JCAP 01(2014) 023.
- [7] S. Hofmann and T. Rug, *A Quantum Bound-State Description of Black Holes*, Nucl. Phys. B902 (2016) 302-325.
- [8] S. W. Hawking, *Particle creation by black holes*, Communications in Mathematical Physics Volume 43 (1975) 199-220.
- [9] S. Hawking, *Breakdown of Predictability in Gravitational Collapse*, Phys. Rev. D 14 (1976) 2460-2473.
- [10] J. M. Maldacena, *The Large N Limit of Superconformal Field Theories and Supergravity*, Adv. Theor. Math. Phys. 2 (1998) 231-252.
- [11] E. Witten, *Anti-de Sitter space and holography*, Adv. Theor. Math. Phys. 2 (1998) 253-291.
- [12] S. S. Gubser, I. R. Klebanov, and A. M. Polyakov, *Gauge theory correlators from noncritical string theory*, Phys. Lett. B428 (1998) 105.

- [13] L. Susskind, *The World as a hologram*, J. Math. Phys. 36 (1995) 6377-6396.
- [14] R. J. Glauber, *The Quantum Theory of Optical Coherence*, Phys. Rev. 130 (1963) 2529.
- [15] T. Muta, *Foundations of Quantum Chromodynamics*, World Scientific Lecture Notes in Physics Vol. 78.
- [16] G. Dvali, C. Gomez, L. Gruending and T. Rug, *Towards a Quantum Theory of Solitons*, Nucl. Phys. B901 (2015) 338-353.
- [17] A. A. Belavin, A. M. Polyakov, A. S. Schwartz, Y. S. Tyupkin, *Pseudoparticle solutions of the Yang-Mills equations*, Phys. Lett. B59 (1975) 8587.
- [18] L. Randall and R. Sundrum, *A Large Mass Hierarchy from a Small Extra Dimension*, Phys. Rev. Lett. 83 (1999) 3370-3373.
- [19] L. Randall and R. Sundrum, *An Alternative to compactification*, Phys. Rev. Lett. 83 (1999) 4690-4693.
- [20] S. Deser and O. Levin, *Accelerated detectors and temperature in (anti)-de Sitter spaces*, Class. Quant. Grav. 14 (1997) L163-L168.
- [21] A. Einstein, *Zur allgemeinen Relativitätstheorie*, Preussische Akademie der Wissenschaften (1915) 778.
- [22] A. Einstein, *Zur allgemeinen Relativitätstheorie (Nachtrag)*, Preussische Akademie der Wissenschaften (1915) 779.
- [23] T. Jacobson, *Introduction to Quantum Fields in Curved Spacetime and the Hawking Effect*, arXiv:gr-qc/0308048.
- [24] C. W. Misner, K. S. Thorne and J. A. Wheeler, *Gravitation*, Freeman and Company.
- [25] R. M. Wald, *General Relativity*, University of Chicago Press.
- [26] K. Hinterbichler, *Theoretical Aspects of Massive Gravity*, Rev. Mod. Phys. 84 (2012) 671-710.
- [27] P. A. M. Dirac, *Lectures on quantum mechanics*, Belfer Graduate School of Science 1964.
- [28] C. P. Burgess, *Introduction to Effective Field Theory*, Ann. Rev. Nucl. Part. Sci. 57 (2007) 329-362.
- [29] C. P. Burgess, *Quantum Gravity in Everyday Life: General Relativity as an Effective Field Theory*, Living Rev. Rel. 7 (2004) 5.

- [30] N. Arkani-Hamed, H. Georgi and M. D. Schwartz, *Effective Field Theory for Massive Gravitons and Gravity in Theory Space*, Ann. Phys. 305 (2003) 96-118.
- [31] J. Polchinski, *String Theory Vol. I: An Introduction to the Bosonic String*, Cambridge University Press.
- [32] J. Polchinski, *String Theory Vol. II: Superstring Theory and Beyond*, Cambridge University Press.
- [33] M. D. Schwarz, *Quantum Field Theory and the Standard Model*, Cambridge University Press.
- [34] J. D. Brown and M. Henneaux, *Central Charges in the Canonical Realization of Asymptotic Symmetries: An Example from Three Dimensional Gravity*, Comm. Math. Phys. 104 (1986) 207-226.
- [35] M. Henneaux and C. Teitelboim, *Asymptotically anti-de Sitter spaces*, Comm. Math. Phys. Volume 98 (1985) 391-424.
- [36] H. Bondi, M. G. J. van der Burg and A. W. K. Metzner, *Gravitational waves in general relativity VII. Waves from isolated axisymmetric systems*, Proc. Roy. Soc. Lond. A 269 (1962) 21.
- [37] R. K. Sachs, *Gravitational waves in general relativity VIII. Waves in asymptotically at space-time*, Proc. Roy. Soc. Lond. A 270 (1962) 103.
- [38] A. Strominger, *On BMS Invariance of Gravitational Scattering*, JHEP 07 (2014) 152.
- [39] A. Averin, G. Dvali, C. Gomez and D. Lust, *Gravitational Black Hole Hair from Event Horizon Supertranslations*, JHEP 06 (2016) 088.
- [40] Karl Schwarzschild, *Über das Gravitationsfeld eines Massenpunktes nach der Einsteinschen Theorie*, Sitzungsberichte der Königlich-Preussischen Akademie der Wissenschaften (1916) 189-196.
- [41] D. N. Page, *Information in black hole radiation*, Phys. Rev. Lett. 71 (1993) 3743-3746.
- [42] D. N. Page, *Black Hole Information*, arXiv:hep-th/9305040.
- [43] S. D. Mathur, *The information paradox: A pedagogical introduction*, Class. Quant. Grav. 26 (2009) 224001.
- [44] L. Susskind, L. Thorlacius and J. Uglum, *The Stretched Horizon and Black Hole Complementarity*, Phys. Rev. D48 (1993) 3743 .
- [45] L. Susskind and L. Thorlacius, *Gedanken experiments involving black holes*, Phys.Rev. D 49 (1994) 966-974.

- [46] Ahmed Almheiri, Donald Marolf, Joseph Polchinski and James Sully, *Black Holes: Complementarity or Firewalls?*, JHEP 02 (2013) 062.
- [47] S. Mathur, *The Fuzzball proposal for black holes: An Elementary review*, Fortsch. Phys. 53 (2005) 793-827.
- [48] T. Banks, W. Fischler, I. R. Klebanov and L. Susskind, *Schwarzschild Black Holes from Matrix Theory*, Phys. Rev. B 80 (1998) 226.
- [49] G. Dvali, *Non-Thermal Corrections to Hawking Radiation Versus the Information Paradox*, Fortsch. Phys. 64 (2016) 106-108.
- [50] G. Dvali, C. Gomez, D. Lust, R. S. Isermann and S. Stieberger, *Black hole formation and classicalization in ultra-Planckian 2 to N scattering*, Nucl. Phys. B 893 (2015) 187.
- [51] G. 't Hooft, *A planar diagram theory for strong interactions*, Nucl. Phys. B 72 (1974) 461.
- [52] E. Witten, *Baryons in the 1/n Expansion*, Nucl. Phys. B160 (1979) 57-115.
- [53] G. Dvali and C. Gomez, *Black Holes as Critical Point of Quantum Phase Transition*, Eur. Phys. J. C74 (2014) 2752.
- [54] V. F. Foit and N. Wintergerst, *Self-similar Evaporation and Collapse in the Quantum Portrait of Black Holes*, Phys. Rev. D 92 (2015) 6, 064043.
- [55] R. Ruffini and J.A. Wheeler, *Introducing the Black Hole* Physics Today 24 (1971) 30.
- [56] W. Israel, *Event horizons in static vacuum space-times*, Phys. Rev. 164 (1967) 1776.
- [57] W. Israel, *Event horizons in static electrovac space-times*, Comm. Math. Phys. 8 (1968) 245.
- [58] B. Carter, *Axisymmetric Black Hole Has Only Two Degrees of Freedom*, Phys. Rev. Lett. 26 (1971) 331.
- [59] R. B. Wald, *Final states of gravitational collapse*, Phys. Rev. Lett. 26 (1971) 1653.
- [60] J. D. Bekenstein, *Nonexistence of Baryon Number for Black Holes II*, Phys. Rev. D 5 (1972) 2403.
- [61] G. Dvali and A. Gussmann, *Skyrmion Black Hole Hair: Conservation of Baryon Number by Black Holes and Observable Manifestations*, arXiv:1605.00543.
- [62] J. D. Bekenstein, *Black holes and entropy*, Phys. Rev. D7 (1973) 2333.
- [63] D. Page, *Hawking Radiation and Black Hole Thermodynamics*, New Journal of Physics 7 (2004) 203.

- [64] Y. Sekino and L. Susskind, *Fast Scramblers*, JHEP 0810 (2008) 065.
- [65] G. Dvali, D. Flassig, C. Gomez, A. Pritzel and N. Wintergerst, *Scrambling in the Black Hole Portrait*, Phys. Rev. D 88 (2013) 124041.
- [66] Daniel Flassig, Alexander Pritzel and Nico Wintergerst, *Black holes and quantumness on macroscopic scales*, Phys. Rev. D87 (2013) 084007.
- [67] M. Shifman, *Advanced Topics in Quantum Field Theory*, Cambridge University Press (2012).
- [68] S. R. Coleman, *Fate of the false vacuum: Semiclassical theory*, Phys. Rev. D 15 (1977) 2929.
- [69] S. R. Coleman, *Gravitational Effects on and of vacuum decay*, Phys. Rev. D 21 (1980) 3305.
- [70] S. Coleman and J. Mandula, *All Possible Symmetries of the S Matrix*, Phys. Rev. 159 (1967) 1251.
- [71] J. Wess and J. Bagger, *Supersymmetry and Supergravity*, Princeton University Press (1992).
- [72] N. Seiberg, *The Power of holomorphy: Exact results in 4D SUSY field theories*, arXiv:9408013 [hep-th] (1994).
- [73] E. Witten, *Dynamical Breaking of Supersymmetry*, Nucl. Phys. B 188 (1981) 513.
- [74] M. Shifman and A. Vainshtein, *Instantons versus supersymmetry: Fifteen years later*, ITEP lectures on particle physics and field theory Vol 2 (1999) 482-647.
- [75] P. W. Higgs, *Broken symmetries, massless particles and gauge fields*, Phys. Lett. 12 (1964) 132.
- [76] J. Zinn-Justin and U.D. Jentschura, *Multi-instantons and exact results I: Conjectures, WKB expansions, and instanton interactions*, Annals Phys 313 (2004) 197.
- [77] S. Weinberg, *A new light boson?*, Phys. Rev. Lett. 40 (1978) 223.
- [78] R.D. Peccei and H.R. Quinn, *CP Conservation in the Presence of Pseudoparticles*, Phys. Rev. D 16 (1977) 1791.
- [79] G. Dvali, *Three-Form Gauging of axion Symmetries and Gravity*, arXiv:hep-th/0507215.
- [80] G. Dvali and L. Funcke, *Small neutrino masses from gravitational θ -term*, Phys. Rev. D 93 (2016) 113002.

- [81] L. Susskind and E. Witten, *The Holographic Bound in Anti-de Sitter Space*, arXiv:hep-th/9805114.
- [82] S. Ryu and T. Takayanagi, *Holographic Derivation of Entanglement Entropy from AdS/CFT*, Phys. Rev. Lett. 96 (2006) 181602.
- [83] M. J. Duff, *Quantum Tree Graphs and the Schwarzschild Solution*, Phys. Rev. D 7 (1973) 2317.
- [84] M. A. Shifman, A. I. Vainshtein and V. I. Zakharov, *QCD and Resonance Physics. Sum Rules*, Nucl. Phys. 47 (1979) 385.
- [85] M. A. Shifman, A. I. Vainshtein and V. I. Zakharov, *QCD and Resonance Physics: Applications*, Nucl. Phys. 47 (1979) 448.
- [86] L. Gruending, S. Hofmann, S. Mueller and T. Rug, *Probing the Constituent Structure of Black Holes*, JHEP 1505 (2015) 047.
- [87] G. Barnich, *The Coulomb solution as a coherent state of unphysical photons*, Gen. Rel. Grav. 43 (2011) 2527-2530.
- [88] S. R. Coleman, *The Quantum Sine-Gordon Equation as the Massive Thirring Model*, Phys. Rev. D 11 (1975) 2088.
- [89] S. Mandelstam, *Soliton operators for the quantized sine-Gordon equation*, Phys. Rev. D 11 (1975) 3026.
- [90] C. Bachas, G. Lazarides, Q. Sha and G. Tiktopoulos, *Quantum mechanical tunneling at high-energy*, Phys. Lett B 268 (1991) 401-407.
- [91] G. Dvali and C. Gomez, *Corpuscular Breaking of Supersymmetry*, (2014) arxiv:1406.6014 [hep-th].
- [92] M. E. Peskin and D.V. Schroeder, *An Introduction To Quantum Field Theory*, Westview Press.
- [93] G. Dvali, C. Gomez, L. Gruending and T. Rug, *Towards a Quantum Theory of Instantons*
- [94] B. D. Josephson, *Possible new effects in superconductive tunnelling*, Phys. Lett. 1 (1962) 251-253.
- [95] A. M. Polyakov, *Quark Confinement and Topology of Gauge Theories*, Nucl. Phys. B 120 (1977) 429.
- [96] G. Dvali and M. Shifman, *Dynamical compactification as a mechanism of spontaneous supersymmetry breaking*, Nucl. Phys. B 504 (1997) 127-146.

- [97] G. Dvali, H.B. Nielsen and N. Tetradis, *Localization of gauge fields and monopole tunneling*, Phys.Rev. D77 (2008) 085005.
- [98] G. Dvali and M. A. Shifman, *Domain walls in strongly coupled theories*, Phys. Lett. B396 (1997) 64-69, Phys. Lett. B407 (1997) 452.
- [99] D. Flassig and A. Pritzel, *Localization of gauge fields and Maxwell-Chern-Simons theory*, Phys.Rev. D84 (2011) 125024.
- [100] M. Dierigl and A. Pritzel, *Topological Model for Domain Walls in (Super-)Yang-Mills Theories*, Phys.Rev. D90 (2014) 10, 105008.
- [101] I. Affleck, *On Constrained Instantons*, Nucl. Phys. B191 (1981) 429.
- [102] G. Dvali, C. Gomez, L. Gruending, T. Rug and D. Sarkar, *Towards a microscopic Description of AdS*, to appear 2017.
- [103] L. Gruending, T. Rug and D. Sarkar, *Effects of quantum compositeness on Quantum Field theories in AdS*, to appear 2017.
- [104] G. Dvali, and C. Gomez, *Quantum Exclusion of Positive Cosmological Constant?*, arXiv:1412.8077 [hep-th] (2014).
- [105] G. Dvali and S. Zell, *Quantum Break-Time of de Sitter*, arXiv:1701.08776 [hep-th] (2017).
- [106] G. Dvali, S. Hofmann and J. Khoury, *Degravitation of the Cosmological Constant and Graviton Width*, Phys. Rev. D 76 (2007) 084006.
- [107] G. Dvali, C. Gomez and D. Luest, *Classical Limit of Black Hole Quantum N-Portrait and BMS Symmetry*, Phys. Lett. B753 (2016) 173.
- [108] E. Alvarez and C. Gomez, *Geometric holography, the renormalization group and the c theorem*, Nucl. Phys. B 541, (1999) 441.
- [109] L. Girardello, M. Petrini, M. Porrati and A. Zaffaroni, *Novel local CFT and exact results on perturbations of N=4 superYang Mills from AdS dynamics*, JHEP 9812 (1998) 022.
- [110] D. Freedman, S. Gubser, K. Pilch and N. P. Warner, *Renormalization group flows from holography supersymmetry and a c theorem*, Adv. Theor. Math. Phys. 3 (1999) 363.
- [111] I. Heemskerk and J. Polchinski, *Holographic and Wilsonian Renormalization Groups*, JHEP 1106, (2011) 031.
- [112] D. Sarkar, *(A)dS holography with a cutoff*, Phys. Rev. D 90 (2014) 086005.

- [113] N. Arkani-Hamed, S. Dimopoulos and G. R. Dvali, *The Hierarchy problem and new dimensions at a millimeter*, Phys. Lett. B 429 (1998) 263.
- [114] D. Jennings, *On the response of a particle detector in Anti-de Sitter spacetime*, Class. Quant. Grav. 27 (2010) 205005.

Acknowledgements

First of all, I would like to thank Gia Dvali for his support during my PhD time. In particular, I am grateful for the physical discussion and for the guidance in many physical questions. Additionally, it was a great experience to have the opportunity to collaborate with Gia.

It is a pleasure to thank Stefan Hofmann and Cesar Gomez for their support and the physical insights they shared with me over the past years. In particular, I am thankful for many fruitful discussions which helped me to improve my understanding of physics.

Additionally, I would especially like to thank all my collaborators over the past years: Gia Dvali, Tehseen Rug, Stefan Hofmann, Cesar Gomez, Debayoti Sarkar and Sophia Mueller.

Furthermore, I would like to thank my colleagues at the Max-Planck institute and the Arnold-Sommerfeld Center like, for instance, Tehseen, Daniel, Nico, Mischa, Alex P., Alex G., Claudius, Marc, Reinke, Max, Sophia, Sebastian Z., Sebastian K., Artem, Lena, Deb, Andre and others for the many fruitful discussions.

Finally, I want to thank the Max-Planck institute for the financial support during my PhD time.